Inorg. Chem. **2008**, *47*, 1727−1752

Forum

Mechanisms of Water Oxidation from the Blue Dimer to Photosystem II

Feng Liu, **Javier J. Concepcion**, **Jonah W. Jurss**, **Thomas Cardolaccia**, **Joseph L. Templeton**, **and Thomas J. Meyer***

Department of Chemistry, University of North Carolina at Chapel Hill, CB 3290, Chapel Hill, North Carolina 27599-3290

Received June 25, 2007

The blue dimer, *cis,cis*-$[(bpy)_2(H_2O)Ru^{III}ORu^{III}(H_2O)(bpy)_2]^{4+}$, is the first designed, well-defined molecule known to function as a catalyst for water oxidation. It meets the stoichiometric requirements for water oxidation, $2H_2O \xrightarrow{-4e^-,\ -4H^+} O{-}O$, by utilizing proton-coupled electron-transfer (PCET) reactions in which both electrons and protons are transferred. This avoids charge buildup, allowing for the accumulation of multiple oxidative equivalents at the Ru−O−Ru core. PCET and pathways involving coupled electron–proton transfer (EPT) are also used to avoid high-energy intermediates. Application of density functional theory calculations to molecular and electronic structure supports the proposal of strong electronic coupling across the μ-oxo bridge. The results of this analysis provide explanations for important details of the descriptive chemistry. Stepwise e^-/H^+ loss leads to the higher oxidation states $[(bpy)_2(O)Ru^{V}ORu^{IV}(O)(bpy)_2]^{3+}$ ($Ru^{V}ORu^{IV}$) and $[(bpy)_2(O)Ru^{V}ORu^{V}(O)(bpy)_2]^{4+}$ ($Ru^{V}ORu^{V}$). Both oxidize water, $Ru^{V}ORu^{IV}$ stoichiometrically and $Ru^{V}ORu^{V}$ catalytically. In strongly acidic solutions (HNO_3, $HClO_4$, and HSO_3CF_3) with excess Ce^{IV}, the catalytic mechanism involves O---O coupling following oxidation to $Ru^{V}ORu^{V}$, which does not build up as a detectable intermediate. Direct evidence has been found for intervention of a peroxidic intermediate. Oxidation of water by $Ru^{V}ORu^{IV}$ is far slower. It plays a role late in the catalytic cycle when Ce^{IV} is depleted and is one origin of anated intermediates such as $[(bpy)_2(HO)Ru^{IV}ORu^{IV}(NO_3)(bpy)_2]^{4+}$, which are deleterious in tying up active components in the catalytic cycle. These intermediates slowly return to $[(bpy)_2(H_2O)Ru^{IV}ORu^{III}(OH_2)(bpy)_2]^{5+}$ with anion release followed by water oxidation. The results of a recent analysis of water oxidation in the oxygen-evolving complex (OEC) of photosystem II reveal similarities in the mechanism with the blue dimer and significant differences. The OEC resides in the thylakoid membrane in the chloroplasts of green plants, and careful attention is paid in the structure to PCET, EPT, and long-range proton transfer by sequential local proton transfers. The active site for water oxidation is a $CaMn_4$ cluster, which includes an appended Mn site, Mn(4), where O---O coupling is thought to occur. Photochemical electron transfer results in oxidation of tyrosine Y_Z to $Y_Z^{\cdot}$, which is ∼7 Å from Mn(4). It subsequently oxidizes the OEC through the stepwise stages of the Kok cycle. O---O coupling appears to occur through an initial peroxidic intermediate formed by redox nucleophilic attack of coordinated OH^- in $Ca{-}OH^-$ on $Mn^{IV}{=}O$.

1. Introduction

Water oxidation is a key reaction at the heart of *photosynthesis*, providing a basis for much of life as we know it.[1−12] It also provides a basis for *artificial photosynthesis* in reactions such as those shown below, where the goal is to

* To whom correspondence should be addressed. E-mail: tjmeyer@unc.edu.

(1) Tommos, C.; Babcock, G. T. *Acc. Chem. Res.* **1998**, *31*(1), 18–25.
(2) Proshlyakov, D. A.; Pressler, M. A.; Babcock, G. T. *Proc. Natl. Acad. Sci. U.S.A.* **1998**, *95*(14), 8020–8025.
(3) Ruettinger, W.; Dismukes, G. C. *Chem. Rev.* **1997**, *97*(1), 1–24.
(4) Barber, J. *Q. Rev. Biophys.* **2003**, *36*(1), 71–89.
(5) Diner, B. A.; Rappaport, F. *Annu. Rev. Plant Biol.* **2002**, *53*, 551–580.

10.1021/ic701249s CCC: $40.75 © 2008 American Chemical Society
Published on Web 03/10/2008

use the energy of the sun to produce high-energy chemicals for energy storage and conversion.[13–19]

$$2H_2O + 4h\nu \rightarrow 2H_2 + O_2 \quad (\Delta G^\circ = +4.92\ \text{eV})$$

$$2H_2O + 2CO_2 + 4h\nu \rightarrow 2HCOOH + O_2 \quad (\Delta G^\circ = +5.80\ \text{eV})$$

As implied by the O_2/H_2O half-reaction $2H_2O \xrightarrow{-4e^-} O{-}O + 4e^- + 4H^+$ [E°(pH = 7, NHE) = 0.815 V], mechanistic and thermodynamic demands associated with water oxidation are imposing. There is a requirement for loss of four electrons and four protons and the formation of an O---O bond. The reaction needs to be carried out as near to the thermodynamic potential for the O_2/H_2O couple as possible to maximize efficiencies for energy storage and conversion. Reaction pathways involving single electron transfer and •OH as an initial intermediate are slow or require powerful oxidizing agents because E°(•OH/H_2O) = 2.31 V.

Avoiding one-electron intermediates requires a mechanism in which multiple redox equivalents are accumulated at a single catalyst site or cluster. This presents its own set of challenges arising from the effects of charge buildup on redox potentials as electrons are removed. The charge effect can be overcome by proton-coupled electron transfer (PCET) in which loss of electrons is accompanied by loss of protons.[20] *Proton loss provides charge compensation but also requires proton management*. This is a considerable challenge in the nonaqueous environment of the thylakoid membranes of green plant chloroplasts where oxygen is evolved. As noted in section 6, this appears to be accomplished by a combination of coupled electron–proton transfers, local proton transfers, and a long-range proton-transfer channel in an intricate structure that has been decribed as being "wired for protons".[12]

An additional set of challenges arises from demands on the catalyst. It must accumulate and use multiple oxidative equivalents at high redox potentials and carry out a difficult, multielectron reaction or reactions without reacting with itself or its surroundings. In artificial photosynthesis, the catalyst must be incorporated into a molecular assembly or other microscopic structure or on an electrode surface, where it can be integrated with other functional elements for light absorption, electron transfer, and catalysis.

As discussed in section 6, a working model for water oxidation is available in the reaction center of photosystem II (PSII) in green plants where oxygen is evolved at the oxygen-evolving complex (OEC). The OEC is activated following excitation of a separate antenna array, which sensitizes the lowest singlet excited state of spatially proximate chlorophyll P_{680} or a nearest-neighbor pheophytin.[21] Oxidative quenching to give P_{680}^+ provides oxidative equivalents that drive water oxidation at the OEC through the intervening redox relay tyrosine Y_Z.

To put the challenges for catalyst design into perspective, damage to the reaction center of PSII, largely due to chemical damage following singlet oxygen formation by energy transfer to the O_2 product, requires synthesis of a new reaction center after ~30 min of operation under ambient sunlight.

Even given the difficulties of effecting water oxidation, catalysts are known. They include metal oxide and nanoparticle RuO_2[22–24] and IrO_2,[25–27] ruthenium−ammine complex precursors to catalysts of unknown composition,[28–31] and a few molecular catalysts based on complexes of manganese[32–38] and ruthenium.[39–42] The first example of a

(6) Wydrzynski, T. J. *Photosystem II*; Springer: Dordrecht, The Netherlands, 2005.
(7) Nelson, N.; Yocum, C. F. *Annu. Rev. Plant Biol.* **2006**, *57*(1), 521–565.
(8) Kern, J.; Biesiadka, J.; Loll, B.; Saenger, W.; Zouni, A. *Photosynth. Res.* **2007**, *92*(3), 389–405.
(9) Barber, J. *Biochem. Soc. Trans.* **2006**, *34*(5), 619–631.
(10) McEvoy, J. P.; Brudvig, G. W. *Chem. Rev.* **2006**, *106*(11), 4455–4483.
(11) Ke, B. *Photosynthesis: Photochemistry and Photobiophysics*; Kluwer Academic: Dordrecht, The Netherlands, 2001.
(12) Meyer, T. J.; Huynh, M. H. V.; Thorp, H. H. *Angew. Chem., Int. Ed.* **2007**, *46*, 5284–5304.
(13) Alstrum-Acevedo, J. H.; Brennaman, M. K.; Meyer, T. J. *Inorg. Chem.* **2005**, *44*, 6802–6827.
(14) Gust, D.; Moore, T. A.; Moore, A. L. *Acc. Chem. Res.* **2001**, *34*(1), 40–48.
(15) Gust, D.; Moore, T. A. *The Porphyrin Handbook*; Academic Press: New York, 1999; pp 153–190..
(16) Meyer, T. J. *Acc. Chem. Res.* **1989**, *22*(5), 163–170.
(17) Wasielewski, M. R. *Chem. Rev.* **1992**, *92*(3), 435–461.
(18) Arakawa, H.; Aresta, M.; Armor, J. N.; Barteau, M. A.; Beckman, E. J.; Bell, A. T.; Bercaw, J. E.; Creutz, C.; Dinjus, E.; Dixon, D. A.; Domen, K.; DuBois, D. L.; Eckert, J.; Fujita, E.; Gibson, D. H.; Goddard, W. A.; Goodman, D. W.; Keller, J.; Kubas, G. J.; Kung, H. H.; Lyons, J. E.; Manzer, L. E.; Marks, T. J.; Morokuma, K.; Nicholas, K. M.; Periana, R.; Que, L.; Rostrup-Nielson, J.; Sachtler, W. M. H.; Schmidt, L. D.; Sen, A.; Somorjai, G. A.; Stair, P. C.; Stults, B. R.; Tumas, W. *Chem. Rev.* **2001**, *101*(4), 953–996.
(19) Balzani, V.; Credi, A.; Venturi, M. *Molecular Devices and Machines: a Journey into the Nanoworld*; Wiley-VCH: Weinheim, Germany, 2003; pp 132–173..
(20) Huynh, M. H. V.; Meyer, T. J. *Chem. Rev.* **2007**, *107*(11), 5004–5064.
(21) Holzwarth, A. R.; Mueller, M. G.; Reus, M.; Nowaczyk, M.; Sander, J.; Roegner, M. *Proc. Natl. Acad. Sci.* **2006**, *103*(18), 6895–6900.
(22) Kadowaki, H.; Saito, N.; Nishiyama, H.; Kobayashi, H.; Shimodaira, Y.; Inoue, Y. *J. Phys. Chem. C* **2007**, *111*(1), 439–444.
(23) King, N. C.; Dickinson, C.; Zhou, W.; Bruce, D. W. *Dalton Trans.* **2005**, *6*, 1027–1032.
(24) Sato, J.; Saito, N.; Yamada, Y.; Maeda, K.; Takata, T.; Kondo, J. N.; Hara, M.; Kobayashi, H.; Domen, K.; Inoue, Y. *J. Am. Chem. Soc.* **2005**, *127*(12), 4150–4151.
(25) Hara, M.; Lean, J. T.; Mallouk, T. E. *Chem. Mater.* **2001**, *13*(12), 4668–4675.
(26) Yagi, M.; Tomita, E.; Kuwabara, T. *J. Electroanal. Chem.* **2005**, *579*(1), 83–88.
(27) Yagi, M.; Tomita, E.; Sakita, S.; Kuwabara, T.; Nagai, K. *J. Phys. Chem. B* **2005**, *109*(46), 21489–21491.
(28) Yagi, M.; Kaneko, M. *Chem. Rev.* **2001**, *101*, 21–35.
(29) Shiroishi, H.; Sayama, H.; Moroi, T.; Kaneko, M. *J. Electroanal. Chem.* **2001**, *502*(1–2), 132–137.
(30) Shiroishi, H.; Yamashita, S.; Kaneko, M. *J. Mol. Catal. A: Chem.* **2001**, *169*(1–2), 269–273.
(31) Mills, A.; Russell, T. *J. Chem. Soc., Faraday Trans.* **1991**, *87*, 313–318.
(32) Yagi, M.; Narita, K. *J. Am. Chem. Soc.* **2004**, *126*(26), 8084–8085.
(33) Narita, K.; Kuwabara, T.; Sone, K.; Shimizu, K.; Yagi, M. *J. Phys. Chem. B* **2006**, *110*(46), 23107–23114.
(34) Yagi, M.; Wolf, K. V.; Baesjou, P. J.; Bernasek, S. L.; Dismukes, G. C. *Angew. Chem., Int. Ed.* **2001**, *40*(15), 2925–2928.
(35) Poulsen, A. K.; Rompel, A.; McKenzie, C. J. *Angew. Chem., Int. Ed.* **2005**, *44*(42), 6916–6920.
(36) Shimazaki, Y.; Nagano, T.; Takesue, H.; Ye, B.-H.; Tani, F.; Naruta, Y. *Angew. Chem., Int. Ed.* **2004**, *43*(1), 98–100.
(37) Limburg, J.; Vrettos, J. S.; Liable-Sands, L. M.; Rheingold, A. L.; Robert, H.; Crabtree, R. H.; Brudvig, G. W. *Science* **1999**, *283*, 1524–1527.
(38) Limburg, J.; Vrettos, J. S.; Chen, H.; de Paula, J. C.; Crabtree, R. H.; Brudvig, G. W. *J. Am. Chem. Soc.* **2001**, *123*(3), 423–430.

well-defined molecular catalyst, investigated in mechanistic detail, is the μ-oxo-bridged "blue dimer", *cis*,*cis*-$[(bpy)_2(H_2O)RuORu(H_2O)(bpy)_2]^{4+}$.[43–46]

The blue dimer and the OEC of photosynthesis and how they make oxygen are the focus of this account. Recent X-ray diffraction (XRD) and EXAFS studies on PSII have provided molecular level insight into its structure[47–50] and, with it, possible pathways for oxidative activation and water oxidation.[1–12,51–64]

Both the blue dimer and OEC are discrete molecular entities, activated by electron transfer. In both, the significant demands arising from the net reaction are met by building up multiple oxidative equivalents in sequential steps with loss of protons by PCET. The use of PCET achieves "redox potential leveling" and, through the use of coupled electron–proton transfer (EPT) pathways, avoids high-energy intermediates.[20,65] The OEC is part of a membrane-bound molecular assembly that includes separate components for light absorption and electron transfer arranged in a membrane organized by protein folding. In principle, the blue dimer or a derivative is capable of serving the same role if incorporated into a molecular assembly or attached to an electrode surface.

1.1. Water Oxidation and Artificial Photosynthesis. Our interest in water oxidation and artificial photosynthesis arose from experiments in the early 1970s in collaboration with David Whitten and his group at the University of North Carolina (UNC). Following an earlier suggestion by Adamson and co-workers,[66,67] we used flash photolysis techniques to demonstrate electron-transfer quenching of the metal-to-ligand charge-transfer (MLCT) excited-state $Ru(bpy)_3^{2+}*$, $Ru(bpy)_3^{2+}* + MV^{2+} \rightarrow Ru(bpy)_3^{3+} + MV^{\bullet+}$.[68,69] A significant observation was that $Ru(bpy)_3^{3+}$ and $MV^{\bullet+}$, formed by excited-state quenching, were thermodynamically capable of water oxidation, $E^{\circ\prime}(Ru(bpy)_3^{3+/2+}) = 1.26$ V vs NHE, and reduction, $E^{\circ\prime}(MV^{2+/\bullet+}) = -0.4$ V,[70] from pH $\sim$ 0–7. ($E^{\circ\prime}$ values cited here and elsewhere are formal potentials, the potential of the couple in the prevailing medium with the oxidized and reduced forms at equal concentrations.) These potentials revealed that excited-state quenching by electron transfer provided a potential basis for water splitting, $2H_2O \rightarrow 2H_2 + O_2$, by combining electron transfer with catalysis.

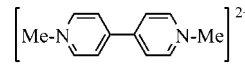

(MV^{2+})

In solution, the oxidative and reductive equivalents formed by excited-state quenching underwent "recombination" by back electron transfer, $Ru(bpy)_3^{3+} + MV^{\bullet+} \rightarrow Ru(bpy)_3^{2+} + MV^{2+}$. This necessitated a strategy in which redox equivalents were separated spatially and used to drive separate catalysts for water oxidation and water reduction. In turn, this led to a modular approach to synthesizing molecular assemblies that contained the essential elements for artificial photosynthesis. A generic structure following from this approach is shown in Figure 1. Key elements are an antenna light absorber array that sensitizes the formation of a molecular excited state in the reaction center, electron-transfer quenching, and electron-transfer activation of catalysts for water oxidation and reduction.[12,16,71]

An important element in such schemes was devising molecular catalysts for water oxidation and reduction. They had to have the required reactivity as discrete modules that could later become components in more complex assemblies activated by electron transfer. Other configurations could be considered, in membranes or on electrodes, for example.

(39) Zong, R.; Thummel, R. P. *J. Am. Chem. Soc.* **2005**, *127*(37), 12802–12803.
(40) Howells, A. R.; Sankarraj, A.; Shannon, C. *J. Am. Chem. Soc.* **2004**, *126*(39), 12258–12259.
(41) Wada, T.; Tsuge, K.; Tanaka, K. *Angew. Chem., Int. Ed.* **2000**, *39*(8), 1479–1482.
(42) Sens, C.; Romero, I.; Rodriguez, M.; Llobet, A.; Parella, T.; Benet-Buchholz, J. *J. Am. Chem. Soc.* **2004**, *126*(25), 7798–7799.
(43) Gersten, S. W.; Samuels, G. J.; Meyer, T. J. *J. Am. Chem. Soc.* **1982**, *104*(14), 4029–4030.
(44) Gilbert, J. A.; Eggleston, D. S.; Murphy, W. R., Jr; Geselowitz, D. A.; Gersten, S. W.; Hodgson, D. J.; Meyer, T. J. *J. Am. Chem. Soc.* **1985**, *107*, 3855–3864.
(45) Chronister, C. W.; Binstead, R. A.; Ni, J.; Meyer, T. J. *Inorg. Chem.* **1997**, *36*(18), 3814–3815.
(46) Hurst, J. K.; Zhou, J.; Lei, Y. *Inorg. Chem.* **1992**, *31*(6), 1010–1017.
(47) Ferreira, K. N.; Iverson, T. M.; Maghlaoui, K.; Barber, J.; Iwata, S. *Science* **2004**, *303*(5665), 1831–1838.
(48) Loll, B.; Kern, J.; Saenger, W.; Zouni, A.; Biesiadka, J. *Nature* **2005**, *438*(7070), 1040–1044.
(49) Yano, J.; Pushkar, Y.; Glatzel, P.; Lewis, A.; Sauer, K.; Messinger, J.; Bergmann, U.; Yachandra, V. *J. Am. Chem. Soc.* **2005**, *127*(43), 14974–14975.
(50) Yano, J.; Kern, J.; Sauer, K.; Latimer, M. J.; Pushkar, Y.; Biesiadka, J.; Loll, B.; Saenger, W.; Messinger, J.; Zouni, A.; Yachandra, V. K. *Science* **2006**, *314*(5800), 821–825.
(51) Hillier, W.; Messinger, J.; Yachandra, V. K. *The Catalytic Manganese Cluster, in Photosystem II: The Water/Plastoquinone Oxido-Reductase of Photosynthesis*; Kluwer Academic Publishers: Dordrecht, The Netherlands, 2005; pp 567–608..
(52) Vrettos, J. S.; Limburg, J.; Brudvig, G. W. *Biochim. Biophys. Acta* **2001**, *1503*(1–2), 229–245.
(53) Pecoraro, V. L.; Baldwin, M. J.; Caudle, M. T.; Hsieh, W.-Y.; Law, N. A. *Pure Appl. Chem.* **1998**, *70*(4), 925–929.
(54) Renger, G. *Biochim. Biophys. Acta* **2004**, *1655*(1–3), 195–204.
(55) Brudvig, G. W.; Crabtree, R. H. *Proc. Natl. Acad. Sci. U.S.A.* **1986**, *83*(13), 4586–4588.
(56) Volkov, A. G. *Bioelectrochem. Bioenerg.* **1989**, *21*(1), 3–24.
(57) Schlodder, E.; Witt, H. T. *J. Biol. Chem.* **1999**, *274*(43), 30387–30392.
(58) Renger, G. *Physiol. Plant* **1997**, *100*(4), 828–841.
(59) Dasgupta, J.; van Willigen, R. T.; Dismukes, G. C. *Phys. Chem. Chem. Phys.* **2004**, *6*(20), 4793–4802.
(60) Messinger, J.; Badger, M.; Wydrzynski, T. *Proc. Natl. Acad. Sci. U.S.A.* **1995**, *92*(8), 3209–3213.
(61) Dau, H.; Iuzzolino, L.; Dittmer, J. *Biochim. Biophys. Acta* **2001**, *1503*(1–2), 24–39.
(62) Limburg, J.; Vrettos, J. S.; Liable-Sands, L. M.; Rheingold, A. L.; Crabtree, R. H.; Brudvig, G. W. *Science* **1999**, *283*(5407), 1524–1527.
(63) Messinger, J. *Phys. Chem. Chem. Phys.* **2004**, *6*(20), 4764–4771.
(64) Siegbahn, P. E. M. *Inorg. Chem.* **2000**, *39*(13), 2923–2935.
(65) Meyer, T. J.; Huynh, M. H. V. *Inorg. Chem.* **2003**, *42*(25), 8140–8160.
(66) Demas, J. N.; Adamson, A. W. *J. Am. Chem. Soc.* **1973**, *95*(16), 5159–5168.
(67) Adamson, A. W.; Demas, J. N. *J. Am. Chem. Soc.* **1971**, *93*(7), 1800–1801.
(68) Bock, C. R.; Meyer, T. J.; Whitten, D. G. *J. Am. Chem. Soc.* **1974**, *96*(14), 4710–4712.
(69) Young, R. C.; Meyer, T. J.; Whitten, D. G. *J. Am. Chem. Soc.* **1976**, *98*(1), 286–287.
(70) Neshvad, G.; Hoffman, M. Z. *J. Phys. Chem.* **1989**, *93*, 2445–2452.
(71) Huynh, M. H. V.; Dattelbaum, D. M.; Meyer, T. J. *Coord. Chem. Rev.* **2005**, *249*(3–4), 457–483.

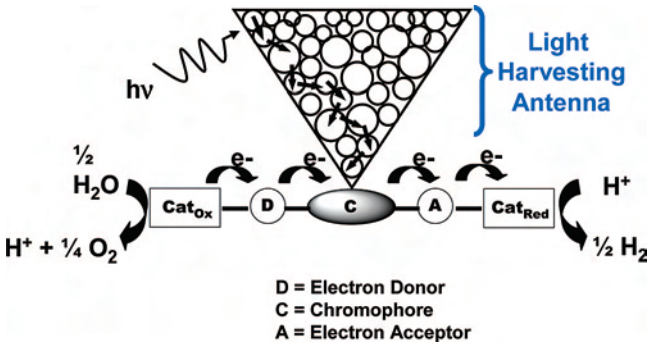

Figure 1. Diagram illustrating the essential elements in an assembly for artificial photosynthesis and the sequence of events that occurs after light is absorbed. The abbreviations are as follows: C = chromophore (light absorber), D = electron-transfer donor, A = electron-transfer acceptor, cat_{red} = catalyst for chemical reduction, and cat_{ox} = catalyst for chemical oxidation. The reaction illustrated is the photochemical splitting of water into H_2 and O_2. In the absence of a light-harvesting array, multilayer structures are required to achieve sufficient light absorption. Reprinted with permission from ref 13. Copyright 2007 Wiley.

With the latter, there was direct overlap with a second area of research interest, chemically modified electrodes for redox catalysis, inspired by a fruitful collaboration with Royce Murray and his group at UNC.[71–80] A target of particular interest was the possibility of devising a reversible electrode for the O_2/H_2O couple much as platinum for the H^+/H_2 couple.

2. Oxo Complexes, PCET, EPT, and Redox Potential Leveling

Although there were numerous early reports that $Ru(bpy)_3^{3+}$ and related oxidized polypyridyl complexes could oxidize water to oxygen, the actual reactions observed were typically oxidation of a coordinated ligand.[81–85] Shortly after the early experiments demonstrating excited-state electron-transfer quenching, Bruce Moyer, a graduate student in the Meyer group, decided to explore aqua complexes as potential water oxidation catalysts. This was in recognition of the coupled e^-/H^+ demands of the net reaction. He prepared the aqua complex derivative of $Ru(bpy)_3^{3+}$, *cis*-$[Ru(bpy)_2(py)(H_2O)]^{2+}$. Upon the addition of 1 equiv of Ce^{IV} in an acidic aqueous solution, the red solution immediately turned pale green [by oxidation of $Ru(bpy)_2(py)(H_2O)^{2+}$ to $Ru^{III}(bpy)_2(py)(OH)^{2+}$]. With the addition of a second equiv, the solution became colorless because of further oxidation to $Ru^{IV}(bpy)_2(py)(O)^{2+}$.[86,87]

Although Bruce waited expectantly for oxygen to evolve, it never did. The ruthenium(IV) oxido complex that he had prepared was just short of being able to oxidize water with $\Delta E^{\circ\prime} = -0.12$ V ($\Delta G^{\circ\prime} = +0.48$ eV) for water oxidation, $2Ru^{IV}(bpy)_2(py)(O)^{2+} + 2H_2O \rightarrow 2Ru(bpy)_2(py)(H_2O)^{2+} + O_2$. What he had found was significant in creating the first member of a family of polypyridylruthenium(IV) oxido and -ruthenium(VI) dioxido complexes that have proven to have an extraordinarily rich stoichiometric, catalytic, and mechanistic oxidation chemistry including reactivity toward a multitude of organic and inorganic substrates.[65]

2.1. PCET. The initial foray into oxido complexes also revealed the very important role that PCET plays in oxidative activation.[1,12,20,88–104] PCET is a natural consequence of the influence of decreased electron content on the pK_a properties of molecules having acidic protons. Acidity increases as the electron content decreases, as illustrated by $pK_{a,1}$ values for $Ru^{II}(bpy)_2(py)(H_2O)^{2+}$ (10.6) and $Ru^{III}(bpy)_2(py)(H_2O)^{3+}$ (0.85).[87] Another example is tyrosine (TyrOH) with $pK_a = 10$ compared to $TyrOH^{\bullet+}$ with $pK_a = -2$.[100,101,105,106]

Oxidation-state-induced changes in pK_a can be dramatic when there are significant changes in bonding with $\Delta pK_a >$

(72) Abruna, H. D.; Denisevich, P.; Umana, M.; Meyer, T. J.; Murray, R. W. *J. Am. Chem. Soc.* **1981**, *103*(1), 1–5.
(73) Abruna, H. D.; Calvert, J. M.; Denisevich, P.; Ellis, C. D.; Meyer, T. J.; Murphy, W. R., Jr.; Murray, R. R.; Sullivan, B. P.; Walsh, J. L. *ACS Symp. Ser.* **1982**, *192*, 133–158.
(74) Vining, W. J.; Meyer, T. J. *J. Electroanal. Chem. Interface Electrochem.* **1987**, *237*(2), 191–208.
(75) O'Toole, T. R.; Meyer, T. J.; Sullivan, B. P. *Chem. Mater.* **1989**, *1*(6), 574–576.
(76) Gould, S.; Meyer, T. J. *J. Am. Chem. Soc.* **1991**, *113*(19), 7442–7443.
(77) Younathan, J. N.; Wood, K. S.; Meyer, T. J. *Inorg. Chem.* **1992**, *31*(15), 3280–3285.
(78) Guadalupe, A. R.; Chen, X.; Sullivan, B. P.; Meyer, T. J. *Inorg. Chem.* **1993**, *32*(24), 5502–5512.
(79) Moss, J. A.; Leasure, R. M.; Meyer, T. J. *Inorg. Chem.* **2000**, *39*(6), 1052–1058.
(80) Vining, W. J.; Meyer, T. J. *Inorg. Chem.* **1986**, *25*(12), 2023–2033.
(81) Roecker, L.; Kutner, W.; Gilbert, J. A.; Simmons, M.; Murray, R. W.; Meyer, T. J. *Inorg. Chem.* **1985**, *24*(23), 3784–3791.
(82) Sagues, J.; Alejandro, A.; Gillard, R. D.; Lancashire, R. J.; Williams, P. A. *J. Chem. Soc., Dalton Trans.* **1979**, *1*, 193–198.
(83) Gillard, R. D. *Coord. Chem. Rev.* **1975**, *16*(1–2), 67–94.
(84) Ghosh, P. K.; Brunschwig, B. S.; Chou, M.; Creutz, C.; Sutin, N. *J. Am. Chem. Soc.* **1984**, *106*(17), 4772–4783.
(85) Nord, G.; Pedersen, B.; Bjergbakke, E. *J. Am. Chem. Soc.* **1983**, *105*(7), 1913–1919.
(86) Moyer, B. A.; Meyer, T. J. *J. Am. Chem. Soc.* **1978**, *100*(11), 3601–3603.
(87) Moyer, B. A.; Meyer, T. J. *Inorg. Chem.* **1981**, *20*(2), 436–444.
(88) Cukier, R. I.; Nocera, D. G. *Annu. Rev. Phys. Chem.* **1998**, *49*, 337–369.
(89) Fang, J.-Y.; Hammes-Schiffer, S. *J. Chem. Phys.* **1997**, *107*(15), 5727–5739.
(90) Hammes-Schiffer, S.; Iordanova, N. *Biochim. Biophys. Acta* **2004**, *1655*(1–3), 29–36.
(91) Mayer, J. M. *Annu. Rev. Phys. Chem.* **2004**, *55*, 363–390.
(92) Mayer, J. M.; Rhile, I. J. *Biochim. Biophys. Acta* **2004**, *1655*(1–3), 51–58.
(93) Chang, C. J.; Chang, M. C. Y.; Damrauer, N. H.; Nocera, D. G. *Biochim. Biophys. Acta* **2004**, *1655*(1–3), 13–28.
(94) Huynh, M. H. V.; Meyer, T. J. *Proc. Natl. Acad. Sci. U.S.A.* **2004**, *101*(36), 13138–13141.
(95) Himo, F.; Siegbahn, P. E. M. *Chem. Rev.* **2003**, *103*(6), 2421–2456.
(96) Lovell, T.; Himo, F.; Han, W.-G.; Noodleman, L. *Coord. Chem. Rev.* **2003**, *238–239*, 211–232.
(97) Sun, L.; Hammarstroem, L.; Akermark, B.; Styring, S. *Chem. Soc. Rev.* **2001**, *30*(1), 36–49.
(98) Sjoedin, M.; Ghanem, R.; Polivka, T.; Pan, J.; Styring, S.; Sun, L.; Sundstroem, V.; Hammarstroem, L. *Phys. Chem. Chem. Phys.* **2004**, *6*(20), 4851–4858.
(99) Reece, S. Y.; Nocera, D. G. *J. Am. Chem. Soc.* **2005**, *127*(26), 9448–9458.
(100) Carra, C.; Iordanova, N.; Hammes-Schiffer, S. *J. Am. Chem. Soc.* **2003**, *125*(34), 10429–10436.
(101) Costentin, C.; Robert, M.; Savéant, J.-M. *J. Am. Chem. Soc.* **2007**, *129*(18), 5870–5879.
(102) Manchanda, R.; Thorp, H. H.; Brudvig, G. W.; Crabtree, R. H. *Inorg. Chem.* **1991**, *30*(3), 494–497.
(103) Manchanda, R.; Thorp, H. H.; Brudvig, G. W.; Crabtree, R. H. *Inorg. Chem.* **1992**, *31*(20), 4040–4041.
(104) Thorp, H. H.; Brudvig, G. W.; Bowden, E. F. *J. Electroanal. Chem. Interface Electrochem.* **1990**, *290*(1–2), 293–301.
(105) Land, E. J.; Porter, G.; Strachan, E. *Trans. Faraday Soc.* **1961**, *57*, 1885–1893.
(106) Sjoedin, M.; Styring, S.; Wolpher, H.; Xu, Y.; Sun, L.; Hammarstroem, L. *J. Am. Chem. Soc.* **2005**, *127*(11), 3855–3863.

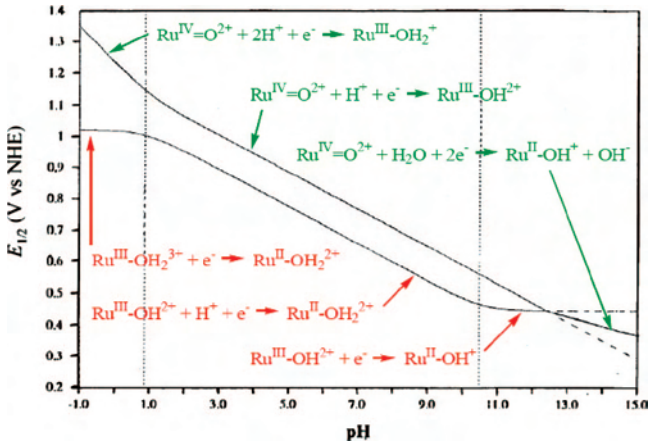

Figure 2. $E_{1/2}$ vs pH diagrams for the $Ru^{IV/III}$ and $Ru^{III/II}$ couples of *cis*-$[Ru^{II}(bpy)_2(py)(H_2O)]^{2+}$ $(Ru^{II}OH_2)^{2+}$ at 25 °C, I = 0.1 M, vs NHE. The vertical dotted lines correspond to $pK_{a,1}$ for *cis*-$[Ru^{II}(bpy)_2(py)(H_2O)]^{2+}$ $(Ru^{II}OH_2^{2+}$, K_a^{II} =10.6) and $pK_{a,1}$ for *cis*-$[Ru^{III}(bpy)_2(py)(H_2O)]^{3+}$ $(Ru^{III}OH_2^{3+}$, K_a^{III} = 0.85). The remaining abbreviations are as follows: *cis*-$[Ru^{IV}(bpy)_2(py)(O)]^{2+}$ (Ru^{IV}=O^{2+}) and *cis*-$[Ru^{III}(bpy)_2(py)(OH)]^{2+}$ ($Ru^{III}OH^{2+}$). The half-cell reactions for the individual couples in the various pH regions are indicated, as are the sixth ligands and whether they are O^{2-}, OH^-, or H_2O. The $E_{1/2}$−pH curves were calculated from the Nernst equation by using known pK_a values, $E_{1/2}$(*cis*-$[Ru^{II}(bpy)_2(py)(H_2O)]^{3+/2+}$) = 1.02 V, and $E_{1/2}$(*cis*-$[Ru^{II}(bpy)_2(py)(OH)]^{2+/+}$) = 0.46 V.[86,87,108–110]

19 between $[Ru^{IV}(bpy)_2(py)(OH)]^{3+}$ (pK_a < −6) and $[Ru^{III}(bpy)_2(py)(OH)]^{2+}$ (pK_a > 13). The latter is a common observation when one of the members of a redox couple involves multiple bond interactions that tie up available orbitals and electron density.

Oxidation-state-dependent acid–base behavior can lead to complex pH-dependent behavior for redox couples. This is illustrated by the results of electrochemical measurments on the $Ru^{IV/III}$ and $Ru^{III/II}$ couples of $Ru^{II}(bpy)_2(py)(H_2O)^{2+}$ in Figure 2. Above pH = 0.85, $pK_{a,1}$ for $Ru^{III}(bpy)_2(py)(H_2O)^{3+}$, the Ru^{III} form of the couple, is deprotonated. $E_{1/2} \sim E^{\circ\prime}$ decreases by 59 mV/pH unit (at 25 °C) as predicted by the Nernst equation. The $Ru^{IV/III}$ couple decreases in parallel because the couple becomes Ru^{IV}=O^{2+}/$Ru^{III}OH^{2+}$ in this pH range. This is a general prediction of the Nernst equation for loss of a single proton with oxidation, e.g., $Ru^{IV}(bpy)_2(py)(O)^{2+} + H^+ + e^- \rightarrow Ru^{III}(bpy)_2(py)(OH)^{2+}$. More generally, for PCET couples at pH values way from the pK_a, $E^{\circ\prime}$ is predicted to vary with pH as $-59(m/n)$ V/pH unit with m the number of protons transferred and n the number of electrons.[107] This accounts for the decrease of 118 mV/pH unit in $E_{1/2}$ in a strongly acidic solution where the $Ru^{IV/III}$ couple becomes Ru^{IV}=O^{2+}/$Ru^{III}OH_2^{3+}$.

There are important insights in the data in Figure 2 about oxidative activation and buildup of multiple redox equivalents at single sites or clusters. The potential difference between the $[Ru(bpy)_2(Cl)_2]^{2+/+}$ ($Ru^{IV/III}$) and $[Ru(bpy)_2(Cl)_2]^{+/0}$ ($Ru^{III/II}$) couples of *cis*-$[Ru^{II}(bpy)_2(Cl)_2]$ in CH_3CN is $\Delta E^{\circ\prime}$ = 1.7 V. The potential difference between the same couples in $Ru^{II}(bpy)_2(py)(H_2O)^{2+}$, where a proton is lost between oxidation states, is 0.11 V at pH = 7.

The dramatic decrease in $\Delta E^{\circ\prime}$ for the aqua couple comes largely from the loss of a proton that avoids the buildup of charge.[20] A second example occurs in the oxidation of *cis*-$[Ru^{II}(bpy)_2(H_2O)_2]^{2+}$ to *cis*-$[Ru^{VI}(bpy)_2(O)_2]^{2+}$, which, from pH = 2–6, occurs through four sequential $1e^-/1H^+$ couples over a potential range of only 0.6 V.[111,112]

Experimental $\Delta E^{\circ\prime}$ values provide a quantitative measure of "comproportionation" equilibria among adjacent oxidation states such as the one shown in eq 1. The magnitude of the comproportionation equilibrium constant, $K_c = \exp(nF\Delta E^{\circ\prime}/RT$ (F is the Faraday constant, 1 eV V^{-1} in SI units), is dictated both by the charge effect mentioned above and by electronic stabilization effects such as the Ru=O multiple bonding in $Ru^{IV}(bpy)_2(py)(O)^{2+}$.

$$Ru^{IV}(bpy)_2(py)(O)^{2+} + Ru^{II}(bpy)_2(py)(OH_2)^{2+} \rightarrow 2Ru^{III}(bpy)_2(py)(OH)^{2+} \quad (1)$$

The combination of charge and electronic effects leads to *redox potential leveling* with multiply oxidized Ru^{IV} accessible at a relatively low potential. *Redox potential leveling is at the core of multielectron redox catalysis, allowing for the buildup of multiple redox equivalents at single chemical sites or clusters*.[20,65]

pH and electronic stabilization effects are also responsible for "missing oxidation states", which are thermodynamically unstable toward *disproportionation*. An example, in Figure 2, is $Ru^{III}(bpy)_2(py)(OH)^{2+}$. Because $pK_{a,1}$ = 10.6 for $Ru^{II}(bpy)_2(py)(H_2O)^{2+}$, the $Ru^{III/II}$ couple becomes $Ru^{III}(bpy)_2(py)(OH)^{2+}/Ru^{II}(bpy)_2(py)(OH)^{+}$ and pH-independent above pH = 10.6. Its potential crosses over that for the pH-dependent $Ru^{IV/III}$ couple at pH = 12.8. Above this pH, $Ru^{III}(bpy)_2(py)(OH)^{2+}$ is a stronger oxidant than $Ru^{IV}(bpy)_2(py)(O)^{2+}$ and reacts with itself to give Ru^{IV}=O^{2+} and $Ru^{II}OH^+$, $2Ru^{III}OH^{2+} + OH^- \rightarrow Ru^{IV}$=$O^{2+} + Ru^{II}OH^+ + H_2O$. This peculiar state of affairs arises from electronic stabilization of Ru^{IV} by oxo formation and from the difference in pH dependences between adjacent couples.

There are even more dramatic examples in the literature with $[Os^{II}(tpy)(H_2O)_3]^{2+}$ undergoing a $3e^-$ oxidation to *trans*-$[Os^{VI}(tpy)(O)(OH)(H_2O)]^{3+}$ over a broad pH range with the intermediate oxidation states Os^{III}, Os^{IV}, and Os^{V} all unstable toward disproportionation.[112–114] As discussed below, oxidation of $[(bpy)_2(OH)Ru^{IV}ORu^{III}(H_2O)(bpy)_2]^{4+}$ occurs by $3e^-$ to give $[(bpy)_2(O)Ru^{V}ORu^{V}(O)(bpy)_2]^{4+}$ below pH = 2.[44]

Because of the difference in electronic configurations between oxidation states, comproportionation equilibria can be manipulated by systematic ligand variations. This has been

(107) More generally for the $Ru^{III/II}$ couple over the entire pH range in Figure 2, $E_{1/2}$ varies with pH as $E_{1/2} = E^{\circ\prime}(Ru{-}OH_2^{3+/2+}) - 0.05916\{\log(K_a^{III} + [H^+]) - \log(K_a^{II} + [H^+])\}$ with K_a^{III} and K_a^{II} the first acid dissociation constants for the ruthenium(III) and ruthenium(II) aqua complexes.

(108) Buckingham, D. A.; Sargeson, A. M.; Dwyer, F. P. J.; Mellor, D. P. *Chelating Agents and Metal Chelates*; Academic Press: New York, 1964.
(109) Heath, G. A.; Moock, K. A.; Sharp, D. W. A.; Yellowlees, L. J. *J. Chem. Soc., Chem. Commun.* **1985**, *21*, 1503–1505.
(110) Lancaster, C. R. D. *FEBS Lett.* **2003**, *545*(1), 52–60.
(111) Dobson, J. C.; Takeuchi, K. J.; Pipes, D. W.; Geselowitz, D. A.; Meyer, T. J. *Inorg. Chem.* **1986**, *25*, 2357.
(112) Pipes, D. W.; Meyer, T. J. *J. Am. Chem. Soc.* **1984**, *106*, 7653.
(113) Dovletoglou, A.; Adeyemi, S. A.; Lynn, M. H.; Hodgson, D. J.; Meyer, T. J. *J. Am. Chem. Soc.* **1990**, *112*, 8989.
(114) Pipes, D. W.; Meyer, T. J. *Inorg. Chem.* **1986**, *25*(18), 3256–3262.

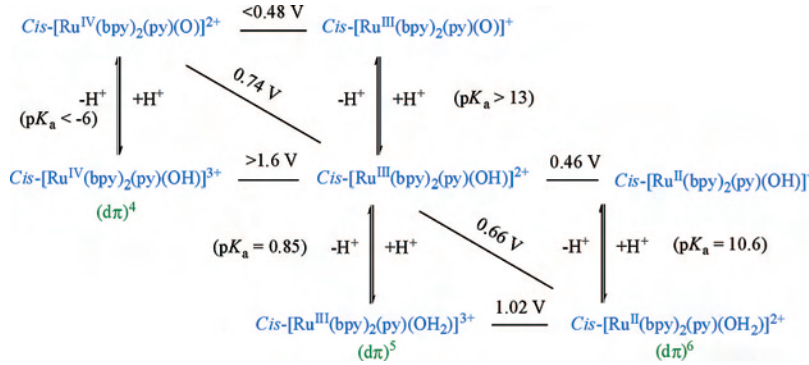

Figure 3. PCET thermodynamics. Acid–base, formal potential ($E^{\circ\prime}-pK_a$) diagram for the $Ru^{IV/III}$ and $Ru^{III/II}$ couples of *cis*-$[Ru^{II}(bpy)_2(py)(H_2O)]^{2+}$ taken from ref 20 showing the dπ electron configurations at the metal. Potentials are vs NHE at 25 °C, $I = 0.1$ M. The vertical lines give pK_a values and the slanted lines formal potentials ($E_{1/2} \sim E^{\circ\prime}$) for pH-dependent couples at pH = 7.

demonstrated for couples related to those in eq 1 by exploiting ligand variations that stabilize Ru^{IV} by σ effects and Ru^{II} by π effects.[115] This approach has been cleverly exploited by Llobet and co-workers to find a ligand set for which $Ru^{III}OH^{2+}$ is unstable with respect to disproportionation over a broad pH range.[116]

2.2. Coupled EPT. There are kinetic consequences arising from PCET and proton loss, and they must be mastered for water oxidation. Their origins for the $Ru^{IV/III}$ and $Ru^{III/II}$ couples of $Ru(bpy)_2(py)(H_2O)^{2+}$ can be surmised from the formal potential, $E^{\circ\prime}-pK_a$ diagram in Figure 3, which provides an informative summary of pK_a and $E^{\circ\prime}$ values at pH = 7.

A proton is lost when $Ru^{II}(bpy)_2(py)(H_2O)^{2+}$ is oxidized to $Ru^{III}(bpy)_2(py)(OH)^{2+}$ over a wide pH range, pH = 0.85−10.6 (Figure 2). As shown in Figure 3, this could occur in three different ways: (i) electron transfer to give $Ru^{III}OH_2^{3+}$ followed by proton transfer to the surrounding medium to give $Ru^{III}OH^{2+}$ (ET−PT); (ii) proton transfer first, to give $Ru^{II}OH^{+}$, followed by electron transfer to give $Ru^{III}OH^{2+}$ (PT−ET); (iii) coupled EPT with simultaneous loss of both an electron and a proton.

Compared to the thermodynamic potential for the $Ru^{III}OH^{2+}/Ru^{II}OH_2^{2+}$ couple, the stepwise mechanisms in (i) or (ii) incur a significant energy penalty in the first step. This occurs because the intermediates, $Ru^{III}OH_2^{3+}$ or $Ru^{II}OH^{2+}$, are at high energy at the prevailing pH. For ET-PT, the initial ET, $Ru^{II}OH_2^{2+} \rightarrow Ru^{III}OH_2^{3+}$, occurs at 1.02 V compared to 0.66 V for the $Ru^{III}OH^{2+}/Ru^{II}OH_2^{2+}$ couple at pH = 7. The ΔG difference of 0.36 eV is recovered in the subsequent PT step, $Ru^{III}OH_2^{3+} \rightarrow Ru^{III}OH^{2+} + H^+$, with $\Delta G^{\circ\prime} = 0.059(pK_{a,1}(Ru^{III}OH_2^{3+}) - pH)$ (at 25 °C). Similarly, the initial PT step in (ii) is unfavorable with $\Delta G = +0.19$ eV. The ΔG difference is recovered in the subsequent ET step, which occurs at 0.46 V.

Mechanisms involving $Ru^{III}OH_2^{3+}$ or $Ru^{II}OH^{2+}$ add energy increments to the reaction barrier and, if they are rate-determining, they can slow the reaction considerably. This is especially onerous for the second oxidation in Figure 3, $Ru^{III}OH^{2+} \xrightarrow{-e^-,-H^+} Ru^{IV}{=}O^{2+}$. For this couple, $\Delta G^{\circ\prime} >$ 0.9 eV for initial ET and $\Delta G^{\circ\prime} > 0.4$ eV for initial PT, both relative to the $Ru^{IV}{=}O^{2+}/Ru^{III}OH^{2+}$ couple at 0.74 V. This inhibits oxidative activation and imposes kinetic inhibitions that appear routinely. An example is oxidation or reduction at electrodes where only sequential ET−PT or PT−ET pathways are available.[101,117,118]

PCET-induced barriers can be circumvented by utilizing coupled EPT pathways. In these pathways, both electrons and protons are transferred simultaneously and, therefore, at the thermodynamic potential for the PCET couple. They differ from H-atom (HAT) or hydride transfer where electrons and protons are transferred from the same chemical bond. *In EPT, electrons are transferred from different orbitals on the donor to different orbitals on the acceptor.*[12,20,65]

The first well-documented example of an EPT pathway was the comproportionation reaction in eq 1, which occurs with a $k(H_2O)/k(D_2O)$ kinetic isotope effect of 16.1. This reaction occurs by preassociation and hydrogen bonding followed by the coupled electron–proton transfer step shown in eq 2. In this pathway, electron transfer occurs between orbitals largely d_π Ru in character and proton transfer from σ_{O-H} to a lone pair on the oxo group.[119–121] Even though microscopically more complex than ET or PT, EPT in eq 2 is favored by >0.66 eV over ET and it dominates reactivity.

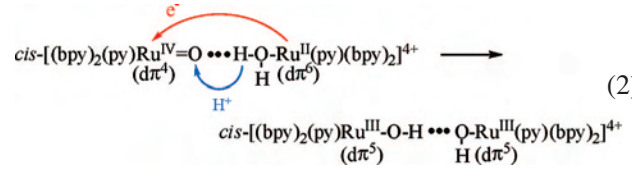

(2)

Managing protons by EPT and proton transfer is critical in oxidative activation. The extraordinary example of the membrane-bound OEC of PII will be discussed in section 6.

PCET and EPT are kinetically important in oxidizing $Ru^{III}(bpy)_2(py)(OH)^{2+}$ to *cis*-$[Ru^{IV}(bpy)_2(py)(O)]^{2+}$ and the blue dimer to its oxidatively activated forms. An electro-

(115) Dovletoglou, A.; Adeyemi, S. A.; Meyer, T. J. *Inorg. Chem.* **1996**, *35*(14), 4120–4127.
(116) Masllorens, E.; Rodriguez, M.; Romero, I.; Roglans, A.; Parella, T.; Benet-Buchholz, J.; Poyatos, M.; Llobet, A. *J. Am. Chem. Soc.* **2006**, *128*(16), 5306–5307.
(117) Lebeau, E. L.; Binstead, R. A.; Meyer, T. J. *J. Am. Chem. Soc.* **2001**, *123*(43), 10535–10544.
(118) Hammes-Schiffer, S. *ChemPhysChem* **2002**, *3*(1), 33–42.
(119) Binstead, R. A.; Meyer, T. J. *J. Am. Chem. Soc.* **1987**, *109*(11), 3287–3297.
(120) Binstead, R. A.; Moyer, B. A.; Samuels, G. J.; Meyer, T. J. *J. Am. Chem. Soc.* **1981**, *103*(10), 2897–2899.
(121) Binstead, R. A.; Stultz, L. K.; Meyer, T. J. *Inorg. Chem.* **1995**, *34*(3), 546–551.

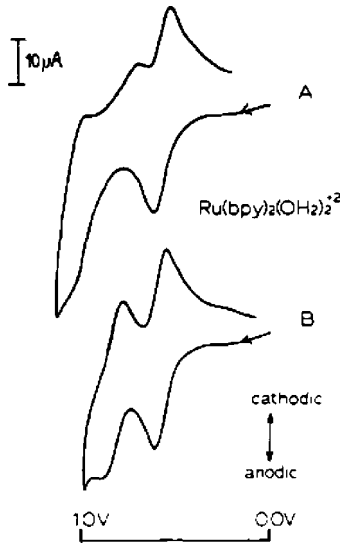

Figure 4. Cyclic voltammogram of *cis*-$[Ru(bpy)_2(H_2O)_2]^{2+}$ at pH = 2.5 at untreated (A) and oxidatively activated (B) glassy carbon electrodes (scan rate = 20 mV s^{-1} vs SCE). Reprinted with permission from ref 122. Copyright 1985 American Chemical Society.

chemical example is illustrated in Figure 4, which shows the influence of oxidative activation of a carbon electrode on the cyclic voltammetric response of the $Ru^{III}(H_2O)(OH)^{2+}/Ru^{II}(H_2O)_2^{2+}-Ru^{IV}(H_2O)(O)^{2+}/Ru^{III}(H_2O)(OH)^{2+}$ couples of *cis*-$[Ru(bpy)_2(H_2O)_2]^{2+}$.[122] In this comparison, oxidative pretreatment converts the kinetically irreversible, electron-transfer-limited $Ru^{IV/III}$ wave into an electrochemically reversible wave. Oxidative pretreatment is known to create O-containing surface functional groups. They provide a basis for surface EPT pathways that greatly facilitate oxidation and reduction at the surface by avoiding high-energy ET intermediates.[122–131]

Although molecular level details of how surface oxidative activation enhances the rate of interfacial electron transfer are unknown, pathways analogous to EPT in eq 2 can be surmised in which surface sites are involved. This is illustrated in Figure 5 for reversible oxidation of $Ru^{III}OH^{2+}$ at an oxidatively activated carbon electrode. A related mechanism has been proposed for the oxidation of hydroquinone by $Ru^{IV}(bpy)_2(py)(O)^{2+}$.[132]

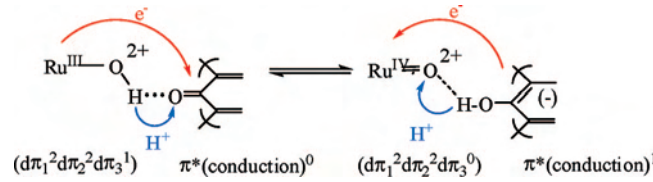

Figure 5. Schematic diagram illustrating possible reversible EPT to and from an oxidatively activated carbon electrode for oxidation of *cis*-$[Ru^{III}(bpy)_2(py)(OH)]^{2+}$ to *cis*-$[Ru^{IV}(bpy)_2(py)(O)]^{2+}$. Changes in the electronic configuration are indicated in the diagram.

3. The Blue Dimer: Electronic and Molecular Structure

Although the initial foray into oxo chemistry was unsuccessful in finding an oxidation catalyst, it pointed the way to further developments that did. A strategy that seemed reasonable to pursue, given the $4e^-/4H^+$ nature of the O_2/H_2O couple, was to link two Ru=O redox sites each having its own $2e^-/2H^+$ character.

In a related investigation, we had been exploring the multiple electron-transfer chemistry of a variety of molecular assemblies and clusters.[133–135]

One study involved μ-oxo-bridged ruthenium complexes such as *cis*,*cis*-$[(bpy)_2ClRu^{III}ORu^{III}Cl(bpy)_2]^{2+}$, which had been initially reported by Dwyer and co-workers.[136,137] Given Moyer's results, we were interested in preparing the aqua version and a synthetic procedure was developed that led to *cis*,*cis*-$[(bpy)_2(H_2O)Ru^{III}ORu^{III}(OH_2)(bpy)_2]^{4+}$, the "blue dimer".[43,44] Also isolated in low yields was the trimeric, ruthenium red analogue $[(bpy)_2(H_2O)Ru^{III}ORu^{IV}(bpy)_2ORu^{III}(OH_2)(bpy)_2]^{6+}$.[138]

3.1. Structure. The structure of the blue dimer cation was determined by XRD and is shown in Figure 6.[44] The structure shown is one of two enantiomers, the Δ,Δ form. Equal amounts of the Λ,Λ isomer were also present in the crystal. This terminology refers to a form of optical activity associated with octahedral bischelates such as *cis*-$Ru(bpy)_2XY$, for which there are mirror image enantiomers.

Molecular models for the three possible isomers of the blue dimer are illustrated in Figure 7. H atoms have been omitted, and only the inner chelate rings of the bpy ligands are shown for clarity. In the meso form, the coordination geometry at one site is Δ and that at the other Λ. The enantiomeric and meso forms are chemically different, and recent results at UNC suggest that they are separable by high-performance liquid chromatography.

Because of steric interactions across the μ-oxo bridge, there are also discrete rotamers within the same structural isomer

(122) Cabaniss, G. E.; Diamantis, A. A.; Murphy, W. R.; Linton, R. W.; Meyer, T. J. *J. Am. Chem. Soc.* **1985**, *107*, 1845.
(123) Engstrom, R. C. *Anal. Chem.* **1982**, *54*(13), 2310–2314. Engstrom, R. C.; Strasser, V. A. *Anal. Chem.* **1984**, *56*(2), 136–141.
(124) Diamantis, A. A.; Murphy, W. R., Jr.; Meyer, T. J. *Inorg. Chem.* **1984**, *23*(20), 3230–3234.
(125) Ray, K. R.; McCreery, R. L. *J. Electrochem. Soc.* **1999**, *469*, 150.
(126) Pariente, F.; Tobalina, F.; Moreno, G.; Hernandez, L.; Lorenzo, E.; Abruna, H. D. *Anal. Chem.* **1997**, *69*, 4065.
(127) Blaedel, W. J.; Jenkins, R. A. *Anal. Chem.* **1976**, *48*, 1240.
(128) Huck, H.; Schmidt, H. L. *Angew. Chem., Int. Ed. Engl.* **1981**, *20*, 402.
(129) Che, C. M.; Wong, K. Y.; Anson, F. C. *J. Electroanal. Chem. Interface Electrochem.* **1987**, *226*(1–2), 211–226.
(130) Lai, Y.-K.; Wong, K.-Y. *J. Electroanal. Chem.* **1994**, *374*(1–2), 255–261.
(131) Evans, J. F.; Kuwana, T. *Anal. Chem.* **1979**, *51*(3), 358–365.
(132) Binstead, R. A.; McGuire, M. E.; Dovletoglou, A.; Seok, W. K.; Roecker, L. E.; Meyer, T. J. *J. Am. Chem. Soc.* **1992**, *114*, 173.
(133) Meyer, T. J. *Prog. Inorg. Chem.* **1975**, *19*, 1–50.
(134) Brown, G. M.; Callahan, R. W.; Johnson, E. C.; Meyer, T. J.; Weaver, T. R. *ACS Symp. Ser.* **1975**, *5*, 66.
(135) Meyer, T. J. *Inorganic Compounds with Unusual Properties*; Advances in Chemistry Series 150; American Chemical Society: Washington, DC, 1976.
(136) Dwyer, F. P.; Goodwin, H. A.; Gyarfas, E. C. *Aust. J. Chem.* **1963**, *16*(4), 544–548.
(137) Weaver, T. R.; Meyer, T. J.; Adeyemi, S. A.; Brown, G. M.; Eckberg, R. P.; Hatfield, W. E.; Johnson, E. C.; Murray, R. W.; Untereker, D. *J. Am. Chem. Soc.* **1975**, *97*(11), 3039–3048.
(138) Geselowitz, D. A.; Kutner, W.; Meyer, T. J. *Inorg. Chem.* **1986**, *25*(12), 2015–2023.

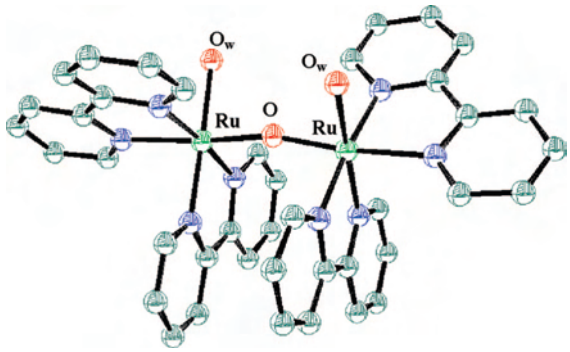

Figure 6. Structure of the blue dimer, *cis*,*cis*-$[(bpy)_2(H_2O)Ru^{III}ORu^{III}(OH_2)(bpy)_2]^{4+}$ in the salt, $[(bpy)_2(H_2O)Ru^{III}ORu^{III}(OH_2)(bpy)_2](ClO_4)_4 \cdot 2H_2O$. The CIF file was taken from the Cambridge Crystallographic Database and corresponds to the structure published in ref 44.

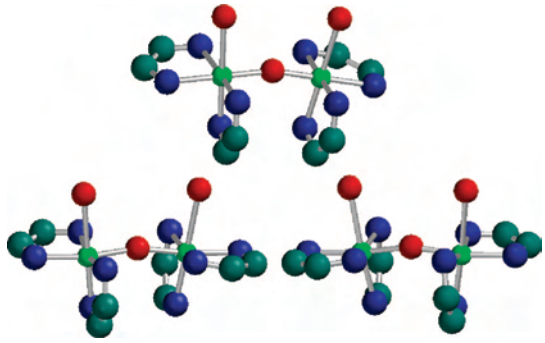

Figure 7. Simplified structure of the blue dimer, *cis*,*cis*-$[(bpy)_2(H_2O)Ru^{III}ORu^{III}(OH_2)(bpy)_2]^{4+}$, showing only the inner chelate rings illustrating the meso (top) and enantiomeric (bottom) pair; see the text.

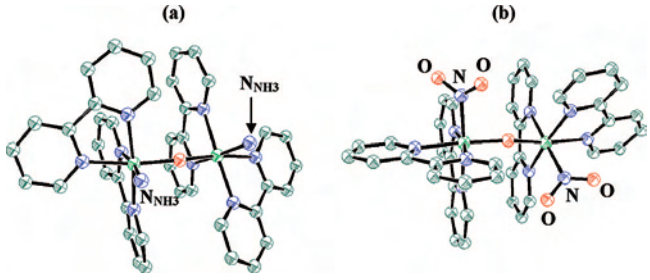

Figure 8. X-ray structures of *cis*,*cis*-$[(bpy)_2(H_3N)Ru^{III}ORu^{III}(NH_3)(bpy)_2]^{4+}$ (a) in the salt $[(bpy)_2(H_3N)Ru^{III}ORu^{III}(NH_3)(bpy)_2](ClO_4)_4$ and *cis*,*cis*-$[(bpy)_2(O_2N)Ru^{III}ORu^{III}(NO_2)(bpy)_2]^{2+}$ (b) in the salt $[(bpy)_2(O_2N)Ru^{III}ORu^{III}(NO_2)(bpy)_2](ClO_4)_2 \cdot 2H_2O$. The CIF files were taken from the Cambridge Crystallographic Database and correspond to the structures published in refs 140 and 141, respectively.

that can differ significantly in energy.[139] Two low-energy rotamers, "interior" and "exterior", have been identified for the enantiomeric form of the blue dimer in density functional theory (DFT) calculations. For blue dimer derivatives of the type $[(bpy)_2(X)Ru^{III}ORu^{III}(X)(bpy)_2]^{n+}$, structures in which the dihedral angle X−Ru−Ru−X is less than 90° belong to the "interior" category and those in which the angle is larger than 90° belong to the "exterior" category. Representative X-ray structures are shown in Figure 8, with $[(bpy)_2(H_3N)Ru^{III}ORu^{III}(NH_3)(bpy)_2]^{4+}$ (Figure 8a) an example of an "interior" rotamer with a $H_3N-Ru-Ru-NH_3$ dihedral angle of 28.5°.[140] The dihedral angle is 0° in $[(bpy)_2(H_3N)Ru^{III}ORu^{III}(OH)(bpy)_2]^{3+}$.[141] The structure of $[(bpy)_2(O_2N)Ru^{III}ORu^{III}(NO_2)(bpy)_2]^{2+}$ in Figure 8b[142] illustrates an example of an "exterior" rotamer with $\angle O_2N-Ru-Ru-NO_2 = 115.9°$. All of these structures are of the enantiomeric form.

For $[(bpy)_2(H_2O)Ru^{III}ORu^{III}(OH_2)(bpy)_2]^{4+}$, the "interior" rotamer is favored over the "exterior" one by 3.9 kcal mol^{-1} based on DFT calculations.[139] It is the rotamer observed in the crystal structure and is characterized by $\angle H_2O-Ru-O-Ru-OH_2 = 65.7°$ and a H_2O---OH_2 separation distance of 4.72 Å. Yang and Baik[143] reported two structural isomers for $[(bpy)_2(H_2O)Ru^{III}ORu^{III}(OH_2)(bpy)_2]^{4+}$ from DFT calculations, "staggered" and "eclipsed". The reported structures are actually two "interior" rotamers of the same enantiomeric pair.

In the blue dimer structure, there is evidence for Ru−O multiple bonding in the μ-oxo bridge by the short μ-Ru−O distances of 1.869 Å compared to 2.136 Å for terminal $Ru-OH_2$. The bridging angle is $\angle Ru-O-Ru = 165.4°$.[44] The water-to-water O---O separation distance in $[(bpy)_2(H_2O)Ru^{III}ORu^{III}(OH_2)(bpy)_2]^{4+}$ is 4.725 Å. This structural feature could be of relevance for a water oxidation pathway involving O---O coupling, and evidence for such a pathway has been found based on ^{18}O-labeling studies.[144] The results of gas-phase DFT calculations predict a nearly linear Ru−O−Ru bridge in $[(O)Ru^{V}ORu^{V}(O)]^{4+}$ with $\angle Ru-O-Ru = 178°$, $r(Ru{=}O) = 1.86$ Å, and a shortened O---O separation distance.[139]

The structure of the once-oxidized form, $Ru^{IV}ORu^{III}$, was also determined by XRD in the salt *cis*,*cis*-$[(bpy)_2(HO)Ru^{IV}ORu^{III}(OH_2)(bpy)_2](ClO_4)_4 \cdot 2H_2O$ as the enantiomeric pair.[141] In this structure, $\angle Ru-O-Ru$ was increased to 170.0° and the μ-Ru−O bridge distances decreased to 1.847 and 1.823 Å. The asymmetry in the Ru−O−Ru bridge is consistent with the asymmetry of the two sides in proton content. In the rotamer observed in the crystal, the O---O distance is increased to 5.555 Å. The structural differences between the blue dimer and its $Ru^{IV}ORu^{III}$ form can be rationalized based on strong electronic coupling across the μ-oxo bridge as described in the next section.

3.2. Electronic Structure. Although the blue dimer has been modeled theoretically by assuming weak $Ru^{III}-Ru^{III}$ electronic coupling across the μ-oxo bridge,[143,145,146] there is clear experimental evidence to the contrary. The evidence comes from a variety of sources: (1) A $Ru(3d_{3/2})$ X-ray photoelectron spectroscopy (XPS) binding energy of 280.5 eV is observed by XPS, which is closer to Ru^{II} in *cis*-$Ru(bpy)_2Cl_2$ (279.9 eV) than to Ru^{III} in *cis*-$Ru(bpy)_2Cl_2^+$

(139) Bartolotti, L. J.; Pedersen, L. G.; Meyer, T. J. *Int. J. Quantum Chem.* **2001**, *83*(3/4), 143–149.
(140) Ishitani, O.; White, P. S.; Meyer, T. J. *Inorg. Chem.* **1996**, *35*, 2167–2168.
(141) Schoonover, J. R.; Ni, J.; Roecker, L.; White, P. S.; Meyer, T. J. *Inorg. Chem.* **1996**, *35*(20), 5885–5892.
(142) Phelps, D. W.; Kahn, E. M.; Hodgson, D. J. *Inorg. Chem.* **1975**, *14*, 2486.
(143) Yang, X.; Baik, M.-H. *J. Am. Chem. Soc.* **2006**, *128*(23), 7476–7485.
(144) Geselowitz, D.; Meyer, T. J. *Inorg. Chem.* **1990**, *29*(19), 3894–3896.
(145) Yang, X.; Baik, M.-H. *J. Am. Chem. Soc.* **2004**, *126*(41), 13222–13223.
(146) Batista, E. R.; Martin, R. L. *J. Am. Chem. Soc.* **2007**, *129*(23), 7224–7225.

Table 1. Comparison of Reduction Potentials in CH_3CN, $I = 0.1$, 23 ± 2 °C, in V vs NHE[149]

	$Ru^{III/II}$	$E^{\circ\prime}([(bpy)_2ClRu^{III/II}L]^{+/0})$		
L	Cl^-	$(ORu^{II}Cl(bpy)_2{}^{o})]$	pyridine	$(ORu^{III}Cl(bpy)_2{}^{+})$
	0.0	−0.75	0.55	−0.07
	$Ru^{IV/III}$	$E^{\circ\prime}([(bpy)_2ClRu^{IV/III}L]^{2+/+})$		
L	Cl^-	$(ORu^{III}Cl(bpy)_2{}^{+})$		
	1.7	0.43		

(281.9 eV).[137] (2) A complex pattern of electronic absorption bands appears from the UV into the near-IR including the intense band at 636 nm, which makes the blue dimer blue. There is no precedence for such bands in monomeric complexes of Ru^{III}. (3) The relatively short Ru−O bond distances in the μ-oxo bridge. (4) The magnitudes of comparative redox potentials (see below).

The blue dimer is paramagnetic in the solid state with a moment of 1.60 μ_B per dimer for the ClO_4^- salt. It is also paramagnetic in solution, as shown by ^1H NMR measurements that reveal narrow-line, paramagnetically shifted resonances over a range in excess of 40 ppm.[147] Temperature-dependent magnetic measurements reveal that the nitrite analogue, *cis*,*cis*-$[(bpy)_2(O_2N)Ru^{III}ORu^{III}(NO_2)(bpy)_2](ClO_4)_2$, has a singlet ground state with a low-lying triplet excited state. The magnetism can be rationalized by assuming strong electronic coupling across the μ-oxo bridge, see below, or a moderate magnetic interaction between spin-paired d^5 Ru^{III} ions.[137] Low-temperature EPR measurements are consistent with a singlet ground state in the blue dimer.[148]

The influence of strong electronic coupling, and its significant impact on redox properties, is seen in the reduction potential comparisons in Table 1.[149] For the blue dimer derivative *cis*,*cis*-$[(bpy)_2(Cl)Ru^{III}ORu^{III}(Cl)(bpy)_2]^{2+}$, the first $Ru^{III} \rightarrow Ru^{II}$ reduction occurs at $E_{1/2} = -0.07$ V in CH_3CN ($I = 0.1$) compared to 0.6 V in *cis*-$[Ru^{III}(bpy)_2(py)(Cl)]^{2+}$. Based on this comparison, the "ligand" $\{-ORu^{III}Cl(bpy)_2{}^{+}\}$ in *cis*,*cis*-$[(bpy)_2(Cl)Ru^{III}\{-ORu^{III}(Cl)(bpy)_2\}]^{2+}$ is strongly electron-*donating* relative to py in $-[Ru^{III}(bpy)_2(py)(Cl)]^{2+}$.

Similarly, the second $Ru^{III} \rightarrow Ru^{II}$ reduction, $[(bpy)_2(Cl)Ru^{III}\{-ORu^{II}(Cl)(bpy)_2\}]^+ + e^- \rightarrow [(bpy)_2(Cl)Ru^{II}\{-ORu^{II}(Cl)(bpy)_2\}]$, occurs at −0.75 V compared to the reduction of *cis*-$[Ru^{III}(bpy)_2(Cl)_2]^+$ to $[Ru^{II}(bpy)_2(Cl)_2]$ at 0 V. This comparison shows that $\{-ORu^{II}(Cl)(bpy)_2{}^{0}\}$ is strongly electron-donating relative to $L = Cl^-$.

Similar effects exist in the oxidation of Ru^{III} to Ru^{IV}. $E_{1/2} = 0.43$ V for oxidation of $[(bpy)_2(Cl)Ru^{III}\{-ORu^{III}(Cl)(bpy)_2\}]^{2+}$ to $[(bpy)_2(Cl)Ru^{IV}\{-ORu^{III}(Cl)(bpy)_2\}]^{3+}$. Oxidation of *cis*-$[Ru^{III}(bpy)_2(Cl)_2]^+$ to $[Ru^{III}(bpy)_2(Cl)_2]^{2+}$ occurs at 1.7 V.

The effects of electronic coupling across the μ-oxo bridge are also seen in acid–base properties. For example, the first acid dissociation constant in $[Ru^{III}(bpy)_2(py)(H_2O)]^{3+}$ is $K_{a,1} = 0.85$. It increases to 6.8 in $[(bpy)_2(H_2O)Ru^{III}ORu^{III}(OH_2)(bpy)_2]^{4+}$. Part of this difference is attributable to the difference in the charge type.[44]

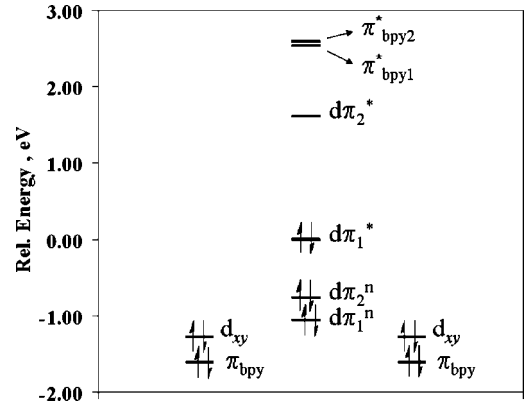

Figure 9. Molecular orbital diagram for *cis*,*cis*-$[(bpy)_2(H_2O)Ru_1^{III}ORu_2^{III}(OH_2)(bpy)_2]^{4+}$ from DFT calculations (assuming a closed-shell singlet by using the B3LYP functional and the LANL2DZ basis set). The energy levels are labeled by their dominant orbital compositions with d_π and d_{π^*} (t_{2g} in O_h symmetry) directed along the μ-Ru−O axes and mixed with $2p_\pi$ O orbitals of the bridge. The d_{xy} (d_δ) orbitals are orthogonal to the μ-Ru−O axes.[151]

The influence of electronic coupling across the Ru−O−Ru bridge is 2-fold. On one hand, it decreases $E^{\circ\prime}$ values for $Ru^{III/II}$ couples, making them no longer viable for water oxidation. For the $Ru(bpy)_3{}^{3+/2+}$ couple in water $E^{\circ\prime} = 1.26$ V, which is sufficient to oxidize water even in 1 M H^+ with $E^\circ = 1.23$ V for the O_2/H_2O couple. By contrast, $E^{\circ\prime}$ for the first $Ru^{III/II}$ couple in $[(bpy)_2(Cl)Ru^{III}ORu^{III}(Cl)(bpy)_2]^{2+}$ *is decreased by more than 2 V to −0.75 V*.

The second influence of electronic coupling, combined with PCET, is that it provides access to higher oxidation states—Ru^{IV}, Ru^{V}, and Ru^{VI}—and they have the thermodynamic driving force required for water oxidation, section 4.1.

It is possible to account for $E^{\circ\prime}$ values and assign the electronic spectrum of the blue dimer if it is assumed that significant electronic coupling and delocalization exist across the μ-oxo bridge.[139] A delocalized model was first proposed by Dunitz and Orgel for $Cl_5RuORuCl_5$[150] and modified for the blue dimer.[137] An energy level diagram from a recent DFT calculation is shown in Figure 9.[151]

In a recent publication,[146] Batista and Martin proposed a variation on the original weak coupling model of Baik and co-workers.[143–145] Based on results obtained from DFT (B3LYP) and complete active space self-consistent-field (CASSCF) calculations, the authors concluded that the ground state of the blue dimer is a weakly antiferromagentically coupled singlet state. In this model, partial delocalization occurs by mixing of d_π rather than by mixing of d_δ orbitals as calculated by Baik and co-workers.

The models assuming weak coupling are based solely on the total energies of possible configurations. A detailed comparison between optimized geometries for these configurations and the actual X-ray structure reveal significant differences with the closed-shell singlet giving a more reasonable geometry. They fail to account adequately for either structure or structural changes that occur upon oxidation. Both can be explained by assuming strong electronic coupling. For example, in the series $[(bpy)_2(L)Ru^{III}ORu^{III}$

(147) Dobson, J. C.; Sullivan, B. P.; Doppelt, P.; Meyer, T. J. *Inorg. Chem.* **1988**, *27*(21), 3863–3866.
(148) Lei, Y.; Hurst, J. K. *Inorg. Chem.* **1994**, *33*(20), 4460–4467.
(149) Doppelt, P.; Meyer, T. J. *Inorg. Chem.* **1987**, *26*(13), 2027–2034.
(150) Dunitz, J. D.; Orgel, L. E. *J. Chem. Soc.* **1953**, 2594–2596.
(151) Concepcion, J. J.; Meyer, T. J. , manuscript in preparation.

$(L)(bpy)_2]^{n+}$ (L is H_2O, NH_3, or NO_2^-; $n = 2$ or 4), the average μ-Ru−O bridge distance is 1.882 Å.[44,140,141] In $[(bpy)_2(HO)Ru^{IV}ORu^{III}(OH_2)(bpy)_2]^{4+}$, the average distance is 1.835 Å, in $[(phen)(py\text{-}ph)(Cl)Ru^{IV}ORu^{III}(py\text{-}ph)(phen)]^+$ [phen is 1,10-phenanthroline; py-ph is 2-(2-pyridyl)phenyl], it is 1.832 Å,[152] and in $[(bpy)_2(Cl)Ru^{IV}ORu^{III}(Cl)(bpy)_2]^{3+}$, it is 1.836 Å.[151] No structural information is available for the series $[(bpy)_2(L)RuORu(L)(bpy)_2]^{n+}$ past IV,III. However, there is structural information for $[(Cl)_5Ru^{IV}ORu^{IV}(Cl)_5]^4$,[153] $[(CH_3CN)_2(Cl)_3Ru^{IV}ORu^{IV}(Cl)_3(CH_3CN)_2]$,[154] [(OEP)(Cl)$Ru^{IV}ORu^{IV}$(Cl)(OEP)] (OEP is octaethylporphyrinato),[155] and [(PPP)(Cl)$Ru^{IV}ORu^{IV}$ (Cl)(PPP)] [PPP is 5,10,15,20-tetrakis(pentafluorophenyl)porphyrinato][156] where the average μ-Ru−O bridge distance is 1.793 Å. These data show that there is an average decrease in μ-Ru−O of 0.092 Å when III,III is oxidized to IV,IV.

We have extended earlier DFT calculations on $[(bpy)_2(H_2O)Ru^{III}ORu^{III}(H_2O)(bpy)_2]^{4+}$ [139] based on a closed-shell singlet ground state by using the B3LYP functional and LANL2DZ basis set as implemented in *Gaussian03*. These calculations account, at least qualitatively, for both structural details and changes in structure upon oxidation. An energy level diagram is shown in Figure 9. In this diagram, the highest occupied molecular orbital, d_{π_1}*, is antibonding with regard to the Ru−O−Ru bridge. Oxidation occurs by loss of antibonding electrons, which increases bond order and decreases μ-Ru−O bond distances. Similarly, reduction occurs at d_{π_2}*, which is also antibonding with regard to the Ru−O−Ru bridge. This is consistent with reduction leading to loss of the Ru−O−Ru bridge, $[(bpy)_2(H_2O)Ru^{III}ORu^{III}(H_2O)(bpy)_2]^{4+} + H_2O \xrightarrow{+2e^-,\ 2H^+} 2[Ru^{II}(bpy)_2(H_2O)_2]^{2+}$, section 4.4.

UV–visible, near-IR absorption bands, and band assignments from time-dependent DFT (TDDFT) based on the strong coupling model are shown in Figure 10.[151]

There are notable features in the spectrum in Figure 9 and the assignments in Figure 10. The visible absorption band that makes the blue dimer blue arises from overlapping $d_\pi \rightarrow \pi_{bpy}$* (MLCT) and bridge-based $d_\pi \rightarrow d_{\pi^*}$ transitions. The appearance of visible MLCT bands is common for ruthenium(II) polypyridyl complexes, but these bands typically appear in the UV for Ru^{III}. This is another manifestation of strong electronic coupling across the μ-oxo bridge.

Low-energy absorption features at 1205, 1125, and 915 nm arise from interconfigurational transitions within the set of largely d_π orbitals, d_{xy}, $d_{\pi_n} \rightarrow d_{\pi^*}$. In more typical Ru^{III} complexes, these bands appear in the IR from 2000 to 1430 nm and are of low absorptivity.[157,158]

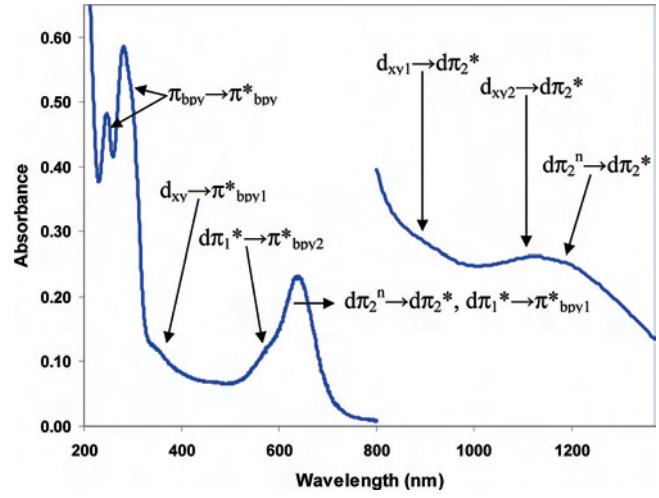

Figure 10. UV–visible−near-IR spectrum of *cis,cis*-$[(bpy)_2(H_2O)Ru^{III}ORu^{III}(OH_2)(bpy)_2]^{4+}$ in water at pH = 7. Band assignments are based on the orbital labeling scheme in Figure 9. π^*_{bpy1} and π^*_{bpy2} are the first and second lowest unoccupied molecular orbitals on the bpy's.[151]

4. The Blue Dimer: Oxidation and Higher Oxidation States

It was exciting to observe that the addition of Ce^{IV} to acidic solutions of the blue dimer resulted in obvious gas evolution. Gas chromatographic and mass spectrometric measurements verified that the gas was oxygen.[43,44] In fact, the blue dimer proved to be the first of a class of μ-oxo complexes of general formula $[(PP)_2(H_2O)Ru^{III}ORu^{III}(OH_2)(PP)_2]^{4+}$ (PP = 1,10-phenanthroline or 4,4′-X_2-bpy with X = Me, COOH)[43–46,159–165] that function as catalysts for water oxidation in acidic solution with added Ce^{IV} or Co^{3+}. In catalytic studies, it was shown that the blue dimer underwent multiple turnovers in solution or in polymer films by electrochemical oxidation or oxidation with added Ce^{IV}. Rate constants for oxygen evolution were reported in the range $k \sim 10^{-1}-10^{-3}$ s^{-1} at 25 °C; however, see section 5.[45,162–164]

4.1. Oxidation of the Blue Dimer. Thermodynamics and Oxidation States. Important questions remained. What form of the blue dimer is oxidatively active toward water oxidation and how is it reached? What is the mechanism or mechanisms of water oxidation?

Involvement of oxidation states was addressed by electrochemical measurements over an extended pH range and by

(152) Ryabov, A. D.; Le Lagadec, R.; Estevez, H.; Toscano, R. A.; Hernandez, S.; Alexandrova, L.; Kurova, V. S.; Fischer, A.; Sirlin, C.; Pfeffer, M. *Inorg. Chem.* **2005**, *44*, 1626.
(153) Efimenko, I. A.; Balakaeva, T. A.; Kurbakova, A. P.; Gorbunova, Y. E.; Mikhailov, Y. N. *Koord. Khim.* **1994**, *20*, 294.
(154) Tyrlik, S. K.; Kisielinska, M.; Huffman, J. C. *Transition Met. Chem.* **1995**, *20*, 413.
(155) Masuda, H.; Taga, T.; Osaki, K.; Sugimoto, H.; Mori, M.; Ogoshi, H. *Bull. Chem. Soc. Jpn.* **1982**, *55*, 3887.
(156) Zhang, J.-L.; Che, C.-M. *Chem.−Eur. J.* **2005**, *11*, 3899.
(157) Hudson, A.; Kennedy, M. J. *J. Am. Chem. Soc.* **1969**, *7*, 1116–1120.
(158) Bhattacharya, S.; Ghosh, P.; Chakravorty, A. *Inorg. Chem.* **1985**, *24*(20), 3224–3230.
(159) Yamada, H.; Hurst, J. K. *J. Am. Chem. Soc.* **2000**, *122*(22), 5303–5311.
(160) Rotzinger, F. P.; Munavalli, S.; Comte, P.; Hurst, J. K.; Grätzel, M.; Pern, F. J.; Frank, A. J. *J. Am. Chem. Soc.* **1987**, *109*(22), 6619–6626.
(161) Comte, P.; Nazeeruddin, M. K.; Rotzinger, F. P.; Frank, A. J.; Grätzel, M. *J. Mol. Catal.* **1989**, *52*(1), 63–84.
(162) Binstead, R. A.; Chronister, C. W.; Ni, J.; Hartshorn, C. M.; Meyer, T. J. *J. Am. Chem. Soc.* **2000**, *122*(35), 8464–8473.
(163) Nagoshi, K.; Yamashita, S.; Yagi, M.; Kaneko, M. *J. Mol. Catal. A: Chem.* **1999**, *144*(1), 71–76.
(164) Hurst, J. K. *Coord. Chem. Rev.* **2005**, *249*(3–4), 313–328. Yamada, H.; Hurst, J. K. *J. Am. Chem. Soc.* **2000**, *122*(22), 5303–5311.
(165) Petach, H. H.; Elliott, C. M. *J. Electrochem. Soc.* **1992**, *139*(8), 2217–2221.

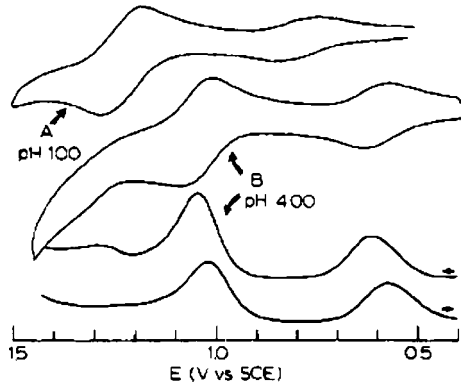

Figure 11. Cyclic voltammograms (top) and differential pulse voltammograms (bottom) for $[(bpy)_2(H_2O)Ru^{III}ORu^{III}(OH_2)(bpy)_2]^{4+}$ at pH 1 and 4 at a scan rate of 50 mV s^{-1} at an oxidatively activated glassy carbon electrode vs the saturated calomel electrode (SCE) at 0.246 V vs NHE. Reprinted from ref 44. Copyright 1985 American Chemical Society.

mixing experiments with added Ce^{IV} in strongly acidic solutions. Ce^{IV} is a powerful oxidant with $E^{\circ\prime}(Ce^{IV/III}) = 1.7$ V in 1 M $HClO_4$, but its use is limited to strongly acidic solutions because of complex hydrolysis phenomena above pH $\sim$ 1.

Representative cyclic voltammograms and pulse voltammograms of the blue dimer in solution at two different pHs are shown in Figure 11.[44] These measurements show that there is a 1:2:1 electron loss pattern for oxidation at pH 4 and the sequence $Ru^{III}ORu^{III} \xrightarrow{-e^-} Ru^{IV}ORu^{III} \xrightarrow{-2e^-} Ru^{V}ORu^{IV} \xrightarrow{-e^-} Ru^{V}ORu^{V}$. The intermediate oxidation state $Ru^{IV}ORu^{IV}$ is "missing" because of its instability toward disproportionation; note section 2.1. The voltammetric waves are pH-dependent, as can be seen in Figure 11. With the pH decreased to 1, the electron loss pattern changes to $Ru^{III}ORu^{III} \xrightarrow{-e^-} Ru^{IV}ORu^{III} \xrightarrow{-3e^-} Ru^{V}ORu^{V}$, with both $Ru^{IV}ORu^{IV}$ and $Ru^{V}ORu^{IV}$ missing oxidation states and with both unstable toward disproportionation.

Obtaining reliable, reproducible electrochemical data for the blue dimer and related oxo-based couples is an art form and relies on the oxidative activation procedures for carbon electrodes mentioned in section 2. Complications arise from the PCET nature of the couples and unstable intermediates that result from simple electron transfer or proton transfer. In conducting the electrochemical experiments, it is difficult to find functional electrode materials at the extremely positive potentials required for the oxidations. As an example, the higher oxidation states of the dimer catalyze the oxidation of carbon electrodes.

The pH dependences of the blue dimer redox couples are shown in the $E_{1/2}$−pH diagram in Figure 12. These data reveal a complex pH dependence that arises largely from the acid–base properties of couples involving the lower oxidation states $Ru^{III}ORu^{III}$ and $Ru^{IV}ORu^{III}$. The studies of pH dependence reveal that the higher oxidation states $Ru^{V}ORu^{IV}$ and $Ru^{V}ORu^{V}$ exist as the dioxido forms over an extended pH range, although there is spectral evidence that $Ru^{V}ORu^{IV}$ is protonated in a strongly acidic solution, where it is unstable toward disproportionation (see below).[162,164,169]

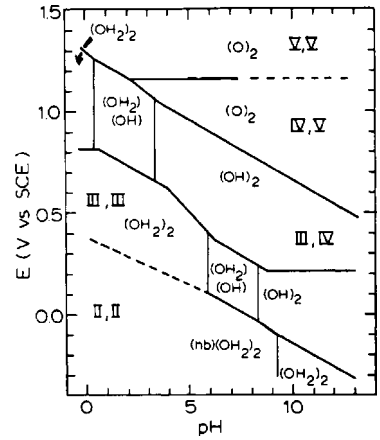

Figure 12. $E_{1/2}$−pH diagram vs SCE (0.246 V vs NHE) for $[(bpy)_2(H_2O)RuORu(OH_2)(bpy)_2]^{4+}$ as in Figure 2, with the vertical lines indicating pK_a values for the lower oxidation state. The labels III,III, etc., indicate the potential−pH regions where these oxidation state distributions dominate. The state of protonation of the initial H_2O ligands, and whether they are O^{2-}, OH^-, or H_2O, is also indicated. Reprinted from ref 166. Copyright 1986 American Chemical Society.

In the diagram in Figure 12, as in Figure 2, pK_a values appear as vertical lines and oxidation state and proton compositions are indicated in those potential pH regions where they are dominant.

Related results were obtained for the blue dimer derivative $[(4,4'\text{-}(COOH)_2bpy)_2(H_2O)RuORu(OH_2)(4,4'\text{-}(COOH)_2\text{-}bpy)_2]^{4+}$ in 0.5 M acid. The substituent effect of the carboxylic acid groups increased $E_{1/2}$ for the $Ru^{IV}ORu^{III}/Ru^{III}ORu^{III}$ couple to 1.23 V in 1 M H_2SO_4. A catalytic wave, presumably due to oxidation of $Ru^{IV}ORu^{III}$ to $Ru^{V}ORu^{V}$ followed by water oxidation, was also observed.[160,161]

Inspection of the data in Figure 12 reveals that $Ru^{IV}ORu^{IV}$ does not appear as a thermodynamically stable oxidation state over the entire pH range. Its instability toward disproportionation is a consequence of its acid–base properties, the influence of electronic coupling in stabilizing intermediate oxidation states, and the pH dependences of adjacent redox couples as described in section 2. As discussed in section 5, anated forms of $Ru^{IV}ORu^{IV}$ do appear as transient, deleterious intermediates in water oxidation by the blue dimer.

Nearly the same pattern of pH-dependent behavior is observed for the osmium analogue, *cis*,*cis*-$[(bpy)_2(H_2O)Os^{III}\text{-}OOs^{III}(OH_2)(bpy)_2]^{4+}$ but with $E^{\circ\prime}$ values characteristically lower by 0.3–0.4 V. For this complex, $Os^{IV}OOs^{IV}$ does appear as a stable oxidation state but only in an acidic solution between pH $\sim$ 0 and 4. Above pH = 4, disproportionation of $Os^{IV}OOs^{IV}$ is driven by the difference in pH dependences between adjacent $Os^{V}OOs^{IV}/Os^{IV}OOs^{IV}$ and $Os^{IV}OOs^{IV}/Os^{IV}OOs^{III}$ couples.[166] There is a narrow potential pH range between pH = 4 and 5, where all four 1e$^-$ couples, $Os^{V}OOs^{V}/Os^{V}OOs^{IV}$, $Os^{V}OOs^{IV}/Os^{IV}OOs^{IV}$, $Os^{IV}OOs^{IV}/Os^{IV}OOs^{III}$, and $Os^{IV}OOs^{III}/Os^{III}OOs^{III}$, coexist. Below pH = 4, $Os^{V}OOs^{IV}$ is unstable with respect to disproportionation and oxidation of $Os^{IV}OOs^{IV}$ occurs to give $Os^{V}OOs^{V}$.

The osmium analogue offers insights for the blue dimer. Given the instability of $Ru^{IV}ORu^{IV}$ toward disproportionation,

(166) Gilbert, J. A.; Geselowitz, D.; Meyer, T. J. *J. Am. Chem. Soc.* **1986**, *108*(7), 1493–1501.

the potential for the $[(O)Ru^{V}ORu^{IV}(O)]^{3+} + e^{-} + 2H^{+} \rightarrow \{[(HO)Ru^{IV}ORu^{IV}(OH)]^{4+}\}$ couple is decreased below the potential for the $\{[(HO)Ru^{IV}ORu^{IV}(OH)]^{4+}\} + e^{-} \rightarrow [(HO)Ru^{IV}ORu^{III}(OH)]^{3+}$ couple. Gas-phase DFT calculations favor the formulation $[(HO)Ru^{IV}ORu^{IV}(OH)]^{4+}$ over $[(O)Ru^{V}ORu^{III}(OH_2)]^{4+}$ for $Ru^{IV}ORu^{IV}$.[139] Instability toward disproportionation in $Ru^{IV}ORu^{IV}$ must be a consequence of electronic stabilization effects, with a contribution from dioxo formation in $Ru^{V}ORu^{IV}$ and of differences in pH dependences between the two couples. These effects combine to destabilize $Ru^{IV}ORu^{IV}$ toward disproportionation over the entire pH range.

As noted above, in acidic solutions below pH $\sim$ 2, $[(O)Ru^{V}ORu^{IV}(O)]^{3+}$is also unstable with respect to disproportionation, $3[(O)Ru^{V}ORu^{IV}(O)]^{3+} + 3H^{+} \rightarrow 2[O)Ru^{V}ORu^{V}(O)]^{4+} + [(HO)Ru^{IV}ORu^{III}(OH_2)]^{4+}$. This is due to the difference in pH dependences for the $Ru^{V}ORu^{V}/Ru^{V}ORu^{IV}$ and $Ru^{V}ORu^{IV}/Ru^{IV}ORu^{III}$ couples (Figure 12).

Given the thermodynamic instabilities of $Ru^{V}ORu^{IV}$ and $Ru^{IV}ORu^{IV}$, in strongly acidic solutions, they are both stronger oxidants than $Ru^{V}ORu^{V}$, with $Ru^{IV}ORu^{IV}$ the most powerful oxidant of the three. Further, given the potential of the O_2/H_2O couple (1.23 V vs NHE at pH = 0) and its pH dependence, all three oxidation states, $Ru^{V}ORu^{V}$, $Ru^{V}ORu^{IV}$, and $Ru^{IV}ORu^{IV}$, are thermodynamically capable of water oxidation from pH = 0 to 14.

As discussed in section 2, the remarkable interplay of closely lying oxidation states for the blue dimer results from a combination of factors. Redox potential leveling, due to the acid–base properties of bound H_2O, plays a role, as do electronic stabilization effects from electronic coupling across the bridge and terminal Ru=O bond formation.

4.2. Oxidation of Related μ-Oxo Dimers. $[(tpy)(H_2O)_2Ru^{III}ORu^{III}(H_2O)_2(tpy)]^{4+}$ (tpy is 2,2′:6′,2″-terpyridine). In this dimer, there is an additional water molecule in the coordination sphere of each Ru. In contrast to the blue dimer, stepwise oxidation occurs through successive $1e^{-}$ oxidations. Redox potentials are well separated, and $Ru^{IV}ORu^{IV}$ is a stable oxidation state. From pH = 4.5–9, the successive couples ($E^{\circ\prime}$ vs NHE at pH = 7 in parentheses) are $[(HO)Ru^{IV}ORu^{III}(OH)]^{3+}/[(HO)Ru^{III}ORu^{III}(H_2O)]^{3+}$ (0.40 V), $[(HO)Ru^{IV}ORu^{IV}(OH)_2]^{3+}/[(HO)Ru^{IV}ORu^{III}(OH)]^{3+}$ (0.66 V), $[(O)Ru^{V}ORu^{IV}(O)]^{3+}/[(HO)Ru^{IV}ORu^{IV}(OH)_2]^{3+}$ (1.12 V), and $[(O)Ru^{V}ORu^{V}(O)]^{4+}/[(O)Ru^{V}ORu^{IV}(O)]^{3+}$ (1.45 V).[167]

There are useful insights about the blue dimer in these data as well. As for the blue dimer, the difference in pH dependences between the $Ru^{V}ORu^{V}/Ru^{V}ORu^{IV}$ and $Ru^{V}ORu^{IV}/Ru^{IV}ORu^{III}$ couples causes $[(O)Ru^{V}ORu^{IV}(O)]^{3+}$ to be unstable with respect to disproportionation into $[(O)Ru^{V}ORu^{V}(O)]^{4+}$ and $[(HO)Ru^{IV}ORu^{IV}(OH_2)]^{5+}$ below pH = 1.7. For the tpy dimer, $Ru^{IV}ORu^{IV}$ is a stable oxidation state because the additional coordinated water molecules allow loss of an additional proton to give $[(HO)Ru^{IV}ORu^{IV}(OH)_2]^{3+}$ (or $[(HO)Ru^{IV}ORu^{IV}(O)(H_2O)]^{3+}$; the actual proton formulation is unknown). Both $Ru^{V}ORu^{V}$ and $Ru^{V}ORu^{IV}$ are thermodynamically capable of water oxidation.

$[(bpy)_2(H_2O)Ru^{III}ORu^{III}(py)(bpy)_2]^{4+}$ (py is pyridine). In this mixed-ligand complex, there is a single coordinated water molecule and the highest accessible oxidation state is $[(bpy)_2(O)Ru^{V}ORu^{III}(py)(bpy)_2]^{4+}$. It has pH-dependent electrochemical properties that are related to those of $Ru^{II}(bpy)_2(py)(H_2O)^{2+}$ but based on $Ru^{V/IV}$ and $Ru^{IV/III}$ couples due to strong electronic coupling across the Ru−O−Ru bridge.[168] Electronic coupling also influences pK_a values with $pK_{a,1} = 6.8$ compared to 0.85 for $Ru^{III}(bpy)_2(py)(H_2O)^{3+}$ and $pK_a \sim 11.2$ for $Ru^{IV}OH$ compared to $pK_a < -6$ for $Ru^{IV}(bpy)_2(py)(OH)^{2+}$. Both $1e^{-}$ and $2e^{-}$ couples are thermodynamically capable of water oxidation with $E^{\circ\prime} \sim$ 1.1 V at pH = 7 for the $[(bpy)_2(O)Ru^{V}ORu^{III}(py)(bpy)_2]^{5+}/[(bpy)_2(HO)Ru^{IV}ORu^{III}(py)(bpy)_2]^{4+}$ couple.

4.3. Higher Oxidation States. Structure and Spectroscopy. $[(bpy)_2(OH)Ru^{IV}ORu^{III}(H_2O)(bpy)_2]^{4+}$. As noted above, the $1e^{-}$-oxidized form of the blue dimer, as $[(bpy)_2(HO)Ru^{IV}ORu^{III}(OH_2)(bpy)_2]^{4+}$, has been characterized structurally by XRD.[141] In $Ru^{IV}ORu^{III}$, ∠Ru−O−Ru increases from 165 to 170° compared to the blue dimer and μ-Ru−O bond distances in the asymmetric bridge decrease from 1.869 to 1.847 and 1.823 Å.[139]

In resonance Raman spectra, the symmetric Ru−O−Ru stretch, ν_{sym}(RuORu), appears at 384 cm^{-1} for the blue dimer, at 389 cm^{-1} for $[(bpy)_2(OH)Ru^{IV}ORu^{III}(OH_2)(bpy)_2]^{4+}$, and at 398 cm^{-1} for $[(bpy)_2(H_2O)Ru^{IV}ORu^{III}(OH_2)(bpy)_2]^{5+}$.[141] The UV–visible spectrum is correspondingly pH-dependent with bridge-based $d_\pi \rightarrow d_{\pi^*}$ bands appearing in the visible at 446 ± 2 nm (ϵ = 22 000 M^{-1} cm^{-1}) for $[(H_2O)Ru^{IV}ORu^{III}(OH_2)]^{5+}$, at 495 ± 2 nm for $[(HO)Ru^{IV}ORu^{II-III}(OH_2)]^{4+}$, and at 488 ± 2 nm for $[(OH)Ru^{IV}ORu^{III}(OH)]^{3+}$. A characteristic, interconfigurational $d_\pi \rightarrow d_\pi$ band appears in the near-IR at 1173 nm ($\epsilon \sim 400$ M^{-1} cm^{-1}). The $pK_{a,1}$ for $[(H_2O)Ru^{IV}ORu^{III}(OH_2)]^{5+}$ is 0.4, and $pK_{a,2} = 3.2$ at 25 °C (I = 1).[44]

$Ru^{IV}ORu^{IV}$. From the electrochemical results in Figure 12, $Ru^{IV}ORu^{IV}$ is an unstable oxidation state from pH = 0–14. It does appear as a kinetic intermediate in the oxidation of $Ru^{IV}ORu^{III}$ by Ce^{IV}.[162] In 1 M $HClO_4$ or CF_3CSO_3H, intermediates appear that persist on the 10−100 s time scale (section 5). There is also good evidence that anated $Ru^{IV}ORu^{IV}$ intermediates such as $[(bpy)_2(HO)Ru^{IV}ORu^{IV}(NO_3)(bpy)_2]^{3+}$ appear and build up late in blue-dimer-catalyzed water oxidation cycles. UV–visible−near-IR spectra are pH-dependent because of acid–base equilibria, $[(bpy)_2(HO)Ru^{IV}ORu^{IV}(NO_3)(bpy)_2]^{4+}$ (λ_{max} = 455 nm) ⇌ $[(bpy)_2(O)Ru^{V}ORu^{III}(NO_3)(bpy)_2]^{3+}$ (λ_{max} = 488 nm) + H^{+} (pK_a = 1.4). For an apparent deprotonated triflate analogue, section 5.3, λ_{max} = 489 nm with ν_{sym}(RuORu) = 358 cm^{-1} in its resonance Raman spectrum.[148,164,169]

Gas-phase DFT calculations on $Ru^{IV}ORu^{IV}$ favor the dihydroxido form, $[(bpy)_2(OH)Ru^{IV}ORu^{IV}(OH)(bpy)_2]^{4+}$ over the asymmetrical oxido−aqua form, $[(bpy)_2(O)Ru^{V}ORu^{III}(H_2O)(bpy)_2]^{4+}$ by 16 kcal mol^{-1}. DFT-calculated μ-Ru−O bond lengths were 1.82 Å with ∠Ru−O−Ru = 175.5°.[139]

(167) Lebeau, E. L.; Adeyemi, S. A.; Meyer, T. J. *Inorg. Chem.* **1998**, *37*(25), 6476–6484.

(168) Raven, S. J.; Meyer, T. J. *Inorg. Chem.* **1988**, *27*(24), 4478–4483.

(169) Yamada, H.; Siems, W. F.; Koike, T.; Hurst, J. K. *J. Am. Chem. Soc.* **2004**, *126*, 9786–9795.

$[(bpy)_2(O)Ru^{V}ORu^{IV}(O)(bpy)_2]^{3+}$. Based on the pH-dependent electrochemical data in Figure 12, $Ru^{V}ORu^{IV}$ exists as the dioxido complex $[(bpy)_2(O)Ru^{V}ORu^{IV}(O)(bpy)_2]^{3+}$, at least above pH = 2. In strongly acidic solutions, 1 M HNO_3, there is spectral evidence for protonation with shifts in λ_{max} from 488 nm ($\epsilon = 9700\ M^{-1}\ cm^{-1}$), 710 nm ($\epsilon \sim 600\ M^{-1}\ cm^{-1}$) to 482 nm ($\epsilon = 14\,500\ M^{-1}\ cm^{-1}$), 750 nm ($\epsilon \sim 600\ M^{-1}\ cm^{-1}$).[162] Protonation could occur at an oxo group or at the μ-oxo bridge,[148] assuming the former, the acid–base equilibrium is $[(O)Ru^{V}ORu^{IV}(OH)]^{4+} \rightleftharpoons [(O)Ru^{V}ORu^{IV}(O)]^{3+} + H^+$, pK_a (I = 1 M, 23 °C) ~ 0.3.

In gas-phase DFT calculations on the protonated form, $[(bpy)_2(O)Ru^{V}ORu^{IV}(OH)(bpy)_2]^{4+}$, ∠Ru−O−Ru was calculated to be 175.6° with μ-Ru−O bridge bond lengths of 1.83 and 1.84 Å.

$Ru^{V}ORu^{IV}$ has been generated by electrochemical and HOCl oxidation of $[(bpy)_2(HO)Ru^{IV}ORu^{III}(OH)(bpy)_2]^{4+}$ in a 0.1 M phosphate buffer. It slowly returns to $Ru^{IV}ORu^{III}$ with the evolution of oxygen. The kinetics were initially described as first order in $Ru^{V}ORu^{IV}$,[168] but we find a better fit to second order, equal concentration kinetics with k(23 °C) = $5.5 \times 10^{-4}\ M^{-1}\ s^{-1}$. $Ru^{V}ORu^{IV}$ is also unstable above pH = 7 toward bpy ligand oxidation.[162]

$Ru^{V}ORu^{IV}$ is thermodynamically unstable toward disproportionation below pH = 2. In 1 M $HClO_4$, disproportionation, which is accompanied by water oxidation, occurs by second order, equal concentration kinetics with k(1 M $HClO_4$, 25 °C) = 22 $M^{-1}\ s^{-1}$.[162,182] There is evidence for rate acceleration with added anions and for the appearance of both $Ru^{IV}ORu^{III}$ and anated intermediates such as $[(bpy)_2(HO)Ru^{IV}ORu^{IV}(NO_3)(bpy)_2]^{4+}$ as products at high concentrations of added anions.

$[(bpy)_2(O)Ru^{V}ORu^{V}(O)(bpy)_2]^{4+}$. As discussed below, $[(O)Ru^{V}ORu^{V}(O)]^{4+}$ appears to be the active form of the blue dimer toward water oxidation. Based on the results of stopped-flow measurements, oxidation of $Ru^{V}ORu^{IV}$ to $[(O)Ru^{V}ORu^{V}(O)]^{4+}$ in 1 M $HClO_4$ occurs with k(25 °C) ≥ $10^2\ M^{-1}\ s^{-1}$.[162] In 1 M HNO_3, k(23 °C) = 80 ± 2 $M^{-1}\ s^{-1}$.[182]

As described in sections 5.3 and 5.4, the details of how $Ru^{V}ORu^{V}$ is reached and how water oxidation occurs depend on the nature and strength of the acid used. Even so, there are common mechanistic elements. In 0.1 M HNO_3, rapid oxidation of $Ru^{V}ORu^{IV}$ to $Ru^{V}ORu^{V}$ is followed by the appearance of an intermediate without the buildup of $Ru^{V}ORu^{V}$. The intermediate, thought to be a peroxide, dominates early in the catalytic cycle. In 1 M HNO_3, oxidation of $Ru^{V}ORu^{IV}$ is slower and rate-limiting, and it dominates at the catalytic steady state.

Even given its implied reactivity, it was possible to isolate a black suspension, tentatively identified as $[(bpy)_2(O)Ru^{V}ORu^{V}(O)(bpy)_2](ClO_4)_4$, by adding three equivalents of Ce^{IV} three times to $Ru^{IV}ORu^{III}$ at high concentration in 1 M $HClO_4$ at 5 °C. Under these conditions with added Ce^{IV}, a black microparticulate suspension appeared that was highly explosive when isolated as a solid.[162] Measurements on the suspension revealed UV–visible absorption maxima at ~400 and ~600 nm. In its resonance Raman spectrum, obtained in frozen solutions at 77 K, peaks appeared at 816 cm^{-1} for ν(Ru=O) and at ~357 cm^{-1} for ν_{sym}(Ru−O−Ru). The Raman results were important in suggesting both retention of the Ru−O−Ru μ-oxo bridge and the presence of a Ru=O group or groups in the active form of the catalyst.[162] Upon redissolution of the suspension, which occurs with oxygen evolution, ν(Ru=O) was replaced by a broad band at 650 cm^{-1} and ν_{sym}(Ru−O−Ru) by a new band at 398 cm^{-1}.

Similar conclusions were reached based on Ru K-edge XANES (X-ray absorption near-edge structure) and EXAFS (extended X-ray absorption fine structure) measurements in frozen solutions. Results of these experiments were interpreted as demonstrating a nearly linear Ru−O−Ru bridge and short, terminal Ru−O bonds consistent with Ru=O.[170]

Hurst and co-workers have reached different conclusions based on electrochemical and Ce(IV) oxidation of the blue dimer in HSO_3CF_3 with resonance Raman and UV–visible monitoring.[164,169] Controlled potential electrolysis past 1.3 V Ce(IV) oxidation of $Ru^{IV}ORu^{III}$ with resonance Raman monitoring gave a new species forumulated as $Ru^{IV}ORu^{IV}$ having ν_{sym}(Ru−O−Ru) at 358 cm^{-1} and λ_{max} = 488 nm ($\epsilon = 1.6 \times 10^4\ M^{-1}\ cm^{-1}$). Oxidation, either electrochemically or by the addition of excess Ce(IV), resulted in an additional species, formulated as $Ru^{V}ORu^{V}$, having ν(Ru=O) = 818 cm^{-1} and λ_{max} = 482 nm ($\epsilon = 1.5 \times 10^4\ M^{-1}\ cm^{-1}$). It disappeared with k(23 °C) = $9.5 \times 10^{-3}\ s^{-1}$ [$k(H_2O)/k(D_2O)$ = 1.6] to give the species at λ_{max} = 488 nm. The rate constant for oxygen evolution under the same conditions was comparable with $k(O_2) = 5.2(\pm 1.0) \times 10^{-3}\ s^{-1}$. The intermediate at λ_{max} = 488 nm returned to $Ru^{IV}ORu^{III}$ on a longer time scale.[164,169]

As discussed in section 5.5, it is possible to reconcile these observations as part of a complete cycle for water oxidation by reformulating the species at λ_{max} = 482 nm as a peroxidic intermediate formed rapidly from $Ru^{V}ORu^{V}$ and the species at λ_{max} = 488 nm as with a coordinated anion $Ru^{IV}ORu^{IV}$.

Gas-phase DFT calculations predict a nearly linear Ru−O−Ru bridge in $[(O)Ru^{V}ORu^{V}(O)]^{4+}$ with ∠Ru−O−Ru = 178° and r(Ru=O) = 1.86 Å in either the *interior* or *exterior* rotamers.[139] In a later calculation, which assumed weak electronic coupling, ∠Ru−O−Ru varied from 137 to 177° and r(Ru=O) from 1.73 to 1.80 Å depending upon the rotamer and the details of the magnetic interaction across the μ-oxo bridge.[143]

$[(O)Ru^{VI}ORu^{V}(O)]^{5+}$. There is evidence for "overoxidation" of $[(tpy)(H_2O)(O)Ru^{V}ORu^{V}(O)(OH_2)(tpy)]^{4+}$ to give $Ru^{VI}ORu^{V}$, possibly as $[(tpy)(HO)(O)Ru^{VI}ORu^{V}(O)(OH_2)(tpy)]^{4+}$. The availability of the higher oxidation state is due to loss of a proton from the additional water in the coordination sphere. The oxidized product is unstable toward loss of the μ-oxo bridge to give the known dioxo complex *trans*-$[Ru^{VI}(tpy)(O)_2(H_2O)]^{2+}$ by the reaction $[(tpy)(HO)(O)Ru^{VI}ORu^{V}(O)(OH_2)(tpy)]^{4+} \xrightarrow{-e^-,\ +H^+,\ +H_2O} 2[Ru^{V}(O)_2(OH_2)(tpy)]^{2+}$.[167] The instability arises from strong electronic stabilization of the d^2 *trans*-$M^{VI}(tpy)(O)_2(H_2O)^{2+}$ (M = Ru, Os) product from the *trans*-dioxido bonding interaction.[111–115,171]

Oxidative decomposition has been directly observed for the surface-bound tpy derivative, $[(tpy\text{-}PO_3H_2)(H_2O)_2Ru^{III}ORu^{III}(OH_2)_2(tpy\text{-}PO_3H_2)]_2^{4+}$. In this derivative, the phosphonate groups form stable surface links at monolayer and submonolayer coverages on a variety of oxide surfaces: ITO (In_2O_3/Sn^{IV}), TiO_2, ZrO_2, and SnO_2.[172–174] On these surfaces, a $Ru^{VI}ORu^{V}/Ru^{V}ORu^{V}$couple is observed at 1.3 V vs NHE in cyclic voltammograms. Oxidation past this wave results in catalytically enhanced currents and water oxidation but in competition with the breakdown of the μ-oxo structure to give $[Ru^{VI}(tpy\text{-}PO_3H_2)]_2(O)_2(H_2O)]^{2+}$ on the surface.[174]

4.4. Instabilities and Complications. Obtaining reliable information about oxidation states past $Ru^{IV}ORu^{III}$ and the role that they play in the mechanism of water oxidation has proven to be a major challenge. The difficulties are worth documenting for what they reveal about the underlying chemistry.

(1) The Higher Oxidation States Are Strongly Oxidizing and Difficult to Access by Chemical or Electrochemical Oxidation. The redox potential data in Figure 12 show that potentials above 1.4 V vs NHE are required to oxidize $Ru^{IV}ORu^{III}$ to $Ru^{V}ORu^{V}$. The potentials required to reach $Ru^{IV}ORu^{IV}$ and $Ru^{V}ORu^{IV}$ are even higher. Very few reagents can provide these potentials. Both Ce^{IV} and Co_{aq}^{3+} have been used, but both are limited to a strongly acidic solution to avoid hydrolysis and/or water oxidation. For the $Co^{3+}(aq)/Co^{2+}(aq)$ couple, $E^{\circ\prime} = 1.84$ V. Although oxy anions such as HOCl can be used to access $Ru^{V}ORu^{IV}$ in certain pH ranges,[168] the blue dimer is an effective catalyst for decomposing HOCl into O_2 and Cl^- (section 5.1). *In the study of water oxidation, care must be taken in the use of strongly oxidizing oxy anions and related O-transfer reagents because they may be the source of O_2 by catalyzed decomposition.*

Electrochemical oxidation is difficult as well at such positive potentials because of the instability of typical electrode materials. There is the additional complication of slow electrode kinetics in the absence of surface activation to induce PCET surface pathways (section 2.2). At "unactivated" carbon electrodes, oxidation in the presence of the blue dimer results in sustained currents arising from surface oxidation, complicating the study of water oxidation by electrocatalysis.[44,122,164] Similarly, care must be taken with solvents and other components; for example, 99.8% triflic acid is vacuum-distilled from Ce^{IV} with blue dimer added. High-purity water is essential; we have used water from a Barnstead Milli-Q system.

(2) Polypyridyl Ligand Oxidation Occurs above pH = 7. As discussed in section 2, higher oxidation state polypyridyl complexes of iron, ruthenium, and osmium are unstable as the pH is raised above 7. As noted there, early claims in the literature that $Ru(bpy)_3^{3+}$ oxidizes water are incorrect. More recent studies showed that the actual chemistry involved is the oxidation of a bpy ligand. This chemistry has been summarized recently by Hurst.[164] A common decomposition pathway appears to be oxidation of a coordinated polypyridyl ligand following nucleophilic attack by OH^- with pseudobase formation. These reactions are analogous to reversible nucleophilic attack on pyridinium cations.[82,175–178] Following $2e^-$ oxidation of the OH^- adducts, the partly oxidized rings are kinetically susceptible to further oxidation, resulting in decomposition of the ligands, ultimately giving CO_2 as a product after several redox cycles.

An additional pathway has been suggested for decomposition of M(III) polypyridyl complexes (M = Fe, Ru, Os) at higher pHs involving initial nucleophilic attack by water or OH^- on the metal itself and coordination expansion.[179]

(3) Anation. A number of observations point to complications from anation in which anions in the surrounding solution replace coordinated water molecules. Anation of $[(bpy)_2(H_2O)Ru^{III}ORu^{III}(H_2O)(bpy)_2]^{4+}$ by Cl^- (eq 3) has been monitored by ^1H NMR and UV–visible measurements.[147,180] Anation by sulfate was reported in the oxidation of the carboxylato derivative $[(4,4'\text{-}(COOH)_2bpy)_2(H_2O)Ru^{III}ORu^{III}(OH_2)(4,4'\text{-}(COOH)_2bpy)_2]^{4+}$ to $Ru^{IV}ORu^{III}$.[160,161] As mentioned in the previous section, the monosubstituted blue dimer complexes $[(bpy)_2(H_2O)Ru^{III}ORu^{III}(L)(bpy)_2]^{4+}$ (L = pyridine, NH_3) are known.[149]

$$[(bpy)_2(H_2O)Ru^{III}ORu^{III}(OH_2)(bpy)_2]^{4+} + Cl^- \rightleftharpoons [(bpy)_2(H_2O)Ru^{III}ORu^{III}(Cl)(bpy)_2]^{3+} + H_2O \quad (3)$$

Hurst and co-workers have studied the rate of water exchange in $[(bpy)_2(H_2O)Ru^{III}ORu^{III}(OH_2)(bpy)_2]^{4+}$ by using a resonance Raman technique and found $k(23\ ^\circ C) = 7 \times 10^{-3}\ s^{-1}$. Water exchange in $[(bpy)_2(HO)Ru^{IV}ORu^{III}(OH_2)(bpy)_2]^{4+}$ is far slower with $k \leq 10^{-5}\ s^{-1}$.[181]

There is no sign of equilibrium substitution of the noncoordinating anions $X^- = ClO_4^-$, $F_3CSO_3^-$, or NO_3^- for water in $[(bpy)_2(H_2O)Ru^{III}ORu^{III}(OH_2)(bpy)_2]^{4+}$ or in $[(bpy)_2(H_2O)Ru^{IV}ORu^{III}(H_2O)(bpy)_2]^{5+}$. Anation by SO_4^{2-} does occur in the latter but is induced by electron-transfer catalysis. This was shown by the addition of $Ru^{III}ORu^{III}$ to solutions containing $[(bpy)_2(H_2O)Ru^{IV}ORu^{III}(H_2O)(bpy)_2]^{5+}$ ($\lambda_{max} = 446 \pm 2$ nm) in 1 M H_2SO_4. Kinetic studies show that $[(bpy)_2(SO_4)Ru^{IV}ORu^{III}(SO_4)(bpy)_2]^{1+}$ ($\lambda_{max} = 468 \pm$

(170) Okamoto, K.; Miyawaki, J.; Nagai, K.; Matsumura, D.; Nojima, A.; Yokoyama, T.; Kondoh, H.; Ohta, T. *Inorg. Chem.* **2003**, *42*(26), 8682–8689.
(171) Che, C.-M.; Cheng, J. Y. K.; Cheng, K.-K.; Wong, K.-Y. *J. Chem. Soc., Dalton Trans.* **1997**, *13*, 2347–2350.
(172) Gillaizeau-Gauthier, I.; Odobel, F.; Alebbi, M.; Argazzi, R.; Costa, E.; Bignozzi, C. A.; Qu, P.; Meyer, G. J. *Inorg. Chem.* **2001**, *40*(23), 6073–6079.
(173) Gallagher, L. A.; Meyer, T. J. *J. Am. Chem. Soc.* **2001**, *123*(22), 5308–5312.
(174) Liu, F.; Cardolaccia, T.; Hornstein, B. J.; Schoonover, J. R.; Meyer, T. J. *J. Am. Chem. Soc.* **2007**, *129*(9), 2446–2447.
(175) Bae, E.; Choi, W.; Park, J.; Shin, H. S.; Kim, S. B.; Lee, J. S. *J. Phys. Chem. B* **2004**, *108*, 14093–14101.
(176) Berg-Brennan, C.; Subramanian, P.; Absi, M.; Stern, C.; Hupp, J. T. *Inorg. Chem.* **1996**, *35*(12), 3719–3722.
(177) Zhang, H.-T.; Yan, S. G.; Subramanian, P.; Skeens-Jones, L. M.; Stern, C.; Hupp, J. T. *J. Electroanal. Chem.* **1996**, *414*(1), 23–29.
(178) Bunting, J. W. *Adv. Heterocycl. Chem.* **1979**, *25*, 1–82.
(179) Lay, P. A.; Sasse, W. H. F. *Inorg. Chem.* **1985**, *24*(26), 4707–4710.
(180) Ellis, C. D.; Gilbert, J. A.; Murphy, W. R., Jr.; Meyer, T. J. *J. Am. Chem. Soc.* **1983**, *105*(14), 4842–4843.
(181) Yamada, H.; Koike, T.; Hurst, J. K. *J. Am. Chem. Soc.* **2001**, *123*(51), 12775–12780.

2nm) appears by a rate law first order in $Ru^{III}ORu^{III}$ and first order in sulfate with $k(23\ °C) = 1.2 \times 10^{-3}\ M^{-1}\ s^{-1}$. The bis-sulfato product has been characterized by XRD.[182]

The kinetic observations are consistent with rate-limiting substitution, at $Ru^{III}ORu^{III}$,

$$[(bpy)_2(H_2O)Ru^{III}ORu^{III}(OH_2)(bpy)_2]^{4+} + SO_4^{2-} \rightarrow [(bpy)_2(H_2O)Ru^{III}ORu^{III}(SO_4)(bpy)_2]^{2+} + H_2O \quad (4)$$

followed by a rapid second substitution,

$$[(bpy)_2(H_2O)Ru^{III}ORu^{III}(SO_4)(bpy)_2]^{2+} + SO_4^{2-} \rightarrow [(bpy)_2(SO_4)Ru^{III}ORu^{III}(SO_4)(bpy)_2] + H_2O$$

and electron transfer,

$$[(bpy)_2(SO_4)Ru^{III}ORu^{III}(SO_4)(bpy)_2] + [(bpy)_2(H_2O)Ru^{IV}ORu^{III}(OH_2)(bpy)_2]^{5+} \rightarrow [(bpy)_2(SO_4)Ru^{IV}ORu^{III}(SO_4)(bpy)_2]^{+} + [(bpy)_2(H_2O)Ru^{III}ORu^{III}(OH_2)(bpy)_2]^{4+}$$

This reaction is driven by the difference in redox potentials between the $[(H_2O)RuORu(OH_2)]^{5+/4+}$ and $[(SO_4)RuORu(SO_4)]^{+/0}$ couples.[182]

There is no sign of electron-transfer-induced substitution for the noncoordinating anions $X^- = ClO_4^-$, $F_3CSO_3^-$, or NO_3^- but anated intermediates do play a role in water oxidation. This is evidenced by the appearance of $[(bpy)_2(HO)Ru^{IV}ORu^{IV}(ONO_2)(bpy)_2]^{4+}$ along with $Ru^{V}ORu^{IV}$ late in catalytic cycles in 1 M HNO_3 and in the disproportionation of $Ru^{V}ORu^{IV}$ under the same conditions.

The anion-containing complex is characterized by a bridge-based $d_\pi \rightarrow d_{\pi^*}$ absorption band at $\lambda_{max} = 455$ nm in 1 M H^+ and by low-energy, interconfigurational $d_\pi \rightarrow d_\pi$ bands at 832 and 1164 nm. It is in acid–base equilibrium with the deprotonated form $[(bpy)_2(O)Ru^{V}ORu^{III}(ONO_2)(bpy)_2]^{3+}$ with $\lambda_{max} = 489$ nm. This and related intermediates inhibit further water oxidation and build up in solution as the catalytic rate decreases and Ce^{IV} is depleted. Ultimately, NO_3^- is lost from the coordination sphere of the intermediate, water is oxidized, and $Ru^{IV}ORu^{III}$ reappears as the final product (section 5.3).

As discussed in sections 5.3 and 5.4, there is also evidence for the intervention of transient kinetic intermediates in the cerium(IV) oxidation of $Ru^{IV}ORu^{III}$ in 1 M $HClO_4$ and 1 M CF_3CSO_3H.

(4) Overoxidation. Decomposition by Ligand Loss and Dioxido Formation. Potential complications from overoxidation of $[(tpy)(H_2O)(O)Ru^{V}ORu^{V}(O)(H_2O)(tpy)]^{4+}$ to $Ru^{VI}ORu^{V}$ accompanied by loss of the μ-oxo bridge were mentioned in section 4.3. Ligand labilization appears in higher oxidation states presumably by coordination expansion by added H_2O or OH^- by use of available d orbitals in d^4, d^3, or d^2 Ru^{IV}, Ru^{V}, or Ru^{VI} complexes.[183] Coordination expansion triggers chelate ring opening and ligand loss. Examples include bpy loss and cis to trans isomerization in *cis*-$[Ru^{VI}(bpy)_2(O)_2]^{2+}$ to give *trans*-$[Ru^{VI}(bpy)(H_2O)_2(O)_2]^{2+}$ [111] and oxidative decomposition of $[(bpy)_2(O)Os^{V}OOs^{V}(O)(bpy)_2]^{4+}$ to give *trans*-$[Os^{VI}(bpy)(O)_2(OH_2)_2]^{2+}$.[166] Overoxidation may play a significant role in catalyst deactivation in the presence of large excesses of oxidant.[31]

(5) Oligomerization. An additional complication appears for the tpy dimer arising from oligomerization to give analogs of $[(bpy)_2(H_2O)Ru^{III}ORu^{IV}(bpy)_2ORu^{III}(OH_2)(bpy)_2]^{6+}$,[138] mentioned in section 3, and even higher oligomers.[184] Oligomerization in this case is facile because of the extra water molecules in the coordination sphere of the dimer, which can be displaced with μ-oxo bridge formation.[167]

(6) Reductive Loss of the μ-Oxo Bridge. Although polypyridyl complexes of ruthenium(II) are typically coordinatively stable, reduction of the blue dimer results in loss of the μ-oxo bridge, $[(bpy)_2(H_2O)Ru^{III}ORu^{III}(H_2O)(bpy)_2]^{4+} + H_2O + 2H^+ \xrightarrow{+2e^-} 2Ru(bpy)_2(H_2O)_2^{2+}$.[44,166] This is a general reaction for μ-oxo-bridged complexes of ruthenium(III) and osmium(III). It is another manifestation of strong electronic coupling across the μ-oxo bridge (section 3.2). According to the orbital energy scheme in Figure 9, reduction of $[(bpy)_2(H_2O)Ru^{III}ORu^{III}(H_2O)(bpy)_2]^{4+}$ occurs at d_{π^*} orbitals, which are antibonding with regard to the bridge. The addition of electrons causes a breakdown in the μ-oxo-bridged structure.

5. The Blue Dimer: Oxidative Activation and Water Oxidation

It was important to show that the blue dimer and structurally related derivatives were capable of acting as chemical or electrochemical catalysts for water oxidation, in solution.[43–46,161–163,165,185] By inference, the highest oxidation state, $Ru^{V}ORu^{V}$, appeared to be a potent catalyst for water oxidation. Given the formulation, $[(bpy)_2(O)Ru^{V}ORu^{V}(O)(bpy)_2]^{4+}$ for $Ru^{V}ORu^{V}$, a straightforward strategy for meeting the $4e^-/4H^+$ PCET demands of the O_2/H_2O couple presented itself based on stepwise e^-/H^+ oxidation of $[(bpy)_2(H_2O)Ru^{III}ORu^{III}(H_2O)(bpy)_2]^{4+}$ to $[(bpy)_2(O)Ru^{V}ORu^{V}(O)(bpy)_2]^{4+}$.

The initial strategy for oxidative activation pursued by Moyer had paid off but by using ligand bridging of two sites to achieve $4e^-/4H^+$ oxidation.

The mechanism remained to be established. What step or steps are rate limiting? How can the catalyst be improved to decrease reaction barriers? What are the details of the O---O bond-forming step? Are there multiple mechanisms for water oxidation or just one?

5.1. Oxo Reactivity. The higher oxidation states $[(bpy)_2(O)Ru^{V}ORu^{V}(O)(bpy)_2]^{4+}$ and $[(bpy)_2(O)Ru^{V}ORu^{IV}(O)(bpy)_2]^{3+}$ are oxo or oxido complexes expected to share the reactivity of terminal oxo complexes such as $[Ru^{IV}(bpy)_2(py)(O)]^{2+}$. Enhanced reactivity is expected on thermodynamic grounds because $E^{o\prime} > 1.5$ V vs NHE for the $2e^-/3H^+$ couple $[(O)Ru^{V}ORu^{IV}(O)]^{3+}/[(HO)Ru^{IV}ORu^{III}(OH_2)]^{4+}$ at pH = 1 compared to 1.06 V for the $2e^-/2H^+$ couple $Ru^{IV}{=}O^{2+}/Ru^{II}OH_2^{2+}$.

(182) Concepcion, J. J.; Jurss, J. W.; Liu, F.; Cardolaccia, T., work in progress.
(183) Lay, P. A.; Sasse, W. H. F. *Inorg. Chem.* **1985**, *24*(26), 4707–4710.
(184) Jurss, J. W.; Cardolaccia, T. , work in progress.

There is indirect evidence for enhanced oxo reactivity. It is based on electrocatalyzed oxidation of carbon electrodes and consumption of cerium(IV) without water oxidation in aqueous solutions containing the blue dimer in which solvent–water has not been carefully prepurified.[44,164]

Quantitative reactivity comparisons have been made between $Ru^{IV}(bpy)_2(py)(O)]^{2+}$ and the μ-oxo complexes $[(bpy)_2(O)Ru^{V}ORu^{IV}(O)(bpy)_2]^{3+}$ and $[(bpy)_2(O)Ru^{V}ORu^{III}(py)(bpy)_2]^{+}$. Rate constant measurements for the oxidation of a series of alcohols and olefins, e.g., isopropyl alcohol and $CH_2CH{=}CH(CH_2)_2COO^-$, in water at 25 °C revealed enhanced reactivities of ~300 toward alcohol oxidation and of ~40 toward olefin oxidation.[168]

Cl^- Oxidation. *trans*-$[Ru^{VI}(bpy)_2(O_2)]^{2+}$, $[(bpy)_2(O)Ru^{V}ORu^{V}(O)(bpy)_2]^{4+}$, and $[(bpy)_2(O)Ru^{V}ORu^{III}(py)(bpy)_2]^{4+}$ all react rapidly with Cl^- to give either Cl_2 or HOCl depending on the pH.[74,80,168,180] The potentials for the metal complex and Cl_2/Cl^- and $HOCl/Cl^-$ couples are close, and the reactions are reversible by varying the pH. The reaction in eq 5 is at equilibrium at pH = 3.5. The blue dimer also catalyzes the decomposition of HOCl, $2HOCl \rightarrow 2Cl^- + O_2 + 2H^+$ ($\Delta G° = -24$ kcal mol^{-1}), by a coupled redox cycle involving the $Ru^{V}ORu^{IV}/Ru^{IV}ORu^{III}$ couple.

$$[(bpy)_2(OH)Ru^{IV}ORu^{III}(OH_2)(bpy)_2]^{4+} + HOCl \rightarrow [(bpy)_2(O)Ru^{V}ORu^{IV}(O)(bpy)_2]^{3+} + Cl^- + 2H^+ + H_2O \quad (5)$$

Electrocatalytic Cl^- oxidation to Cl_2-HOCl also occurs for the blue dimer when it is ion-exchanged into sulfonated polystyrene and Nafion polymeric films on glassy carbon electrodes.[74,80] Catalysis in these film environments occurs by as many as 26 000 turnovers but, ultimately, is inhibited by apparent "anation" with catalyst binding to the sulfonate groups in the films.

5.2. Oxidative Activation. Insight into oxidative activation of the blue dimer is available from the electrochemical data in Figure 12 and by mixing experiments with Ce(IV). In summary, (i) $Ru^{IV}ORu^{IV}$, $Ru^{V}ORu^{IV}$ and $Ru^{V}ORu^{V}$ are all thermodynamically capable of water oxidation, (ii) $Ru^{IV}ORu^{IV}$ plays a role as a kinetic intermediate but is thermodynamically unstable toward disproportionation, and (iii) below pH = 2, $Ru^{V}ORu^{IV}$ is also unstable toward disproportionation into $Ru^{V}ORu^{V}$ and $Ru^{IV}ORu^{III}$. It also undergoes slow water oxidation.

Reduction potentials and a PCET summary are given in Scheme 1. For the blue dimer in 1 M H^+, the apparent proton release pattern upon oxidation is 1:1:2:0. In the OEC of PSII, the pattern is 1:0:1:2 (section 6).

The results of a kinetics study at 25 °C in 1 M $HClO_4$, with application of global data analysis (to discern multiply absorbing species), are summarized in Scheme 2.[162] The abbreviations that appear are those used previously with $[(bpy)_2(H_2O)Ru^{III}ORu^{III}(H_2O)(bpy)_2]^{4+}$ abbreviated as $Ru^{III}ORu^{III}$, for example.

Scheme 2 is useful in summarizing the complex set of coupled reactions and key intermediates that play a role in the oxidative activation of the blue dimer: (1) $Ru^{V}ORu^{V}$ is the water oxidation catalyst *but does not appear in the catalytic steady state* (see below). It is formed by Ce(IV) oxidation of $Ru^{V}ORu^{IV}$ with $k(23\ °C) \geq 10^2 M^{-1}\ s^{-1}$ and $k(23\ °C) = 80 \pm 2\ M^{-1}\ s^{-1}$ in HNO_3.[182] (2) $Ru^{V}ORu^{V}$ reacts with water with $k \geq 1\ s^{-1}$ if the reaction is first order in $[Ru^{V}ORu^{V}]$ and $k \geq 2 \times 10^4\ M^{-1}\ s^{-1}$ if the reaction is second order.[162] (3) There is rapid electron-transfer exchange between oxidation states; the rate constant for the reaction between $Ru^{III}ORu^{III}$ and $Ru^{V}ORu^{IV}$ in eq g in Scheme 2 is $\geq 10^6\ M^{-1}\ s^{-1}$.

Initial oxidation of $Ru^{III}ORu^{III}$ to $Ru^{V}ORu^{IV}$ by cesium(IV) occurs with an inverse isotope effect, $k(H_2O)/k(D_2O) = 0.87$.[162] Its appearance can be explained by PCET and the preliminary acid–base equilibrium, $[(H_2O)Ru^{III}ORu^{III}(OH_2)]^{4+} \rightleftharpoons [(HO)Ru^{III}ORu^{III}(OH_2)]^{3+} + H^+$, followed by Ce(IV) oxidation of $[(HO)Ru^{III}ORu^{III}(OH_2)]^{3+}$. For the analogous acid–base equilibrium for $[(H_2O)Ru^{IV}ORu^{III}(OH_2)]^{5+}$, $K_a(H_2O)/K_a(D_2O) = 1.6$.[169] An inverse isotope effect of this magnitude for $pK_{a,1}$ in $[(H_2O)Ru^{III}ORu^{III}(OH_2)]^{4+}$ would account for the inverse kinetic isotope effect.

Because of the litany of complications arising from overoxidation, oligomerization, etc. (section 4.4), $[(tpy)(H_2O)_2Ru^{III}ORu^{III}(H_2O)_2(tpy)]^{4+}$ is not an effective catalyst for water oxidation, managing only a single turnover under

Scheme 1. PCET and $E°'$ values (vs NHE) in 1 M $HClO_4$.[44]

	$E°'$, V
$Ru^{III}ORu^{III} \rightarrow Ru^{IV}ORu^{III}$	
$[(H_2O)Ru^{III}ORu^{III}(OH_2)]^{4+} \xrightarrow{-e^-,-H^+} [(HO)Ru^{IV}ORu^{III}(OH_2)]^{4+}$ ($\rightleftharpoons [(H_2O)Ru^{IV}ORu^{III}(OH_2)]^{5+} + H^+$)	1.06
$Ru^{IV}ORu^{III} \rightarrow Ru^{IV}ORu^{IV}$	
$[(HO)Ru^{IV}ORu^{III}(OH_2)]^{4+} \xrightarrow{-e^-,-H^+} \{[(HO)Ru^{IV}ORu^{IV}(OH]^{4+}\}$	>1.55
$Ru^{IV}ORu^{IV} \rightarrow Ru^{V}ORu^{IV}$	
$\{[(HO)Ru^{IV}ORu^{IV}(OH]^{4+}\} \xrightarrow{-e^-,-2H^+} [(O)Ru^{V}ORu^{IV}(OH)]^{4+}$ ($\rightleftharpoons [(O)Ru^{V}ORu^{IV}(O)]^{3+} + H^+$)	>1.55
$Ru^{V}ORu^{IV} \rightarrow Ru^{V}ORu^{V}$	
$[(O)Ru^{V}ORu^{IV}(O)]^{3+} \xrightarrow{-e^-} [(ORu^{V}ORu^{V}(O)]^{4+}$.	1.42

Scheme 2. Mechanism of Water Oxidation by the Blue Dimer at 25 °C in 1 M $HClO_4$ (Reprinted from ref 162. Copyright 2000 American Chemical Society.)

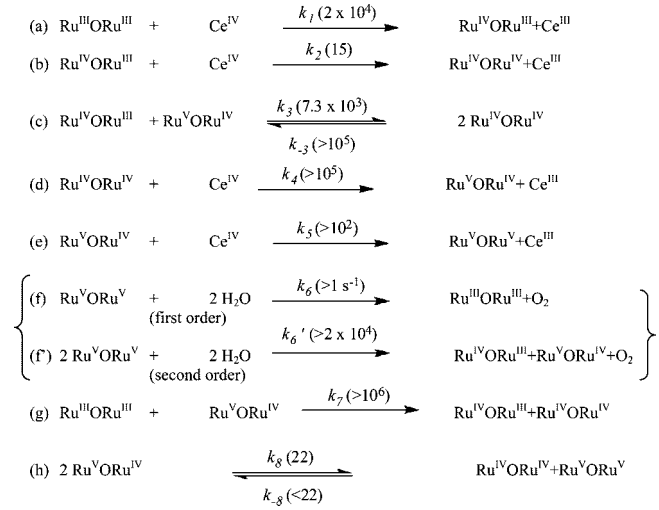

(185) Yagi, M.; Yamase, K.; Kaneko, M. *Electrochim. Acta* **2002**, *47*(12), 2019–2024.

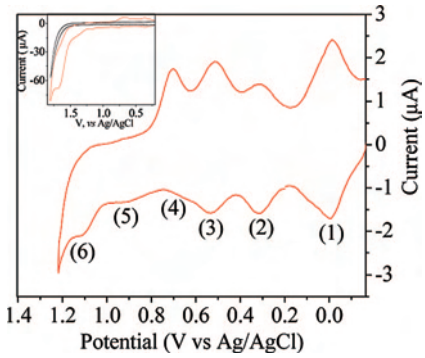

Figure 13. Cyclic voltammogram of $[(tpy\text{-}PO_3H_2)(H_2O)_2RuORu(H_2O)_2(tpy\text{-}PO_3H_2)]^{4+}$ on ITO in a pH = 5.0 buffer solution (I = 0.1 M, CH_3CO_2H/CH_3CO_2Na) at a scan rate of 40 mV s^{-1} vs Ag/AgCl (0.197 V vs NHE). Also shown in the inset is the cyclic voltammogram of the ITO background (black line) at the same scan rate. Reprinted from ref 174. Copyright 2007 American Chemical Society.

maximal conditions.[167] Nonetheless, it was revealing to study oxidative activation of the phosphonated derivative, $[(tpy\text{-}PO_3H_2)(H_2O)_2RuORu(H_2O)_2(tpy\text{-}PO_3H_2)]^{4+}$, on oxide surfaces: ITO, ZrO_2, TiO_2, and SnO_2 (section 4.3).[174] In Figure 13 is shown a cyclic voltammogram on ITO, which illustrates sequential 1e$^-$ oxidations from $Ru^{III}ORu^{III} \xrightarrow{-e^-} Ru^{IV}ORu^{III}$ (wave 2) to $Ru^{V}ORu^{IV} \xrightarrow{-e^-} Ru^{V}ORu^{V}$ (wave 5) and $Ru^{V}ORu^{V} \xrightarrow{-e^-} Ru^{VI}ORu^{V}$ (inset). The increased background currents for the latter two waves is due to catalytic water oxidation.[174] Reduction occurs at the wave labeled (1) in Figure 13. On slower time scales, it results in reductive cleavage of the Ru−O−Ru bridge, a reaction mentioned for the blue dimer in section 4.4, $[(tpy\text{-}PO_3H_2)(H_2O)_2RuORu(H_2O)_2(tpy\text{-}PO_3H_2)]_2^{4+} \xrightarrow{+2e^-,\ 2H^+,\ H_2O} 2[(tpy)PO_3H_2)(Ru(H_2O)_3]^{2+}$.

One advantage of surface attachment is the ability to study water oxidation over an extended pH range, in this case up to pH = 7. At higher pHs, the adsorbed-bound complex is displaced from oxidic surfaces. Another advantage, on surfaces with less than complete monolayer surface coverages, is site isolation without complications from cross surface reactions.[173]

5.3. Water Oxidation. UV–visible spectral changes with time under catalytic conditions with × 30 eq of Ce(IV) added to $[(bpy)_2(H_2O)Ru^{IV}ORu^{III}(H_2O)(bpy)_2]^{5+}$ in 1 M HNO_3 and 0.5 M HSO_3CF_3 are shown in Figure 14.

In 1 M HNO_3 with Ce^{IV} in excess, $Ru^{V}ORu^{IV}$ (λ_{max} = 482 ± 2 nm) appears at the catalytic steady state. The time-dependent changes below 400 nm are largely due to reduction of Ce^{IV} with λ_{max} = 294 nm. At the first observation time of 10 s, ~60% of the added Ce^{IV} had been consumed.

The absorbance−time traces reveal that the addition of 30 equiv of Ce^{IV} to $Ru^{IV}ORu^{III}$ (λ_{max} = 445 ± 2 nm; ϵ = 22 500 M^{-1} cm^{-1}) results in rapid oxidation to $Ru^{V}ORu^{IV}$ (λ_{max} = 482 ± 2 nm, ϵ = 14 500 M^{-1} cm^{-1}) with k(23 °C) = 2 × 10^3 M^{-1} s^{-1}. Under these conditions, there are both protonated and unprotonated forms of $Ru^{V}ORu^{IV}$ in acid–base equilibrium, $[(bpy)_2(O)Ru^{V}ORu^{IV}(OH)(bpy)_2]^{4+} \rightleftharpoons [(bpy)_2(O)Ru^{V}ORu^{IV}(O)(bpy)_2]^{3+} + H^+$ (K_a ~ 0.3), assuming that an oxo group is protonated (section 4.3).

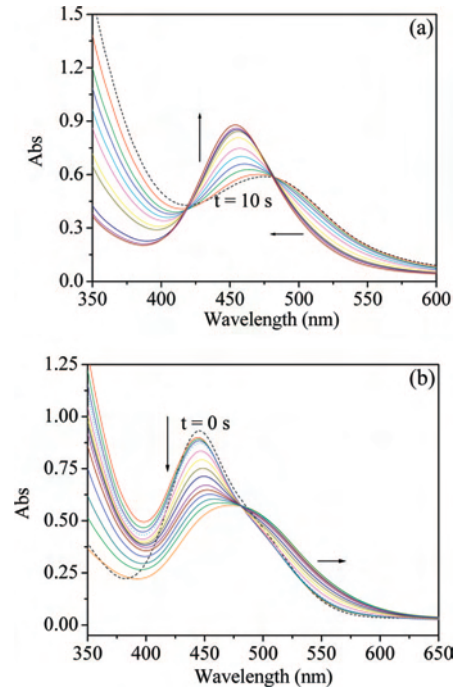

Figure 14. Absorbance−time traces following the addition of 30 equiv of Ce^{IV} to $[(bpy)_2(H_2O)Ru^{IV}ORu^{III}(H_2O)(bpy)_2]^{5+}$ (5 × 10^{-5} M) in (a) 1 M HNO_3 and (b) 0.5 M CF_3SO_3H. (a) The dashed line trace is the spectrum 10 s after the addition of Ce^{IV}. Successive traces, indicated by the direction of the arrows, were recorded at 30, 62, 97, 155, 255, 542, 1030, 2040, 3060, and 4340 s following Ce^{IV} addition. (b) The initial spectrum of $[(bpy)_2(H_2O)Ru^{IV}ORu^{III}(H_2O)(bpy)_2]^{5+}$ is shown by the dashed line trace. Successive traces, indicated by the direction of the arrows, were recorded at 14, 55, 90, 120, 175, 210, 238, 272, 333, 420, 660, 935, 1170, and 1612 s, following the addition of Ce^{IV}.

Once formed, $Ru^{V}ORu^{IV}$ remains the dominant form at the catalytic steady state. Loss of Ce^{IV}, monitored at 360 nm, is first order in both Ce^{IV} and $Ru^{V}ORu^{IV}$ with k(23 °C) = 80 ± 2 M^{-1} s^{-1} consistent with a catalytic cycle rate limited by oxidation of $Ru^{V}ORu^{IV}$ to $Ru^{V}ORu^{V}$. At the end of the catalytic cycle, with Ce^{IV} nearly depleted (~80%), a new species appears characterized by λ_{max} = 455 ± 2 nm with λ_{max} = 832 and 1164 nm in the near-IR. It grows at the expense of $Ru^{V}ORu^{IV}$ as Ce^{IV} is further consumed.

After Ce^{IV} is completely consumed, and on a far slower time scale, the intermediate at 455 nm returns to $[(bpy)_2(H_2O)Ru^{IV}ORu^{III}(OH_2)(bpy)_2]^{4+}$ in a first-order reaction with k(23 °C) = 8 × 10^{-5} s^{-1}.

Stepwise addition of 2 equiv of Fe^{2+} as a reducing agent to solutions containing the long-lived intermediate at λ_{max} = 455 nm leads to quantitative reduction to the blue dimer, $[(bpy)_2(H_2O)Ru^{III}ORu^{III}(OH_2)(bpy)_2]^{4+}$. Increasing the pH to 2 causes reversible spectral shifts from λ_{max} = 455, 832, and 1164 nm to 489 and 1154 nm.[182] The results of a spectrophotometric pH titration were consistent with an acid–base equilibrium with pK_a = 1.4. Asuming that anation has occurred, the acid–base equilibrium is $[(bpy)_2(HO)Ru^{IV}ORu^{IV}(NO_3)(bpy)_2]^{4+}$ (λ_{max} = 455 nm) ⇌ $[(bpy)_2(O)Ru^{V}ORu^{III}(NO_3)(bpy)_2]^{3+}$ (λ_{max} = 489 nm) + H^+.[182]

Based on these observations, the long-lived intermediate in 1 M HNO_3 appears to be the anated complex, $[(bpy)_2(HO)Ru^{IV}ORu^{IV}(ONO_2)(bpy)_2]^{3+}$. The formulation of oxidation states in the two forms of the intermediate is somewhat arbitrary but consistent with the known complex $[(bpy)_2(O)Ru^{V}ORu^{III}(py)(bpy)_2]^{4+}$ for the base form and the DFT result in section 4.3 favoring the formulation $[(bpy)_2(HO)Ru^{IV}ORu^{IV}(OH)(bpy)_2]^{4+}$ over $[(bpy)_2(O)Ru^{V}ORu^{III}(OH_2)(bpy)_2]^{4+}$ for the acid form (section 4.3).

It is significant that the initial consumption of Ce^{IV} is rapid, with ~60% consumed by our first observation time at 10–15 s. Rapid Ce^{IV} consumption shows that blue dimer catalytic water oxidation can be rapid but is clearly medium-dependent given the relatively slow catalysis reported earlier by Hurst et al. in 0.5 M CF_3SO_3H and by Binstead et al. in 1 M $HClO_4$.[162,164,169,181]

Application of spectral deconvolution techniques and the program SPECFIT was used to study the sequence of reactions that occurs on longer time scales after Ce^{IV} was consumed. Based on this analysis, the sequence is $[(bpy)_2(O)Ru^{V}ORu^{IV}(OH)(bpy)_2]^{3+}$ (λ_{max} = 488 nm) → $[(bpy)_2(HO)Ru^{IV}ORu^{IV}(ONO_2)(bpy)_2]^{3+}$ (λ_{max}= 455 nm) → $[(bpy)_2(H_2O)Ru^{IV}ORu^{III}(OH_2)(bpy)_2]^{5+}$ (λ_{max} = 446 nm). Under catalytic conditions, with a large excess of Ce^{IV}, there is also evidence that some anated intermediate forms during the catalytic cycle.

A different observation is made in 0.5 M CF_3SO_3H (Figure 14b), consistent with earlier observations by Hurst et al.[164,169,181] At the initial stages in the catalytic steady state in this medium, a new species appears with $\lambda_{max} = 445 \pm 2$ nm having a slightly increased molar absorptivity compared to $[(bpy)_2(H_2O)Ru^{IV}ORu^{III}(OH_2)(bpy)_2]^{5+}$ at λ_{max} = 446 ± 2 nm. It is distinguished from $Ru^{IV}ORu^{III}$ by a shift in the characteristic $d_\pi \rightarrow d_{\pi^*}$ interconfigurational band from 1173 to 744 nm ($\epsilon \sim 900\ M^{-1}\ cm^{-1}$).

The same intermediate forms rapidly upon the addition of Ce^{IV} (×1) to $Ru^{IV}ORu^{III}$ in 0.5 or 1 M CF_3CSO_3H. When generated stoichiometrically, it subsequently disappears with k(0.5 M CF_3CSO_3H, 23 °C) = $1 \times 10^{-2}\ s^{-1}$ to give $Ru^{IV}ORu^{III}$ and $Ru^{V}ORu^{IV}$. Under catalytic conditions with excess Ce^{IV}, it is replaced early in the catalytic cycle by a second intermediate with λ_{max} = 451 and 750 nm, which is the dominant form during the rest of the catalytic cycle. At the end of the catalytic cycle with Ce^{IV} completely consumed, the intermediate returns to $Ru^{IV}ORu^{III}$ by a stepwise reaction (see below).

Kinetic monitoring of Ce^{IV} loss during the catalytic cycle reveals sequential kinetic regimes occurring on different time scales.[182] The more rapid process is first order in initially added $Ru^{IV}ORu^{III}$ and zero order in Ce^{IV} with k(0.5 M CF_3CSO_3H, 23 °C) = $4 \times 10^{-2}\ s^{-1}$. The slower process is also zero order in Ce^{IV} and first order in added $Ru^{IV}ORu^{III}$ with k(23 °C) ~ $7 \times 10^{-3}\ s^{-1}$.

Our observations and those made earlier[162,164,181] show that catalytic water oxidation is highly medium-dependent. This conclusion is reinforced by measurements in 0.1 M HNO_3 or 0.1 CF_3CSO_3H where still a different observation is made. Under these conditions, the addition of Ce^{IV} (×2) results in the rapid appearance of $Ru^{V}ORu^{IV}$ at λ_{max} = 488 nm with k(0.1 M HNO_3, 23 °C) = $4.5 \times 10^3\ M^{-1}\ s^{-1}$. The addition of a third 1 equiv of Ce^{IV} results in further oxidation of $Ru^{V}ORu^{IV}$ to an intermediate with λ_{max} = 482 and 850 nm. This reaction occurs with k(0.1 M HNO_3, 23 °C) = $2.2 \times 10^2\ M^{-1}\ s^{-1}$. Increasing the acid concentration to 1 M causes λ_{max} for the intermediate to shift to 451 ± 2 nm.

The addition of varying amounts of Fe^{2+}(aq) to solutions containing the intermediate at λ_{max} = 482 nm showed that Fe^{2+}(aq) (×4) were required to reduce it completely, intermediate (482 nm) $\xrightarrow{+4Fe^{2+}(aq)}$ $[(bpy)_2(H_2O)Ru^{III}ORu^{III}(OH_2)(bpy)_2]^{4+}$. This observation is consistent with an intermediate that it is oxidized by $4e^-$ compared to $Ru^{II}{}_{1}ORu^{III}$. A closely related observation has been in 0.5 M CF_3SO_3H by Hurst et al. for an intermediate formulated as $Ru^{V}ORu^{V}$ with λ_{max} = 482 nm. It was formed by electrochemical oxidation of $Ru^{IV}ORu^{III}$ or by its oxidation by using excess Ce^{IV}. This intermediate was reduced to $Ru^{III}ORu^{III}$ by $Os(bpy)_3^{2+}$ (×4).[164,169]

Once formed by stoichiometric oxidation, the intermediate at 482 nm disappears with k(0.1 M HNO_3, 23 °C) = $2.0 \times 10^{-3}\ s^{-1}$. Its probable nature and its decomposition reaction will be discussed in section 5.4.

In 0.1 M HNO_3 under catalytic conditions with Ce^{IV} (×30) added, loss of Ce^{IV} at early times after mixing is rapid, converting $Ru^{IV}ORu^{III}$ into the intermediate at λ_{max} = 482 nm. Under these conditions, loss of Ce^{IV} is first order both in Ce^{IV} and in initially added $Ru^{IV}ORu^{III}$ with k(0.1 M HNO_3, 23 °C) = $1.8 \times 10^2\ M^{-1}\ s^{-1}$. As Ce^{IV} is depleted, $Ru^{V}ORu^{IV}$ appears at the catalytic steady state in competition with the intermediate at 482 nm. It increases at the expense of the intermediate as the Ce^{IV} concentration decreases. Ultimately, $Ru^{V}ORu^{IV}$ and $[(bpy)_2(HO)Ru^{IV}ORu^{IV}(ONO_2)(bpy)_2]^{4+}$ (~30%) are left in the solution. When generated stoichiometrically in 0.1 M HNO_3, $Ru^{V}ORu^{IV}$ returns to $Ru^{IV}ORu^{III}$ by second-order, equal-concentration kinetics with k(0.1 M HNO_3, 23 °C) = $6.8\ M^{-1}\ s^{-1}$.

Water Oxidation by $Ru^{V}ORu^{IV}$. $Ru^{V}ORu^{IV}$ also oxidizes water (eq 6).[168] Loss of $Ru^{V}ORu^{IV}$ is independent of pH from pH = 2.5−6 and second order in $Ru^{V}ORu^{IV}$ with k (25.0 ± 0.1 °C, I = 0.1) = $5.5 \times 10^{-4}\ M^{-1}\ s^{-1}$ in a $H_2PO_4^-/HPO_4^{2-}$ buffer.

$$2[(bpy)_2(O)Ru^{V}ORu^{IV}(O)(bpy)_2]^{3+} + 2H_2O + H^+ \rightarrow 2[(bpy)_2(HO)Ru^{IV}ORu^{III}(OH_2)(bpy)_2]^{4+} + O_2 \quad (6)$$

In acidic solutions, the loss of $Ru^{V}ORu^{IV}$ is greatly accelerated. This reaction also occurs by second-order, equal-concentration kinetics with k(1 M HNO_3, 23 °C) = $20\ M^{-1}\ s^{-1}$. When $Ru^{V}ORu^{IV}$ is generated stoichiometrically in 0.1 M HNO_3, the product is $Ru^{IV}ORu^{III}$. In 1 M HNO_3, the product is a ~1:1 mixture of $Ru^{IV}ORu^{III}$ and the anated intermediate $[(bpy)_2(HO)Ru^{IV}ORu^{IV}(NO_3)(bpy)_2]^{4+}$.

5.4. Water Oxidation. Isotopic Labeling. Key mechanistic issues remain to be resolved including the nature of the O---O coupling step or steps. This point was explored by ^{18}O isotopic labeling. In these experiments, $[(bpy)_2(H_2{}^{18}O)Ru^{III}ORu^{III}(^{18}OH_2)(bpy)_2]^{4+}$ was oxidized by Ce^{IV} in water

of normal isotopic composition before H_2O exchange with solvent had occurred. Hurst et al. have shown that there is no complication from ^{18}O exchange with the μ-oxo bridge under these conditions.[181]

The initial labeling experiments were conducted in 0.1 M CF_3SO_3H with sufficient Ce^{IV}added to oxidize the dimer only to $Ru^{V}ORu^{IV}$ in order to ensure labeling from a single oxidation cycle. In retrospect, they reflect oxidation of water by $[(bpy)_2(O)Ru^{V}ORu^{IV}(O)(bpy)_2]^{3+}$ (eq 6) rather than oxidation by $Ru^{V}ORu^{V}$.

The labeling experiment gave 13% $^{18}O^{18}O$, 64% $^{16}O^{18}O$, and 23% $^{16}O^{16}O$. The appearance of $^{18}O^{18}O$ as a product was significant in revealing O---O coupling by either intramolecular or bimolecular pathways (eq 7).[144] Subsequent cross electron transfer to give the final $Ru^{IV}ORu^{III}$ product, e.g., $[(^{18}O)Ru^{V}ORu^{IV}(^{18}O)]^{3+} + 2[(H_2{}^{16}O)Ru^{III}ORu^{III}(^{16}OH_2)]^{4+} \xrightarrow{+H^+} [(^{18}HO)Ru^{IV}ORu^{III}(^{18}OH_2)]^{4+} + 2[(^{16}HO)Ru^{IV}ORu^{III}(^{16}OH_2)]^{4+}$, followed by exchange between oxidation states, $[(^{18}O)Ru^{V}ORu^{IV}(^{18}O)]^{4+} + [(^{16}HO)Ru^{IV}ORu^{III}(^{16}OH_2)]^{4+} \rightarrow [(^{18}HO)Ru^{IV}ORu^{III}(^{18}OH_2)]^{4+} + [(^{16}O)Ru^{V}ORu^{IV}(^{16}O)]^{3+}$, would lead to scrambling of the ^{18}O label.

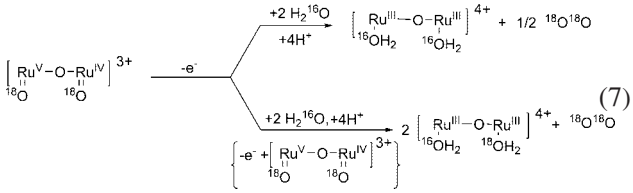

(7)

Based on the kinetics study described in section 5.3, $Ru^{V}ORu^{IV}$ disappears by second-order, equal-concentration kinetics. This rate law is consistent either with the initial disproportionation, $2Ru^{V}ORu^{IV} \rightarrow Ru^{IV}ORu^{III} + Ru^{V}ORu^{V}$, followed by water oxidation by $Ru^{V}ORu^{V}$, or by bimolecular O---O coupling, $[(O)Ru^{IV}ORu^{V}O---ORu^{V}ORu^{IV}(O)]^{6+}$.

Analysis of the labeling data ruled out intramolecular coupling as the sole pathway for exchange in any case.[144] A later study on the oxidation of the ^{15}N-labeled ammine analogue, $[(bpy)_2(H_3{}^{15}N)Ru^{III}ORu^{III}(^{15}NH_3)(bpy)_2]^{4+}$, in the presence of $[(bpy)_2(H_3{}^{14}N)Ru^{III}ORu^{III}(^{14}NH_3)(bpy)_2]^{4+}$ did reveal $^{15}N^{15}N$ and $^{14}N^{14}N$ as the sole N_2 products with no $^{15}N^{14}N$ (eq 8).[186] This result could only be explained by invoking intramolecular N---N coupling between Ru sites across the μ-oxo bridge.

$$[(bpy)_2(H_3N^{15})Ru^{III}ORu^{III}(^{15}NH_3)(bpy)_2]^{4+} \xrightarrow{-6e^-,\ -6H^+,\ +2H_2O} [(bpy)_2(H_2O)Ru^{III}ORu^{III}(OH_2)(bpy)_2]^{4+} + {}^{15}N^{15}N \quad (8)$$

A different result was obtained in a later series of ^{18}O-labeling experiments by Hurst et al., who used excess Ce^{IV} in 0.5 M HSO_3CF_3 under conditions *where water oxidation occurs through* $Ru^{V}ORu^{V}$. They monitored the isotopic composition of evolved oxygen as a function of time through a first catalytic turnover. At 28 °C, they observed comparable amounts of $^{16}O^{18}O$ and $^{16}O^{16}O$ and negligible $^{18}O^{18}O$.[169]

Scheme 3. Proposed Mechanism for Water Oxidation by $Ru^{V}ORu^{V}$ Following Yang and Baik[143] (Transition States Are Bracketed)

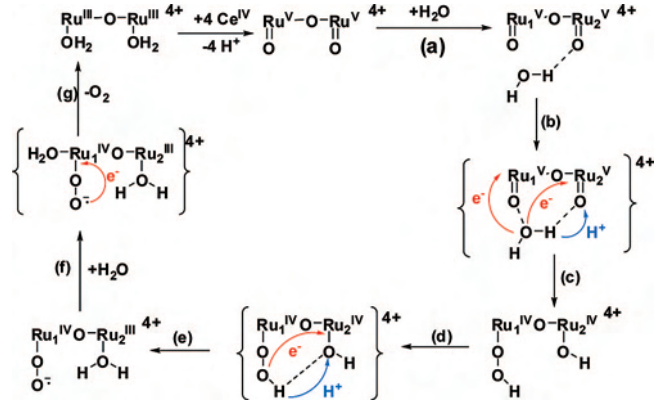

The isotopic ratio was found to be temperature-dependent. The data were treated by reaction rate theory, which gave, for the $^{16}O^{16}O/^{16}O^{18}O$ ratio, $\Delta(\Delta S^{\pm}) \approx 17$ eu and $\Delta(\Delta H^{\pm} \approx 5.3$ kcal mol^{-1}, suggesting competing pathways for oxygen evolution having significantly different microscopic origins.[164,169]

5.5. Water Oxidation Mechanism. Mechanistic pathways accounting for the appearance of $^{16}O^{18}O$ have been proposed involving the initial attack of water on one of the Ru=O sites in $[(O)Ru^{V}ORu^{V}(O)]^{4+}$.[164,168,169] These suggestions have been examined by application of DFT calculations by Yang and Baik, who have proposed a complex series of reactions and intermediates that ultimately lead to O_2 formation and the reappearance of $[(bpy)_2(H_2O)Ru^{III}O-Ru^{III}(OH_2)(bpy)_2]^{4+}$.[143]

Although the detailed mechanism resulting from these calculations is of value, it should be appreciated that the analysis was based on the assumption of relatively weak Ru−O−Ru electronic coupling across the μ-oxo bridge. With this model, it is not possible to account quantitatively for structural changes that occur upon oxidation, the impact of Ru−O−Ru coupling on redox potentials, or the impact of redox events occurring at orbitals delocalized over the μ-oxo bridge.

Rather than reproduce the mechanism proposed by Yang and Baik, a modified version is presented in Scheme 3. In this scheme, the structures in parentheses represent transition states.

It is useful to comment on the key microscopic details for the individual steps in the proposed water oxidation mechanism in Scheme 3:

Step a: Following oxidation to $(O)Ru^{V}ORu^{V}(O)^{4+}$, a water molecule is positioned by hydrogen bonding for subsequent coupled electron–proton transfer (EPT).

Step b: O---O coupling occurs with $2e^-$ transfer, one to Ru_1=O and one to Ru_2=O. ET occurs in concert with PT to Ru_2=O in a EPT step that could be described as $2e^-/1H^+$

(186) Ishitani, O.; Ando, E.; Meyer, T. J. *Inorg. Chem.* **2003**, *42*(5), 1707–1710.

Scheme 4. Proposed Mechanism for Oxidative Activation and Water Oxidation by the Blue Dimer at 23 ± 2 °C

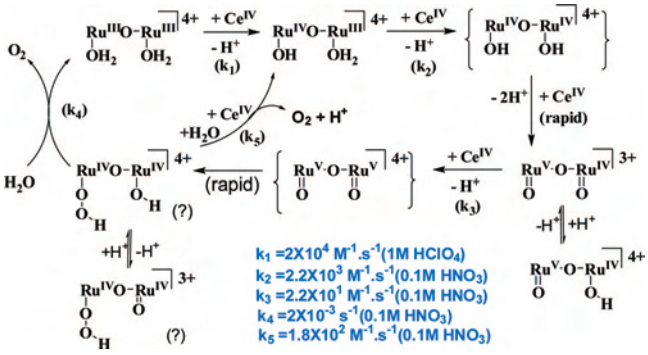

multiple-site EPT (MS-EPT). (Reduction to Ru^{IV} at Ru_2O would greatly increase proton affinity, enhancing the driving force. Note that $pK_a = 11.2$ for $[(bpy)_2(HO)Ru^{IV}ORu^{III}(py)(bpy)_2]^{4+}$; section 4.2).[149]

Step c: Given evidence for the $[(bpy)_2(HO)Ru^{IV}ORu^{IV}(ONO_2)(bpy)_2]^{4+}$/ $[(bpy)_2(O)Ru^{V}ORu^{IV}(ONO_2)(bpy)_2]^{3+}$ acid–base equilibrium, the suggested peroxidic intermediate, $[(HOO)Ru^{IV}ORu^{IV}(OH)]^{4+}$, in step c could also be in acid–base equilibrium with a $Ru^{V}ORu^{III}$ form, $[(HOO)Ru^{IV}ORu^{IV}(OH)]^{4+} \rightleftharpoons [(HOO)Ru^{III}ORu^{V}(O)]^{3+} + H^+$. Evidence for such an equilibrium was mentioned in section 5.3.

Step d: In step d, a second EPT step occurs with $OOH^- \rightarrow Ru^{IV}$ electron transfer coupled with proton transfer from Ru_1OOH to Ru_2OH by a $1e^-/1H^+$ MS-EPT pathway. (Reduction at this stage also enhances basicity; $pK_{a,1} = 6.8$ for $[(bpy)_2(H_2O)Ru^{III}ORu^{III}(py)(bpy)_2]^{4+}$.[149])

Step e: In the mechanism by Yang and Baik, a spin change occurs in the superoxidic intermediate, $[(OO^{\bullet-})Ru^{IV}ORu^{III}(OH_2)]^{4+}$.

Step f: In the final step, internal $OO^{\bullet-} \rightarrow Ru^{IV}$ electron transfer and O_2 release, step g, are accompanied by coordination of H_2O from the solvent, returning the catalyst to its initial $[(H_2O)Ru^{III}ORu^{III}(OH_2)]^{4+}$ form.

The focus of the mechanism in Scheme 3 is the sequence of events that lead to oxygen evolution following oxidation to $Ru^{V}ORu^{V}$. As described in section 5.3, the details of the oxidative activation steps leading to $Ru^{V}ORu^{V}$ and oxygen evolution are also unfolding. A possible mechanism for oxidative activation in 0.1 M HNO_3, derived from the kinetic and mixing studies described in section 5.3 and consistent with Scheme 3, is shown in Scheme 4.

In this mechanism, which reinforces and extends the earlier observations in 1 M $HClO_4$ in Scheme 2, oxidative activation is initiated by stepwise PCET oxidation of the blue dimer, represented below as $[(H_2O)Ru^{III}ORu^{III}(OH_2)]^{4+}$ at pH = 1:

(1) $Ce^{IV} + [(H_2O)Ru^{III}ORu^{III}(OH_2)]^{4+} \rightarrow Ce^{III} + [(HO)Ru^{IV}ORu^{III}(OH_2)]^{4+} + H^+$

(2) $Ce^{IV} + [(HO)Ru^{IV}ORu^{III}(OH_2)]^{4+} \rightarrow Ce^{III} + \{[(HO)Ru^{IV}ORu^{IV}(OH)]^{4+}\} + H^+$

(3) $Ce^{IV} + \{[(HO)Ru^{IV}ORu^{IV}(OH)]^{4+}\} \xrightarrow{\text{rapid}} Ce^{III} + [(O)Ru^{V}ORu^{IV}(O)]^{3+} + 2H^+$.

The slow step is oxidation of $Ru^{IV}ORu^{III}$ to $Ru^{IV}ORu^{IV}$. This is not surprising given the estimated reduction potential of >1.55 V for the $Ru^{IV}ORu^{IV}/Ru^{IV}ORu^{III}$ couple (Scheme 1) and the conclusion that $Ru^{IV}ORu^{IV}$ is the strongest oxidant of the higher oxidation states. This step is the least favored thermodynamically of the three. In 1 M CF_3CSO_3H and $HClO_4$, there is spectral evidence that oxidation of $Ru^{IV}ORu^{III}$ occurs through an anated form of $Ru^{IV}ORu^{IV}$, $Ru^{IV}ORu^{IV}X$ (see below).

The key step in water oxidation occurs following a fourth $1e^-$oxidation, of $Ru^{V}ORu^{IV}$ to $Ru^{V}ORu^{V}$. $Ru^{V}ORu^{V}$ does not build up as a detectable intermediate. Instead, it undergoes a further reaction to produce a detectable intermediate with $\lambda_{max} = 482$ and 850 nm in 0.1 M HNO_3. In 1 M HNO_3, the visible λ_{max} for the intermediate shifts to 451 nm.

The reason why the intermediate appears at the catalytic steady state under these conditions and not in 1 M HNO_3 is due to the enhanced rate of oxidation of $Ru^{V}ORu^{IV}$ in the more dilute acids, k(0.1 M HNO_3, 23 °C) = 2.2×10^2 M^{-1} s^{-1}, compared to 1 M HNO_3, k(23 °C) = 80 M^{-1} s^{-1}.

The stoichiometric experiments with added Ce^{IV} show that the intermediate is $3e^-$ oxidized relative to $Ru^{IV}ORu^{III}$ and $4e^-$ relative to $Ru^{III}ORu^{III}$. This oxidative stoichiometry is consistent with the redox titration with Fe^{2+}(aq), which showed that ×4 equiv of Fe^{2+}(aq) are required to reduce the intermediate to $[(bpy)_2(H_2O)Ru^{III}ORu^{III}(H_2O)(bpy)_2]^{4+}$. The intermediate could be $[(O)Ru^{V}ORu^{V}(O)]^{4+}$, although its spectroscopic signatures at $\lambda_{max} = 482$ and ~850 nm are significantly different from those observed for the black suspension of the ClO_4^- salt mentioned in section 4.3. Another possibility, more consistent with the available evidence, is that it is the deprotonated form of the peroxidic intermediate $[(HO_2)Ru^{III}ORu^{V}(O)]^{3+}$ proposed in Scheme 3. Based on measurements in 1 and 0.1 M HNO_3, this intermediate is in acid–base equilibrium with a protonated form, presumably $[(HO_2)Ru^{IV}ORu^{IV}(OH)]^{4+}$ (eq 9).

$$[(bpy)_2(HO_2)Ru^{IV}ORu^{IV}(OH)(bpy)_2]^{4+}\ (451\text{nm}) \rightleftharpoons [(bpy)_2(HO_2)Ru^{III}ORu^{V}(O)(bpy)_2]^{3+}\ (482\text{nm}) + H^+ \quad (9)$$

The oxo formulation is consistent with the appearance of a ν(Ru=O) stretch at 818 cm^{-1} in CF_3SO_3H as observed by Hurst et al. A similar rate constant for disappearance of the intermediate, k(0.5 M CF_3SO_3H, 23 °C) = 9.5×10^{-3} s^{-1}, was also obtained.[164,169]

When generated under stoichiometric conditions, the peroxidic intermediate disappears with an increase in absorbance for $Ru^{IV}ORu^{IV}$ at $\lambda_{max} = 495$ nm with k(0.1 M HNO_3, 23 °C) = 2×10^{-3} s^{-1}. Loss of the intermediate apparently occurs by the sequence $[(HO_2)Ru^{III}ORu^{V}(O)]^{3+} \xrightarrow{+H_2O,\ +H^+} [(H_2O)Ru^{III}ORu^{III}(OH_2)]^{4+} + O_2$, $[(H_2O)Ru^{III}ORu^{III}(OH_2)]^{4+} + [(HO_2)Ru^{III}ORu^{V}(O)]^{3+} \rightarrow [(HO)Ru^{IV}ORu^{III}(OH_2)]^{4+} + [(HO_2)Ru^{III}ORu^{IV}(OH)]^{3+}$. Evidence for the intermediate $[(HO_2)Ru^{III}ORu^{IV}(OH)]^{3+}$ was obtained by a spectrophotometric titration at the end of this step. It revealed that ×2 Fe^{2+}(aq) based on initial $Ru^{IV}ORu^{III}$ was required for complete reduction to $Ru^{III}ORu^{III}$. The initial self-reduction of $[(HO_2)Ru^{IV}ORu^{IV}(OH)]^{4+}$ is followed by a far slower step with small but discernible changes in the

visible spectrum. This step is presumably due to conversion of $[(HO_2)Ru^{III}ORu^{IV}(OH)]^{3+}$ to $Ru^{IV}ORu^{III}$ with the evolution of oxygen but remains to be studied in detail.

The initial peroxidic intermediate is the dominant form of the catalyst early in the catalytic cycle in both 0.1 M HNO_3 and 0.1 M CF_3CSO_3H. Under these conditions, loss of Ce^{IV} is first order in both Ce^{IV} and initial $Ru^{IV}ORu^{III}$ with k(0.1 M HNO_3, 23 °C) = 1.8×10^2 M^{-1} s^{-1}. This points to further oxidation of the peroxidic intermediate followed by accelerated oxygen evolution, $Ce^{IV} + [(HO_2)Ru^{III}ORu^{V}(O)]^{3+} \rightarrow \{[(HO_2)Ru^{IV}ORu^{V}(O)]^{4+}\} + Ce^{III}$, $\{[(HO_2)Ru^{IV}ORu^{V}(O)]^{4+}\} \xrightarrow{+H_2O} [(HO)Ru^{IV}ORu^{III}(OH_2)]^{4+} + O_2$ (Scheme 4). First-order loss of the peroxidic intermediate is slower by >100 than oxidation by Ce^{IV} at the initial stages of the catalytic cycle.

As the reaction proceeds and Ce^{IV} is consumed, $Ru^{V}ORu^{IV}$ appears and eventually becomes the dominant form at the catalytic steady state. Under these conditions, water oxidation is rate limited by $Ru^{V}ORu^{IV}$ oxidation to $Ru^{V}ORu^{V}$.

In both 1 M CF_3CSO_3H and 1 M $HClO_4$, an additional complication appears. At high concentrations of both of these acids, stoichiometric oxidation by Ce^{IV} results in still a different intermediate, in 1 M CF_3SO_3H characterized by λ_{max} = 445 and 744 nm. A related observation was made in 0.5 M CF_3CSO_3H (section 5.3). The intermediate at 445 nm is in acid–base equilibrium with a deprotonated form at λ_{max} = 493 nm.

The details of these reactions are currently under investigation. The intermediates appear to be $CF_3SO_3^-$ and ClO_4^- analogues of $[(bpy)_2(HO)Ru^{IV}ORu^{IV}(NO_3)(bpy)_2]^{4+}$. Once formed, they enter the catalytic water oxidation cycle by rate-limiting anion loss to give $Ru^{IV}ORu^{IV}$ [k(1 M $HClO_4$, 25 °C) = 4×10^{-2} s^{-1}; k(1 M CF_3SO_3H, 25 °C) = 10^{-2} s^{-1}][162] followed by oxidation to $Ru^{V}ORu^{IV}$ and $Ru^{V}ORu^{V}$. In 0.5 M CF_3CSO_3H, the peroxidic intermediate appears and is dominant at the catalytic steady state. Loss of Ce^{IV} is zero order under these conditions pointing to rate-limiting decomposition of the peroxidic intermediate with k(0.5 M CF_3SO_3H, 25 °C) = 7×10^{-3} s^{-1}.

Isotope Effects. Although the mechanisms in Schemes 3 and 4 are adequate to explain the appearance of $^{16}O^{18}O$ in the labeling experiment with $Ru^{V}ORu^{V}$ as the oxidant, they do not explain $^{16}O^{16}O$. Explanations for $^{16}O^{16}O$ have been advanced based on the following: (i) intermediate formation of a bridging ozonide dianion O_3^{2-} followed by attack by external H_2O on the central oxygen;[187] (ii) intermediate formation of a dihydroperoxide complex, $[(HOO)Ru^{III}ORu^{III}(OOH)]^{2+}$, followed by its decomposition into H_2O_2 or O_2 through a bridging tetroxide;[46] and (iii) intermediate, bpy-based covalent hydrate formation followed by ligand-based oxidation, possibly facilitated by H-atom abstraction to an adjacent Ru=O. It was proposed that further oxidation would give an endoperoxide followed by release of O_2.[164,169]

The first two mechanisms seem unlikely on energetic grounds.[162,169] There is precedence for the initial step proposed in mechanism (iii) from ligand decomposition studies on *cis*-$[Ru^{IV}(bpy)_2(py)(O)]^{2+}$ and $[Ru^{IV}(tpy)(bpy)(O)]^{2+}$ in basic solution. Kinetic results revealed pathways for self-reduction both first and second order in OH^-. However, given the rates observed, these pathways, which rely on the initial OH^- attack on a pyridyl ring, are negligible in strongly acidic solutions.[81]

One explanation for the $^{16}O^{16}O$ labeling result is that isotopic exchange with solvent, although slow in $[(O)Ru^{V}ORu^{IV}(O)]^{3+}$, is competitive with catalytic water oxidation in $[(O)Ru^{V}ORu^{V}(O)]^{4+}$. Ligand substitution is typically enhanced at higher temperatures. Given the temperature-dependent isotopic exchange results of Hurst et al., the low-temperature pathway for oxygen evolution favoring $^{16}O^{18}O$ may arise for water oxidation consistent with the mechanism in Scheme 3. The higher temperature pathway may be associated with isotopic exchange with a solvent, which would explain the appearance of $^{16}O^{16}O$.

5.6. Water Oxidation by $[(bpy)_2(O)Ru^{V}ORu^{IV}(O)(bpy)_2]^{3+}$ and $[(bpy)_2(HO)Ru^{IV}ORu^{IV}(ONO_2)(bpy)_2]^{4+}$. Oxygen evolution measurements over an extended period, well past the catalytic water oxidation stage, reveal that O_2 continues to evolve after Ce^{IV} is consumed. Qualitatively, the rate of oxygen evolution matches the rate of appearance of $Ru^{IV}ORu^{III}$. Depending on the reaction conditions, at the end of catalytic cycles in CF_3SO_3H, $HClO_4$, or HNO_3, the catalyst exists primarily as the putative peroxo intermediate, $[(HO_2)Ru^{IV}ORu^{IV}(OH)]^{3+}$, as $Ru^{V}ORu^{IV}$, as $[(bpy)_2(HO)Ru^{IV}ORu^{IV}(X)(bpy)_2]^{3+}$ (X = $CF_3SO_3^-$, ClO_4^-, NO_3^-), or as a mixture of the three. The final distribution is further complicated by the acid–base equilibria that each of the intermediates undergo, e.g., $[(HO_2)Ru^{IV}ORu^{IV}(OH)]^{3+} \rightleftharpoons [(HO_2)Ru^{III}ORu^{V}(O)]^{3+} + H^+$.

In these solutions, slow oxygen evolution occurs by a series of subsequent reactions involving these three intermediates or a combination of intermediates.

$[(HO_2)Ru^{III}ORu^{V}(O)]^{3+}$. Stepwise decomposition of the putative peroxidic intermediate was discussed in section 5.4. For the deprotonated form, the net reaction is $2[(HO_2)Ru^{III}ORu^{V}(O)]^{3+} + 2H^+ \rightarrow 2[(HO)Ru^{IV}ORu^{III}(OH_2)]^{4+} + O_2$. This is the dominant reaction at the end of catalytic cycles in 0.5 M CF_3SO_3H.

$Ru^{V}ORu^{IV}$. $Ru^{V}ORu^{IV}$ also returns to $Ru^{IV}ORu^{III}$ accompanied by water oxidation (eq 10). It appears at the end of catalytic cycles in both 1 and 0.1 M HNO_3. Loss of $Ru^{IV}ORu^{III}$ occurs by second-order, equal-concentration kinetics. The reaction is highly pH-dependent with k(23 °C) = 5.5×10^{-4} M^{-1} s^{-1} in a 0.1 M $H_2PO_4^-/HPO_4^{2-}$ buffer at pH = 6, k(0.1 M HNO_3, 23 °C) = 4 M^{-1} s^{-1}, and k(1 M HNO_3, 23 °C) = 20 M^{-1} s^{-1}.

$$2[(bpy)_2(O)Ru^{V}ORu^{IV}(O)(bpy)_2]^{3+} + 2H_2O \rightarrow 2[(bpy)_2(HO)Ru^{IV}ORu^{III}(OH)(bpy)_2]^{3+} + O_2 \quad (10)$$

A detailed, pH-dependent kinetic study remains to be undertaken, but the rate enhancement in acidic solutions is presumably due to enhanced reactivity of the protonated form

(187) Meyer, T. J. *Oxygen Complexes and Oxygen Activation by Transition Metals*; Plenum Press: New York, 1988.

of $Ru^{V}ORu^{IV}$. One possible mechanism is initial disproportionation, $2[(O)Ru^{V}ORu^{IV}(OH)]^{4+} \rightarrow [(O)Ru^{V}ORu^{V}(O)]^{4+} + [(HO)Ru^{IV}ORu^{IV}(OH)]^{4+}$, followed by water oxidation by $Ru^{V}ORu^{V}$ as in Scheme 4. The coproduct of this reaction, $[(HO)Ru^{IV}ORu^{IV}(OH)]^{4+}$, is unstable toward disproportionation, $2[(HO)Ru^{IV}ORu^{IV}(OH)]^{4+} + H^{+} \rightarrow [(O)Ru^{V}ORu^{IV}(OH)]^{4+} + [(H_2O)Ru^{IV}ORu^{III}(OH_2)]^{5+}$, and $Ru^{V}ORu^{IV}$ would also re-enter the water oxidation cycle. In the disproportionation step, there could be a role for coupled EPT (eq 11).

$$\begin{aligned} 2[(O)Ru^{IV}ORu^{IV}(OH)]^{4+} &\rightarrow \{[(O)Ru^{V}ORu^{IV}(OH\text{---}O)Ru^{V}ORu^{IV}(OH)]^{8+}\} \rightarrow \\ &\{[(O)Ru^{V}ORu^{V}(O\text{---}HO)Ru^{IV}ORu^{IV}(OH)]^{8+}\} \rightarrow \\ &[(O)Ru^{V}ORu^{V}(O)]^{4+} + [(HO)Ru^{IV}ORu^{IV}(OH)]^{4+} \quad (11) \end{aligned}$$

As noted in the previous section, second-order, equal-concentration kinetics for loss of $Ru^{V}ORu^{IV}$ could also arise from bimolecular O---O coupling, $2[(O)Ru^{V}ORu^{IV}(O)]^{3+} \rightarrow [(O)Ru^{IV}ORu^{V}O\text{---}ORu^{V}ORu^{IV}(O)]^{6+} \xrightarrow{+2H^{+}} [(HO)Ru^{IV}ORu^{IV}O{-}ORu^{IV}ORu^{IV}(OH)]^{8+} \xrightarrow{+2H_2O,\ +2H^{+}} 2[(H_2O)Ru^{IV}ORu^{III}(OH_2)]^{5+} + O_2$. This mechanism would explain the appearance of $^{18}O^{18}O$ in the isotopic labeling experiments.

In 1 M HNO_3, loss of $Ru^{V}ORu^{IV}$ occurs to give a ~1:1 mixture of $Ru^{IV}ORu^{III}$ and $[(bpy)_2(HO)Ru^{IV}ORu^{IV}(ONO_2)(bpy)_2]^{4+}$ (eq 12). As noted in section 5.3, anation also accompanies oxygen evolution during catalytic cycles under these conditions.

$$4[(bpy)_2(O)Ru^{V}ORu^{IV}(OH)(bpy)_2]^{4+} + 4NO_3^{-} + 4H^{+} \rightarrow 4[(bpy)_2(HO)Ru^{IV}ORu^{IV}(ONO_2)(bpy)_2]^{4+} + O_2 + 2H_2O \quad (12)$$

$[(bpy)_2(HO)Ru^{IV}ORu^{IV}(X)(bpy)_2]^{4+}$. Anation is an important, deleterious factor in water oxidation catalysis especially in 1 M HNO_3. Once formed, $[(bpy)_2(HO)Ru^{IV}ORu^{IV}(ONO_2)(bpy)_2]^{4+}$ returns to $Ru^{IV}ORu^{III}$ with the release of oxygen (eq 13), but this reaction is slow with k(1 M HNO_3, 23 °C) = 8×10^{-5} s^{-1}. This ties up the catalyst in an inactive state for extended periods and represents a major pathway for catalyst deactivation. The problem is less severe in 1 M $HClO_4$ or CF_3SO_3H where return to the catalytic cycle is more rapid by $>10^2$. In 1 M $HClO_4$, aquation of the putative analogue of $[(bpy)_2(HO)Ru^{IV}ORu^{IV}(ONO_2)(bpy)_2]^{4+}$ occurs with k(1 M $HClO_4$, 25 °C) = 2.5×10^{-2} s^{-1}.[162]

$$4[(bpy)_2(HO)Ru^{IV}ORu^{IV}(X)(bpy)_2]^{4+} + 6H_2O \rightarrow 4[(bpy)_2(H_2O)Ru^{IV}ORu^{III}(H_2O)(bpy)_2]^{5+} + O_2 + 4X^{-} \quad (13)$$

The mechanism for disappearance of the anated intermediates presumably involves initial aquation to give $Ru^{IV}ORu^{IV}$, $[(bpy)_2(HO)Ru^{IV}ORu^{IV}(X)(bpy)_2]^{4+} + H_2O \rightarrow [(bpy)_2(HO)Ru^{IV}ORu^{IV}(OH)(bpy)_2]^{4+} + H^{+} + X^{-}$ (X = CF_3SO_3, ClO_4, NO_3) followed by disproportionation or further oxidation of $Ru^{IV}ORu^{IV}$ to $Ru^{V}ORu^{IV}$ and $Ru^{V}ORu^{V}$.

The anated intermediates only appear in significant amounts in solutions highly concentrated in added anions. Their appearance in 1 M $HClO_4$ and CF_3SO_3H, coupled with oxidation of $Ru^{IV}ORu^{III}$, suggests a prior equilibrium in $Ru^{IV}ORu^{IV}$ involving anation, $[(H_2O)Ru^{IV}ORu^{III}(OH_2)]^{5+} + X^{-} \rightarrow [(H_2O)(X)Ru^{IV}ORu^{III}(OH_2)]^{4+}$, followed by oxidation, $[(H_2O)(X)Ru^{IV}ORu^{III}(OH_2)]^{4+} + Ce^{IV} \rightarrow [(X)Ru^{IV}ORu^{IV}(OH)]^{4+} + Ce^{III}$. In 1 M HNO_3, $[(bpy)_2(HO)Ru^{IV}ORu^{IV}(ONO_2)(bpy)_2]^{4+}$ also forms as a product of $Ru^{V}ORu^{IV}$ disproportionation and as a product in the oxidation of $[(HO_2)Ru^{IV}ORu^{IV}(OH)]^{4+}$. These reactions are all currently under investigation.

As implied above, in the oxidation of $Ru^{IV}ORu^{III}$ to $Ru^{IV}ORu^{IV}X$, one possibility for anation in the higher oxidation state forms of the blue dimer is the intervention of pathways that involve coordination expansion. This possibility is shown for water oxidation by $Ru^{V}ORu^{IV}$ in 14 in which anation facilitates oxidation to $Ru^{V}ORu^{V}$ by disproportionation followed by intramolecular O---O coupling and intermediate peroxido formation.

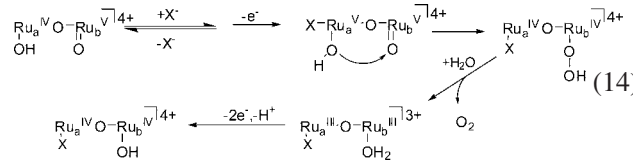

(14)

In d^4 Ru^{IV} and d^3 Ru^{V} complexes, there are orbital vacancies for electron-pair donation and coordination-sphere expansion although at the expense of orbital coupling across the μ-oxo bridge. Coordination-sphere expansion by associative substitution has been suggested as a pathway in water exchange in the blue dimer.[164,181] There is literature precedence for such pathways.[188] Hurst et al. have also considered coordination-sphere expansion as a possible mechanism in water oxidation by H_2O addition to Ru^{V} in $Ru^{V}ORu^{V}$. Literature precedence exists for a seven-coordinate metal complex having lower d electron configurations.[189]

Coordination-sphere expansion may also help to explain the labeling results for water oxidation by $Ru^{V}ORu^{IV}$. As shown in Scheme 5, coordination expansion by $H_2{}^{16}O$ to give $Ru^{V}(OH)_2$ followed by O---O coupling across the μ-oxo bridge would lead to a mixture of $^{16}O^{18}O$ and $^{18}O^{18}O$. The same pathway would provide a basis for solvent exchange and explain the appearance of $^{16}O^{16}O$ as a product.

5.7. Water Oxidation Summary. The results of our analysis of the available data are revealing as to how the blue dimer catalyzes the Ce(IV) oxidation of water. Although the story is not yet complete and mechanistic studies continue, important features can be discerned. After the results are surveyed, the difficulties in analyzing this mechanism become apparent. Two different intermediates intervene, $[(bpy)_2(HO)Ru^{IV}ORu^{IV}(X)(bpy)_2]^{4+}$ and $[(HO_2)Ru^{III}ORu^{IV}(OH)]^{3+}$, and each is involved in its own acid–base equilibrium in the acid range, 1–0.1 M, in which the studies

(188) Rappaport, I.; Helm, L.; Merbach, A. E.; Bernhard, P.; Lundi, A. *Inorg. Chem.* **1988**, *27*, 873–879.
(189) Serpone, N.; Ponterini, G.; Jamieson, M. A.; Bolletta, F.; Maestra, M. *Coord. Chem. Rev.* **1983**, *50*(3), 209–302.

Scheme 5. Possible Coordination Expansion and ^{18}O Labeling in $Ru^{V}ORu^{IV}$

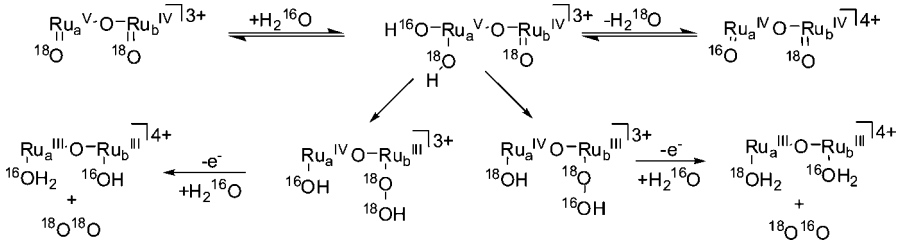

have been conducted. These pH dependences are further exacerbated by acid–base equilibria of both $Ru^{IV}ORu^{III}$ and $Ru^{V}ORu^{IV}$ in the same pH range.

As a mechanistic summary, note the following: (i) The catalytically active form of the blue dimer is $[(bpy)_2(O)Ru^{V}ORu^{V}(O)(bpy)_2]^{4+}$, $Ru^{V}ORu^{V}$. It does not build up in solution as a discernible intermediate but undergoes a rapid reaction with water to form a peroxidic intermediate. (ii) $Ru^{V}ORu^{V}$ is reached by stepwise PCET oxidation of $Ru^{III}ORu^{III}$. In 1 M HNO_3, the slow step is Ce(IV) oxidation of $Ru^{V}ORu^{IV}$ to $Ru^{V}ORu^{V}$. (iii) In 1 M CF_3CSO_3H or $HClO_4$, $1e^-$ oxidation of $Ru^{IV}ORu^{III}$ is accompanied by anation to give $Ru^{IV}ORu^{IV}X$. Following aquation of X^-, rapid oxidation of $Ru^{IV}ORu^{IV}$ through $Ru^{V}ORu^{V}$ occurs to give the peroxidic intermediate. (iii) Decomposition of the peroxidic intermediate, as $[(HO_2)Ru^{IV}ORu^{IV}(OH)]^{4+}$ in 0.5 M CF_3SO_3H, is rate-limiting in the catalytic cycle. Early in the catalytic cycle in 0.1 M HNO_3, cesium(IV) oxidation of $[(HO_2)Ru^{III}ORu^{V}(O)]^{3+}$ is rate-limiting and catalysis is greatly accelerated compared to 0.5 M CF_3SO_3H. (v) Anated intermediates, $[(bpy)_2(HO)Ru^{IV}ORu^{IV}(X)(bpy)_2]^{4+}$ ($X = NO_3$, CF_3SO_3, ClO_4), in acid–base equilibrium with their deprotonated forms $[(bpy)_2(O)Ru^{V}ORu^{III}(X)(bpy)_2]^{3+}$ appear under a variety of conditions: (a) accompanying $1e^-$ oxidation of $Ru^{IV}ORu^{III}$ in 1 M CF_3CSO_3H or $HClO_4$, (b) during catalytic cycles coupled to Ce(IV) oxidation of peroxidic intermediates, and (c) during loss of $Ru^{V}ORu^{IV}$ by second-order, equal-concentration kinetics in the presence of high concentrations of anions. (vi) The anated intermediates subsequently undergo aquation followed by water oxidation through $Ru^{IV}ORu^{IV}$ as an intermediate.

With this interpretation, water oxidation by the blue dimer in its oxidized $Ru^{V}ORu^{V}$ form is rapid. A peroxidic intermediate in acid–base equilibrium is key to the catalytic cycle. Its decomposition or further oxidation is rate-limiting under most conditions. In strongly acidic solutions, anated intermediates intervene deleteriously by tying up $Ru^{IV}ORu^{IV}$.

This is not the end of the story. With this mechanistic insight in hand, we are developing conditions for sustained catalytic oxidation free of anation. A phosphonated version of the blue dimer is on oxide electrode surfaces, and it appears that photochemical pathways for water oxidation exist for some higher oxidation state μ-oxo dimers.

6. Water Oxidation in the OEC

The availability of XRD structural information to 3 and 3.5 Å resolution[47,48] combined with the accumulated insight gained by theory and an impressive array of experimental results has provided molecular-level insight into how oxidative activation and water oxidation occur at the OEC of PSII.

Both of these themes were recently developed in an account that proposed a mechanism for water oxidation in which PCET and proton transfer play major roles.[12] It is useful to revisit this mechanism both for its highlights and for comparison with water oxidation by the blue dimer.

The OEC is part of PSII, a multipolypeptide complex imbedded in the thylakoid membranes of chloroplasts.[47–64,190–196] In green plants, water acts as the electron donor in the net photochemical reduction of CO_2 to carbohydrates. In PSII, H_2O is oxidized to O_2 with the reductive equivalents used to reduce a quinone (Q_A and Q_B) to its hydroquinone. Reductive equivalents are ultimately transferred to photosystem I, where they enter the Calvin cycle for CO_2 reduction.[1–11,47–64,190–196]

Water oxidation occurs in the reaction center of PSII (Figure 15). It is initiated by light absorption in an antenna apparatus, consisting of chlorophylls and organic pigments, which sensitize the lowest singlet state of chlorophyll P_{680} (Chl_{D1} in Figure 15) or neighboring $pheophytin_{D1}$. This excited state subsequently undergoes rapid oxidative quenching with electron transfer to quinone Q_A and oxidation of P_{680} to P_{680}^+. Oxidized P_{680}, in turn, oxidizes tyrosine Tyr_Z, probably in concert with proton transfer to His-190 by EPT. The net reaction is shown in eq 15.

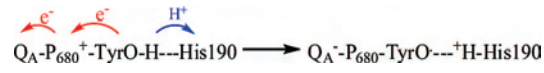

$$Q_A\text{-}P_{680}^{+}\text{-}TyrO\text{-}H\text{---}His190 \xrightarrow{e^-,\ e^-,\ H^+} Q_A^{-}\text{-}P_{680}\text{-}TyrO\cdot\text{---}^{+}H\text{-}His190 \quad (15)$$

The oxidative equivalents transiently stored in TyrO•---$^+$H−His190 (Y_Z•) subsequently oxidize the OEC. The Y_Z•/Y_Z couple (TyrO•---$^+$H−His190/TyrO-H---His190) is thermodynamically capable of water oxidation. Its potential has been estimated as $E^{\circ\prime} = 1.1$–1.2 V,[197] while $E^{\circ\prime} = 0.815$ for the O_2/H_2O couple at pH = 7.

Key elements of the structure of the OEC, based on the XRD data and a recent EXAFS study, are illustrated

(190) Zouni, A.; Witt, H.-T.; Kern, J.; Fromme, P.; Krauss, N.; Saenger, W.; Orth, P. *Nature* **2001**, *409*(6821), 739–743.
(191) Kamiya, N.; Shen, J.-R. *Proc. Natl. Acad. Sci. U.S.A.* **2003**, *100*(1), 98–103.
(192) Goussias, C.; Boussac, A.; Rutherford, A. W. *Philos. Trans. R. Soc. London, Ser. B* **2002**, *357*(1426), 1369–1381.
(193) Sauer, K.; Yachandra, V. K. *Biochim. Biophys. Acta* **2004**, *1655*(1–3), 140–148.
(194) Biesiadka, J.; Loll, B.; Kern, J.; Irrgang, K.-D.; Zouni, A. *Phys. Chem. Chem. Phys.* **2004**, *6*(20), 4733–4736.
(195) McEvoy, J. P.; Brudvig, G. W. *Phys. Chem. Chem. Phys.* **2004**, *6*(20), 4754–4763.
(196) Debus, R. J. *Biochim. Biophys. Acta* **1992**, *1102*(3), 269–352.
(197) Rappaport, F.; Guergova-Kuras, M.; Nixon, P. J.; Diner, B. A.; Lavergne, J. *Biochemistry* **2002**, *41*(26), 8518–8527.

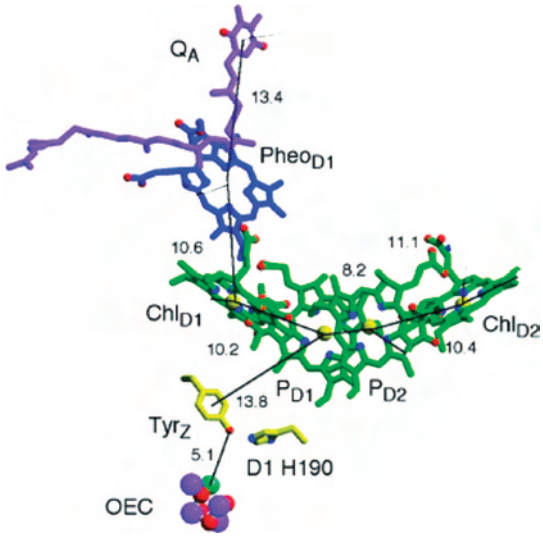

Figure 15. Molecular structure of the reaction center of PSII illustrating the Tyr_Z−$Chl_{D1}(P_{680})$−$Pheo_{D1}$−Q_A donor−chromophore−acceptor (D−C−A−A′) array and the proximity of Tyr_Z to the OEC. Reprinted from ref 47. Copyright 2004 AAAS.

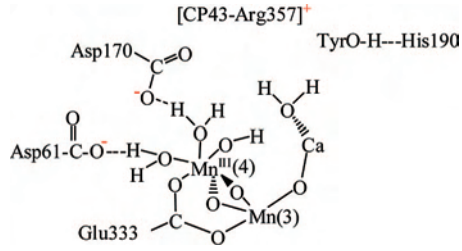

Figure 16. Schematic drawing illustrating possible structural features of the OEC based on EXAFS and XRD data and structures.[12,47–50] The water molecules shown are not observed in either the EXAFS or XRD structures.

schematically in Figure 16. There is still considerable uncertainty in the XRD structures because of the effects of radiation damage and the fact that data are available only to 3 Å resolution. The exact positions of Asp61 and Asp170 are not known and nor is it known whether Glu333 is coordinated as a uni- or bidentate ligand.

The drawing in Figure 16 includes additional features not observed in the XRD structures: coordinated H_2O molecules, μ-oxo bridges, etc. These features are at least consistent with the XRD data and, as suggested below, may play an important role in oxidative activation and oxygen evolution. Key structural elements include the following: (1) Mn(3) and Ca, which are part of a $CaMn_3$ cluster (not shown) important in defining the structure of the OEC and holding it within the membrane environment; (2) an additional Mn, Mn(4), attached to Mn(3) by di-μ-oxo bridging and a bridging glutamate, where oxygen is thought to evolve; (3) Y_Z with Tyr_ZOH ~7 Å from Mn(4); (4) Asp61, which is within the hydrogen-bonding distance of a putative Mn(4)−OH_2 water molecule and the entryway to a long-range proton exit channel to the lumen side of the membrane; (5) Asp170, which appears to be in the second coordination sphere of Mn(4) by XRD and FTIR measurements.[51,198,199]

In oxidizing water, the OEC undergoes four sequential light absorption−electron transfer cycles coupled with the loss of four protons. The sequence of photochemically induced transitions between states from S_0 to S_4 is known as the Kok cycle, with the subscripts identifying the number of electrons lost.[200] In this cycle, it has been proposed that PCET plays a major role both by redox potential leveling and by use of coupled EPT to avoid high-energy intermediates.[1,12]

It is insightful to summarize the ET, PT, EPT, and O---O coupling events that have been proposed for water oxidation in the OEC in a recent account.[12] In contrast to water oxidation by the blue dimer, which occurs in water surrounded by solvent molecules, anions, and acid, water oxidation in the OEC occurs in the hydrophobic thylakoid membrane. This necessitates careful attention to proton management and requires channels for both local and long-range proton transfer.

Summarizing the Proposed Key Features of the Individual Steps in the Kok Cycle. $S_0 \rightarrow S_1$. Although the stable dark resting state for the OEC is S_1, it is convenient to begin with the $S_0 \rightarrow S_1$ transition. A possible oxidation state distribution in S_0 is II,III,IV,IV with the Mn^{II} site at Mn(4), although recent ENDOR data favor the distribution III,III,III,IV.[201,202]

Oxidation of S_0 by $Y_Z^{\bullet}$ has been proposed to occur by MS-EPT (eq 16).[1,12] As shown in eq 16, in this pathway electron transfer occurs from $Mn^{II}OH_2$ to $TyrO_Z^{\bullet}$. It is coupled with a double proton transfer. One proton is transferred from $^+$H-His190 to $TyrO_Z^{\bullet}$ and the other from $Mn^{II}OH_2$ to Asp61.

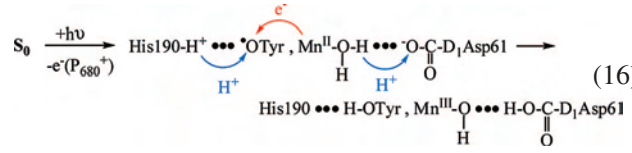

(16)

The requirement to manage protons can be seen in steps proposed following MS-EPT. They are illustrated in eq 17. Initial proton loss occurs to the lumen through the proton exit channel at Asp61 followed by intracoordination-sphere proton transfer. The latter resets the Mn(4)−OH_2---Asp61 interface for additional MS-EPT cycles.

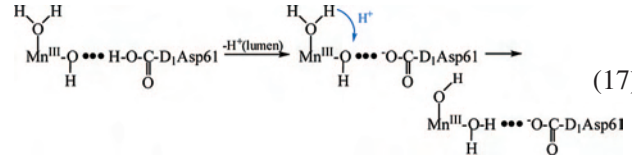

(17)

$S_1 \rightarrow S_2$. There is good experimental evidence that the second oxidation at the OEC occurs at the $CaMn_3$ cluster

(198) Styring, S.; Feyziyev, Y.; Mamedov, F.; Hillier, W.; Babcock, G. T. *Biochemistry* **2003**, *42*(20), 6185–6192.
(199) Debus, R. J.; Strickler, M. A.; Walker, L. M.; Hillier, W. *Biochemistry* **2005**, *44*(5), 1367–1374.
(200) Kok, B.; Forbush, B.; McGloin, M. *Photochem. Photobiol.* **1970**, *11*, 457–475.
(201) Kulik, L. V.; Lubitz, W.; Messinger, J. *Biochemistry* **2005**, *44*(26), 9368–9374.
(202) Kulik, L. V.; Epel, B.; Lubitz, W.; Messinger, J. *J. Am. Chem. Soc.* **2005**, *127*(8), 2392–2393.

rather than at Mn(4), $S_1(\mathrm{Mn(4)^{III}Mn^{III}Mn^{IV}Mn^{IV}}) \xrightarrow{-e^-} S_2(\mathrm{Mn(4)^{III}Mn^{IV}Mn^{IV}Mn^{IV}})$.[12,51] The proton release pattern through the four stages of the Kok cycle is 1:0:1:2 with no protons transferred in the $S_1 \rightarrow S_2$ transition. There is also evidence for a positive charge buildup in S_2.[203]

***S*$_2$ → *S*$_3$.** It has been proposed that O---O coupling occurs at this stage in the Kok cycle and, further, that there are two forms of S_3.[54,204] In the initial series of light-driven events proposed in eq 18, light-driven MS-EPT occurs as in eq 16 but, in this case, with electron transfer from $Mn(4)^{III}$ to $Y_Z^{\bullet}$. This is followed by proton loss to the lumen and intracoordination-sphere proton transfer (eq 18).

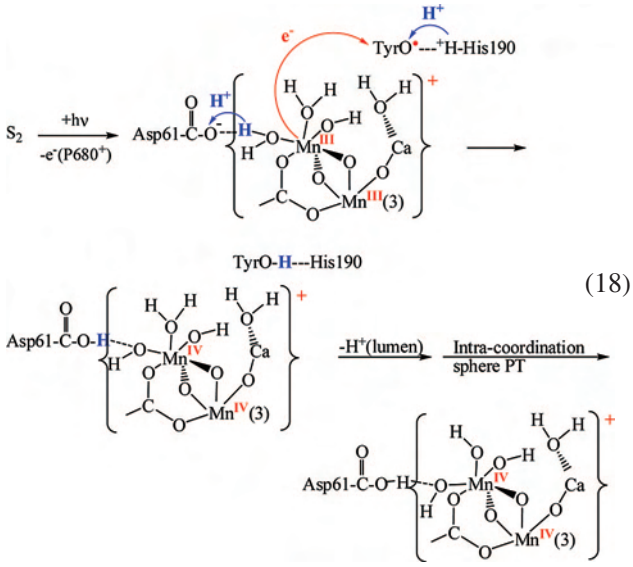

(18)

In the proposed mechanism, activation toward O---O bond formation is preceded by loss of a proton from $CaOH_2$ to Asp170 in the second coordination sphere followed by formation of an oxo site at Mn(4), $Mn(4)^{IV}(O)(H_2O)$, by a $Mn^{IV}(OH)_2 \rightleftharpoons Mn^{IV}(O)(H_2O)$ equilibrium eq 19.

Oxido formation activates the Mn−O bond toward O---O bond formation by redox nucleophilic attack of $CaOH^-$ on electrophilic Mn(4)═O. In this step, one electron is transferred to $Mn(4)^{IV}$ and the other to the cluster shown as $Mn(3)^{IV}$ in eq 19 to give a manganese(III) peroxidic intermediate.

It is interesting to compare details between the key steps that lead to O---O bond formation in the blue dimer and the OEC: *In the membrane-bound OEC*, careful attention is paid to PCET and local proton transfer. Proton transfer fully utilizes proton movement across the coordination face of Mn(4) by intracoordination-sphere proton transfer. As noted above, in solution the blue dimer is surrounded by solvent molecules, protons, and anions.

In the OEC, it has been proposed that O---O coupling occurs after loss of $3e^-$. In the coupling step, $1e^-$ is transferred to $Mn(4)^{IV}$ and one to the cluster to give

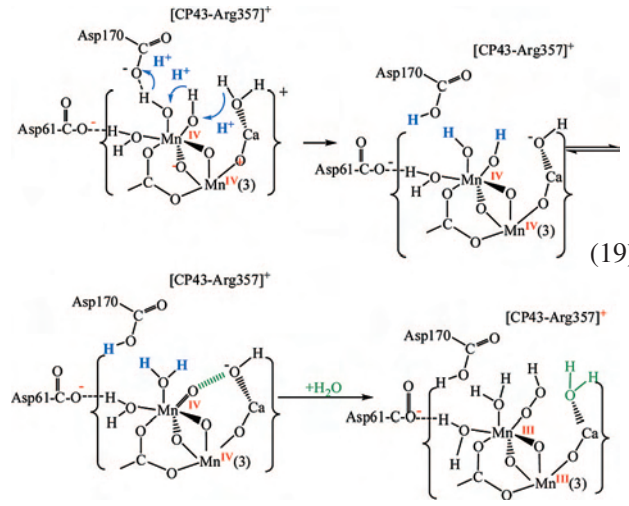

(19)

$Mn^{III}OOH$. *In the blue dimer*, O---O coupling occurs in $Ru^{V}ORu^{V}$ after loss of $4e^-$ to give $Ru^{V}ORu^{V}$ or after $3e^-$ to give $Ru^{V}ORu^{IV}$. As suggested in Scheme 3, O---O coupling in $Ru^{V}ORu^{V}$ may also occur by $1e^-$ transfer to two sites, $Ru_1{}^{V}$ and $Ru_2{}^{V}$ in $[(bpy)_2(O)Ru_1{}^{V}ORu_2{}^{V}(O)(bpy)_2]^{4+}$. A proton is transferred simultaneously in a $2e^-/1H^+$ MS-EPT pathway with proton transfer to Ru_2═O. This also gives a peroxidic intermediate, $Ru^{IV}OOH$.

PCET plays an important role in both reactions. In the OEC, deprotonation of a water molecule coordinated to Ca^{2+} occurs to an internal base to give $CaOH^-$. Coordination and proton loss activate redox nucleophilic attack on $Mn(4)^{IV}$═O. Electron transfer occurs to both $Mn(4)^{IV}$ and $Mn(3)^{IV}$. In the blue dimer, O---O bond formation at $Ru_1{}^{V}$═O occurs in concert with coupled e^-/H^+ transfer to $Ru_2{}^{V}$═O to give $Ru_2{}^{IV}$-OH (eq b in Scheme 3). In the $Ru^{V}ORu^{V}$ form of the blue dimer, the redox equivalents required to complete water oxidation exist within a single molecule. *There is no requirement for prior deprotonation by a neighboring base, and the reaction occurs in strongly acidic environments.* Subsequent $OO^{\bullet-} \rightarrow Ru^{IV}$ electron transfer is followed by O_2 release.

In the OEC, an additional oxidation past the $3e^-$ stage in S_3 is required. In the Kok cycle, S_4 does not build up as an intermediate and oxidation of S_3 is accompanied by oxygen evolution. Evidence for intermediates has been obtained by experiments at high O_2 pressures and by transient X-ray absorption measurements following laser flash photolysis.[205,206]

A stepwise mechanism for the $S_3 \rightarrow \{S_4\} \rightarrow S_0 + O_2$ transition has been proposed involving (i) light-driven $1e^-/H^+$ MS-EPT oxidation of Y_Z by $P_{680}{}^{+}$, (ii) proton transfer across the coordination face of Mn(4) from MnOOH to Asp61 giving $MnOO^-$, (iii) oxidation of $Mn^{III}OO^-$ by $Y_Z^{\bullet}$ by $1e^-/H^+$ MS-EPT with electron transfer from $Mn^{III}OO^-$ to $Y_Z^{\bullet}$ giving $Mn^{III}OO^{\bullet}$, (iv) proton transfer to the lumen followed by release of the second proton (at Asp170) to the lumen accounting for the 1:0:1:2 proton release pattern, and (v) release of O_2, which returns the catalyst to the initial S_0 state.

(203) Rappaport, F.; Blanchard-Desce, M.; Lavergne, J. *Biochim. Biophys. Acta* **1994**, *1184*(2–3), 178–192.
(204) Renger, G. *Biochim. Biophys. Acta* **2001**, *1503*(1–2), 210–228.
(205) Haumann, M.; Liebisch, P.; Mueller, C.; Barra, M.; Grabolle, M.; Dau, H. *Science* **2005**, *310*(5750), 1019–1021.
(206) Clausen, J.; Junge, W. *Nature* **2004**, *430*(6998), 480–483.

Loss of the second proton in step iv and O_2 release in step v are illustrated in eq 20.

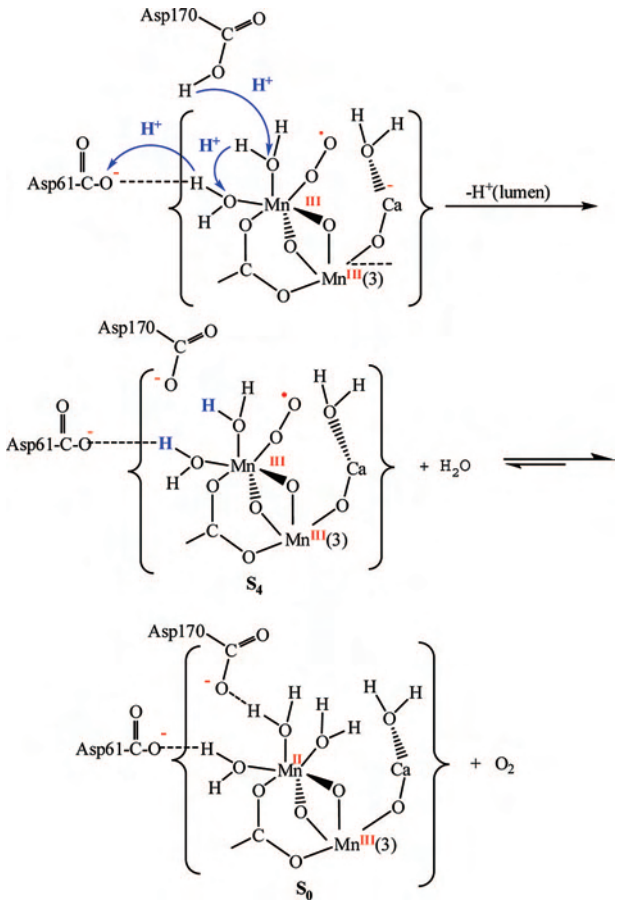

(20)

7. Conclusions and Final Comments

Although many details remain to be evaluated quantitatively, clearer views of how water is oxidized at the OEC of PSII and by the blue dimer are evolving. In both catalysts, oxidative activation occurs by a series of elaborate coupled reactions involving loss of both electrons and protons. PCET plays a central role in redox potential leveling, which allows for the buildup of multiple oxidative equivalents without significant increases in $E°$. PCET also provides essential reaction pathways in which electrons and protons are transferred simultaneously, avoiding high-energy intermediates and decreasing reaction barriers.

Proton management is a key element in the OEC, where the catalytic site is held in the thylakoid membrane. Special provisions are made in its structure for long-range proton transfer to the lumen by a sequence of local proton transfers. It is proposed that short-range proton-transfer channels through coordinated water molecules across the coordination face at Mn(4) play a key role in oxidative activation and proton distribution both before and after the O---O coupling step.

In both catalysts, multiple oxidation provides strongly oxidizing intermediate oxidation states that undergo water oxidation, $O{=}Mn^{IV}(4){-}Mn^{IV}(3)$ in the OEC and $[(O)Ru_1{}^{V}ORu_2{}^{V}(O)]^{4+}$ in the blue dimer. Oxidative activation occurs in structures capable of promoting O---O coupling: between $Mn^{IV}(4){=}O$ and a neighboring $CaOH^{-}$ in the OEC and between $Ru^{V}{=}O$ and a water molecule in the blue dimer. At the OEC, it is suggested that redox nucleophilic attack occurs with $1e^{-}$ transfer to $Mn^{IV}(4){=}O$ and $1e^{-}$ transfer to the oxidized $CaMn_3$ cluster to give a $Mn^{III}(4)OOH$ intermediate. In the oxidized form of the blue dimer, it is proposed that $1e^{-}$ transfer to $Ru_1{}^{V}{=}O$ and $1e^{-}$ transfer to $Ru_2{}^{V}{=}O$ occur to give the intermediate $[HOORu_1{}^{IV}ORu_2{}^{IV}OH]^{4+}$. Water attack at $O{=}Ru_1{}^{V}$ is accompanied by coupled e^{-}/H^{+} transfer to $Ru_2{}^{V}{=}O$. The latter is an important feature because it allows water oxidation to occur even in strongly acidic solutions without prior deprotonation of water. *Attention to structural detail appears to be an essential element in both catalysts*.

The insights gained in these studies will hopefully help unlock the details of water oxidation in photosynthesis, one of the most important reactions in biology. Insights gained for the blue dimer will hopefully guide the next generation of molecular-level catalysts for water oxidation that function with high rates and high catalyst stabilities with possible use in practical devices. There are also implications in these results for the microscopic reverse, reduction of oxygen with electron-transfer control, with the ultimate goal of devising reversible oxygen/water electrodes.[207–210]

Acknowledgments. are made to the National Science Foundation through Grant CHE554561 and Chemical Sciences, Geosciences and Biosciences Division of the Office of Basic Energy Sciences, U.S. Department of Energy, for support of this research.

IC701249S

(207) Boulatov, R.; Collman, J. P.; Shiryaeva, I. M.; Sunderland, C. J. *J. Am. Chem. Soc.* **2002**, *124*(40), 11923–11935.
(208) Collman, J. P.; Devaraj, N. K.; Decreau, R. A.; Yang, Y.; Yan, Y.; Ebina, W.; Eberspacher, T. A.; Chidsey, C. E. D. *Science* **2007**, *315*, 1565–1568.
(209) Chang, C. J.; Deng, Y.; Nocera, D. G.; Shi, C.; Anson, F. C.; Chang, C. K. *Chem. Commun.* **2000**, *1355*, 1356.
(210) Chang, C. J.; Loh, Z.-H.; Shi, C.; Anson, F. C.; Nocera, D. G. *J. Am. Chem. Soc.* **2004**, *126*(32), 10013–10020.